

Ductility Improvement in Magnesium Casting Alloys for Automotive Structural Applications

Konstantinos Korgiopoulos

Department of Mining and Materials Engineering

McGill University, Montreal

July 2021

A thesis submitted to McGill University in partial fulfillment of the requirements
of the degree of Doctor of Philosophy.

© Konstantinos Korgiopoulos, 2021

ABSTRACT

The substitution of heavier steel and aluminum components with lower density magnesium (Mg) alloys has the potential to significantly reduce vehicle weight achieving fuel economy, reduced greenhouse gasses (GHGs) and electrification of future cars. Approximately 30% of the vehicle weight is in body parts (closures, panels, pillars) all of which can be potentially cast in Mg resulting in 10-20% weight reduction. This translates into ~7-15% each of fuel economy and reduced emissions in gasoline powered cars and ~15% range increase for electric vehicles.

This thesis aimed at ductility enhancement of the automotive Mg-6wt%Al (Mg-6Al) alloy by refining its microstructure with trace rare earths additions (Y, Er) for use in the vehicle body applications. Thermodynamic calculations (CALPHAD methods using FactSage software with FTlite database) shed a light on the phase formation and solidification paths of the new alloy and helped determine the mechanism of microstructural refinement. The microstructures were analyzed with electron microscopy and atom probe tomography, effects on the crystal structure were determined with X-Rays Diffraction. The mechanical performance was determined with conventional mechanical testing (i.e., tensile, compression, hardness) and with more complicated ultrasonic methods.

The first part of the study focused on the effect of trace Y additions which found that at trace additions, the Al_4MgY precipitate co-nucleates with $\text{Mg}_{17}\text{Al}_{12}$ leading to its refinement by 47%. This refinement proved to be the key factor in improving tensile ductility. Refinement of the Mg-Al-Mn-Fe precipitates and of α -Mg grain size was also observed at trace Y levels that was lost at high Y levels, leading to a decrease in mechanical properties. Y also modified the lattice constant of the $\text{Mg}_{17}\text{Al}_{12}$ in the Mg-6Al alloy.

The second stage of this research focused on the effect of Y on the intrinsic properties (i.e., the nature of the intermetallic such as but not limited to the elastic moduli, lattice constant, electron to atom ratio, bonding) of $Mg_{17}Al_{12}$. Y caused an increase in the elastic moduli and hardness and altered the lattice constant which decreases for low Y additions and increases with higher additions when the Al_4MgY precipitate forms. It was suggested that Y substitutes both Mg and Al sites showing a complex dependence on the electron-to-atom ratio (e/a). The intermetallic is off-stoichiometric and its e/a suggests that its thermodynamic stabilization is not through Hume-Rothery but through defect structure mechanisms. According to moduli that are determined in this study and first principles calculations reported, the $Mg_{17}Al_{12}$ phase is a ductile phase. Since Y lowers its ductility the role of Y in ductility enhancement is attributable to the morphological refinement of $Mg_{17}Al_{12}$ rather than the change in its intrinsic properties.

The third part of the study applied the knowledge obtained with Y to trace Er additions to Mg-6Al. Er (60-880 ppm) improved the mechanical properties by refining $Mg_{17}Al_{12}$ 56%-44%. Atom probe tomography showed that Er is soluble in $Mg_{17}Al_{12}$ and XRD proves that the lattice constant change. Non-equilibrium thermodynamic calculations indicate that 60 ppm Er, the Al_2Er phase co-precipitates with $Mg_{17}Al_{12}$ nucleating and refining $Mg_{17}Al_{12}$ but this co-precipitation and the refinement are lost at higher Er additions (880 ppm Er). The principles discovered in this study can be used in design novel alloys with trace additions of rare earths to Mg-6Al for vehicle weight reduction.

RÉSUMÉ

Le remplacement des pièces en acier et en aluminium par des alliages de magnésium (Mg) à faible densité a le potentiel de réduire significativement le poids des véhicules automobiles. Cette alternative permet d'économiser du carburant, de réduire les émissions de gaz à effet de serre (GES) ainsi que de promouvoir l'électrification des futures automobiles. En effet, environ 30% du poids du véhicule se trouve dans les pièces de la carrosserie, ce qui permettrait de potentiellement réduire le poids du véhicule de 10 à 20% en coulant ces pièces en Mg. Cette réduction se traduit également par une économie de carburant d'environ 7 à 15%, une réduction des émissions dans les voitures à essence en plus de permettre une augmentation de l'autonomie des véhicules électriques d'environ 15%.

Cette thèse de doctorat visait à améliorer la ductilité de l'alliage automobile Mg-6wt% Al (Mg-6Al) en affinant sa microstructure avec l'ajout de traces de terres rares (Y, Er). Les calculs thermodynamiques (FactSage - FTLite) ont aidé à déterminer le mécanisme de raffinement microstructural. Les microstructures ont été analysées par microscopie électronique et par sonde atomique tomographique, tandis que les effets sur la structure cristalline ont été déterminés par diffraction des rayons X. Les propriétés mécaniques ont pour leur part été déterminées avec des tests mécaniques conventionnels et avec des méthodes ultrasoniques plus compliquées.

La première section de cette étude s'est concentrée sur l'effet des ajouts de trace d'Y. Pour de telles teneurs d'Y, le précipité Al_4MgY co-nuclée avec le $\text{Mg}_{17}\text{Al}_{12}$, conduisant à un raffinement de 47%. Ce raffinement s'est avéré être le facteur clé dans l'amélioration de la ductilité en traction. Un raffinement des précipités de Mg-Al-Mn-Fe et des grains α -Mg a également été observé à des faibles traces d'Y, phénomène qui est perdu à des niveaux d'Y élevés, conduisant à une détérioration des propriétés mécaniques. L'Y a également modifié la constante de structure cristalline du $\text{Mg}_{17}\text{Al}_{12}$ dans l'alliage Mg-6Al.

La deuxième étape de cette recherche s'est concentrée sur l'effet de l'Y sur les propriétés intrinsèques du $Mg_{17}Al_{12}$. L'Y a provoqué une augmentation des modules d'élasticité et de la dureté et a modifié la constante de structure cristalline du matériau, qui diminue pour les faibles ajouts d'Y et augmente avec les ajouts plus élevés lors de la formation du précipité Al_4MgY . Il a été suggéré que l'Y substitue à la fois les sites du Mg et de l'Al, montrant une dépendance complexe du ratio électron-atome (e/a). L'intermétallique est non stoechiométrique et son e/a suggère que sa stabilisation thermodynamique ne se fait pas selon les règles d'Hume-Rothery mais par des mécanismes de défauts de structure. Selon les modules qui sont déterminés dans cette étude et les premiers principes des calculs rapportés, la phase $Mg_{17}Al_{12}$ est une phase ductile. Puisque l'Y diminue sa ductilité, le rôle de l'Y dans l'amélioration de la ductilité est attribuable au raffinement morphologique de $Mg_{17}Al_{12}$ plutôt qu'au changement de ses propriétés intrinsèques.

La troisième section de l'étude a appliqué les connaissances obtenues avec l'Y pour évaluer les ajouts de traces d'Er à l'alliage Mg-6Al. L'Er (60-880 ppm) a amélioré les propriétés mécaniques en raffinant l'alliage $Mg_{17}Al_{12}$ 56%-44%. Les analyses par sonde atomique tomographique ont montré que l'Er est soluble dans $Mg_{17}Al_{12}$ et l'analyse XRD prouve que la constante de structure cristalline est modifiée. Les calculs thermodynamiques hors équilibre indiquent qu'à une teneur de 60 ppm d'Er, la phase Al_2Er co-précipite avec $Mg_{17}Al_{12}$, promouvant ainsi la nucléation et le raffinage du $Mg_{17}Al_{12}$. Cette coprécipitation et ce raffinement sont perdus à des teneurs d'Er plus élevées. Les principes découverts dans cette étude peuvent être utilisés dans la conception de nouveaux alliages avec l'ajout de traces de terres rares au Mg-6Al pour réduire le poids des véhicules.

ACKNOWLEDGMENTS

There are many people that I would like to thank for their support during my PhD journey. First and foremost, I would like to thank my supervisor Prof. Pekguleryuz who introduced me in the amazing world of light alloys and especially in magnesium alloys. It was an honor for me that she taught me physical metallurgy and novel ways of thinking. She is always there to encourage me and support me in any decision I made. Thank you, Professor!

I am also grateful to my colleague Dr. Luis Angel Villegas Armenta for his invaluable support in all the aspects of the PhD life, personal and professional. I would also like to say a big thank to Dr. Amir Farkoosh who supported and guided me at the beginning of my PhD research. I would like to express my gratitude to Pierre Vermette for his invaluable experimental assistance and his technical tips. I am grateful to Dr. Florence Paray who was always supporting my research through her leading role in McGill Materials Characterization Labs.

I would also like to thank my colleagues for their support and friendship during my PhD journey; Karan Narang, Stéphanie Bessette, Dr. Evelin Barbosa de Melo, Brian Cook, Dr. Mert Celikin, Dr. Baoqi Guo, Dr. Maryam Golozar and Raul Arriaga Benitez. I am also grateful to Dr. Xue-Dong Liu and Weawkamol Leelapornpisit from the McGill Facility for Electron Microscopy Research, and Lang Shi and Dr. Longbo Yang from the Department of Earth and Planetary Sciences. I would like to say a big thank to my friend Andreas Katsaris for the scientific discussions and support. I am also grateful to Prof. Alireza Sadeghi and Dr. Brian Langelier for the scientific discussions, the experimental support and journal papers preparation.

A big thanks to all the technicians who supported me during my experimental work; Aleksandra Djuric, Robert Paquette, Monique Riendeau as well as all the personnel of the machine shop. I am also grateful to Barbara Hanley, Leslie Bernier, June Persaud, Diti Anastasopoulos, Heather Holowathy and Genevieve Snider for their continuous support on administrative issues.

I am grateful to my partner in life Christina Katsari for her never-ending support and love all these years. Thank you for being always there for me and making me a better person every day. I would also like to thank my family for their love and encouragement. I am grateful to my beloved parents Maria and Aristofanis, and my sister Christina for supporting me in all aspects of my life.

I would like to gratefully acknowledge McGill University and the Department of Mining and Materials Engineering for the financial support through MEDA, GREAT, Graduate Mobility and Graduate Excellence awards. I would also thank the Hellenic Scholarship Foundation for the Sam and Mary Charalambakis Family award as well as REGAL for the special prize during the ASM student night poster competition. I wish to acknowledge the Natural Sciences and Engineering Research Council of Canada (NSERC) for the financial support during my PhD research.

CONTRIBUTION OF AUTHORS

The current manuscript-based thesis consists of four manuscripts written by the candidate according to the guidelines of McGill Graduate and Postdoctoral Studies. All the manuscripts have been published or accepted for publication as indicated below:

Chapter 3: **Korgiopoulos, K.**, & Pekguleryuz, M. (2020). *The significant effect of trace yttrium level on the mechanical properties of cast Mg-6Al alloy through a refinement mechanism. **Materials Science and Engineering: A**, 775, 138966.*

Chapter 4: **Korgiopoulos, K.**, & Pekguleryuz, M. (2021). *The effect of Y on the microstructure and mechanical performance of an Mg-Al-Y casting alloy. **Experimental Results**, 2, E7. doi:10.1017/exp.2020.63.*

Chapter 5: **Korgiopoulos, K.**, Sadeghi, A., & Pekguleryuz, M. (2021). *Mg₁₇Al₁₂ intermetallic modified with yttrium additions **Intermetallics (in press).***

Chapter 6: **Korgiopoulos, K.**, Langelier, B., & Pekguleryuz, M. (2021). *Mg₁₇Al₁₂ Phase Refinement and the Improved Mechanical Performance of Mg-6Al alloy with trace Erbium Addition. **Materials Science and Engineering: A**, 141075.*

The candidate designed and performed the experimental and simulations work. All the manuscripts are co-authored by Prof. Pekguleryuz as the supervisor of the candidate who provided guidance throughout the research project. Prof. Sadeghi (School of Mechanical Engineering, University of Tehran) and his research group conducted the diffusion experiments for the chapter 5 and he also reviewed and provided helpful discussion for the chapter preparation. Dr. Langelier (Canadian Centre for Electron Microscopy, McMaster University) conducted the atom probe tomography experiments and the analysis of the data for the chapter 6. He also provided useful discussion and reviewed the chapter.

TABLE OF CONTENTS

CHAPTER 1	1
Introduction.....	1
1.1 Introduction.....	1
1.2 Research objectives.....	3
1.3 Thesis outline and chapters description	4
1.4 References.....	4
CHAPTER 2	7
Literature Review.....	7
2.1 Introduction.....	7
2.2 The inherent ductility of hexagonal close-packed metals and of magnesium	8
2.3 Crystal structure and plastic deformation behaviour of pure magnesium	9
2.3.1 Slip	9
2.3.2 Twinning.....	11
2.3.3 Strain hardening curve of Mg under tensile loading.....	13
2.3.4 Stacking Fault (SF).....	14
2.3.5 Effect of solutes on crystal structure and plastic deformation of Mg.....	16
2.3.6 Effect of solutes on axial ratio and twinning	18
2.3.7 Effect of solutes on stacking fault energy in magnesium	19
2.4 Ductility in Mg-Al casting alloys	21
2.4.1 Mg-Al based cast alloys (AM).....	21
2.4.2 Ductility improvement of Mg-Al based cast alloys.....	23
2.4.2.1 Modification of AM alloys with trace additions	23
2.4.2.2 Ductility of the α -Mg matrix	26
2.4.2.3 Role of dispersoid in tensile toughness	26
2.5 References.....	27
CHAPTER 3	40
The significant effect of trace Yttrium level on the mechanical properties of cast Mg-6Al alloy through a refinement mechanism.....	40
ABSTRACT.....	41
3.1 Introduction.....	41
3.2 Experimental Procedures	44
3.3 Results and Discussion	46

3.3.1	Mechanical Properties.....	46
3.3.2	Alloy Microstructures, Phase Selection and Mg ₁₇ Al ₁₂ Refinement.....	48
3.3.3	The Effect of Mg ₁₇ Al ₁₂ Refinement on Ductility	51
3.3.4	The Role of Y on Mg ₁₇ Al ₁₂ Refinement.....	52
3.3.4.1	Experimental Study	52
3.3.4.2	Thermodynamic Simulations.....	57
3.4	Conclusions.....	62
3.5	Acknowledgements.....	63
3.6	References.....	63
CHAPTER 4	70
	The effect of Y on the microstructure and mechanical performance of an Mg-Al-Y casting alloy	70
	ABSTRACT.....	71
4.1	Introduction.....	71
4.2	Objective.....	72
4.3	Methods.....	72
4.4	Results and Discussion	73
4.5	Conclusions.....	78
4.6	Funding Information and Acknowledgements.....	78
4.7	References.....	78
CHAPTER 5	81
	Mg ₁₇ Al ₁₂ intermetallic modified with Yttrium additions.....	81
	ABSTRACT.....	82
5.1	Introduction.....	82
5.2	Material and Methods	85
5.2.1	Synthesis	85
5.2.2	Thermodynamic calculations	86
5.2.3	Characterization	87
5.2.4	Mechanical Properties.....	87
5.2.5	Diffusion Couple.....	88
5.3	Results.....	88
5.3.1	Thermodynamic Calculations	88
5.3.2	Microstructural Investigation.....	90

<i>As-cast Intermetallics</i>	90
5.3.3 Crystal structure.....	94
5.3.4 Mechanical Properties.....	95
5.4 Discussion.....	96
5.5 Conclusions.....	101
5.6 Acknowledgements.....	101
5.7 References.....	102
CHAPTER 6	107
Mg ₁₇ Al ₁₂ Phase Refinement and the Improved	107
Mechanical Performance of Mg-6Al alloy	107
with trace Erbium Addition	107
ABSTRACT.....	108
6.1 Introduction.....	109
6.2 Experimental Procedures	111
6.3 Results.....	113
6.3.1 Mechanical Properties.....	113
6.3.2 Microstructural Investigation.....	114
6.3.2.1 Scanning Electron Microscopy.....	114
6.3.2.2 Atom Probe Tomography	117
6.4 Crystallographic Analysis.....	118
6.5 Thermodynamic Simulations	119
6.6 Discussion.....	122
6.6.1 Modification of β -Mg ₁₇ Al ₁₂ crystal structure	122
6.6.2 Microstructural Refinement	123
6.6.3 The Effect of Microstructural Refinement and the Modification of β -phase on the Mechanical Properties of Mg-6Al	124
6.7 Conclusions.....	126
6.8 Acknowledgements.....	127
6.9 References.....	128
CHAPTER 7	133
Concluding Discussion and Proposed Future Work	133
7.1 General Discussion	133

7.1.1	The Microstructural Refinement of the Mg-6Al alloy with Y and Er and the Mechanism of such Refinement.....	134
7.1.2	Modification of the intrinsic properties of β -Mg ₁₇ Al ₁₂	136
7.1.3	The Effect of Y and Er on the Tensile Properties of Mg-6Al.....	138
7.2	General conclusions	139
7.3	Strategies for Future Work.....	140
7.3.1	Scientific research objectives.....	140
7.3.2	Commercial development objectives	141
CHAPTER 8	142
	Contributions to Original Knowledge.....	142
8.1	Yttrium (Y) Alloying of Mg-6Al Alloy.....	142
8.2	Erbium addition in Mg-Al Alloy	143
8.3	Modification of Mg ₁₇ Al ₁₂ intrinsic properties	143
8.4	Commercial and Environmental Contribution.....	144
Appendix A	145
	Experimental Details and Sources of Error	145

LIST OF FIGURES

Fig. 1.1	Example of vehicle's door panel using Mg-Al-Mn based alloy (AM50) [11].	2
Fig. 2.1	The HCP structure of magnesium with (a) the basal, prismatic and pyramidal planes, (b) extension and contraction deformation twins [24] (reprinted/adapted by permission from [Springer Nature]:[Springer][Metallurgical and Materials Transactions A] by [J. F. Nie et al] [2020]).....	10
Fig. 2.2	Twinning shear versus axial ratio (twin mode is active at filled circles). Redrawn from [9,15]......	12
Fig. 2.3	Three stages of strain hardening in metallic single crystals. Redrawn from [20].	14
Fig. 2.4	(a) Calculated Mg-Al phase diagram with the structure of Mg ₁₇ Al ₁₂ using FactSage (FTlite database) [59]. The light blue area represents the Al range (wt%) of the commercial Mg-Al system. (b) BSE-SEM micrograph showing the as-cast microstructure of a commercial Mg-Al based alloy (AM60B) synthesized and cast at McGill.....	21
Fig. 2.5	(a) Effect of Al content on ultimate tensile strength, yield strength (0.2% offset) and elongation in AM series alloys. Redrawn from [35,63]......	22
Fig. 3.1	(a) Tensile and (b) compression stress-strain curves for the best performing samples. The best performing samples were considered to have the effects of casting defects removed... ..	47
Fig. 3.2	As-cast microstructures of (a) Mg-6Al, (b) Alloy 1, (c) Alloy 2, (d) Alloy 3.	48

Fig. 3.3 EDS mapping analysis in Alloy 2 (100ppmY). Alloy 3 (300ppmY) has similar microstructure.	49
Fig. 3.4 XRD diffraction peaks.....	53
Fig. 3.5 TEM investigation on Alloy 3 (300 ppmY) with Mg-Al-Y-Mn-Fe precipitate as per EDS (Cu signal is coming from the holder and Cl is impurity from the sample preparation) (a) Bright field (b) Dark field imaging.	55
Fig. 3.6 (a) SEM-BSE (Alloy 3) image showing the association of AlMgY particle with Mg ₁₇ Al ₁₂ . The yellow square dot line shows the area where the TEM cross section sample was extracted. (b) TEM bright field imaging. In red dot line is the AlMgY precipitate.	56
Fig. 3.7 HAADF image with the 3 elemental maps for Mg, Al and Y.....	56
Fig. 3.8 (a) HRTEM of the MgAlY/Mg ₁₇ Al ₁₂ interface with the corresponding FFT. The region where further analysis was conducted appears in the red dotted square. (b) Inverse FFT imaging of the interface. The area in the square depicts the interface and the yellow.	57
Fig. 3.9 Equilibrium isopleth for Mg-6Al-(0-0.1) Y showing the solidification path for alloys 1, 2, 3 (round dot vertical lines).....	58
Fig. 3.10 Equilibrium phase diagram of Mg-Al-Y with 0.03wt%Y showing the aluminum range of Al ₄ MgY and Mg ₁₇ Al ₁₂ (~ 43-45 wt% Al).....	59
Fig. 3.11 Non-equilibrium calculations with (a) 0ppmY, (b) 0.1ppmY, (c) 5ppmY, (d) 300ppmY. The wt% in the parentheses present the amount of each precipitate in the end of solidification.	61
Fig. 4.1 SEM/BSE as-cast microstructure of Mg-6Al-0.3Y and EDS maps. The red square shows the close associations of Y enriched precipitates with Mg ₁₇ Al ₁₂	74
Fig. 4.2 Mg-Al-0.3Y alloy after matrix extraction. The red circles show the Al ₂ Y associated with the Mg ₁₇ Al ₁₂ phase.....	74
Fig. 4.3 XRD results (a) Bulk alloy, (b) after matrix extraction.	75
Fig. 5.1 (a) Crystal structure of Mg ₁₇ Al ₁₂ , (b) Substitution example of Mg(I) atoms with La and Al atoms with Zn according to reference [10].	84
Fig. 5.2 Mg-Al-Y Pseudo Binary Equilibrium phase diagrams, containing (a) 300 ppm and (b) 5000 ppm Y.....	89
Fig. 5.3 Schematic drawing indicating the crystallization difference of the two intermetallic containing 300 and 5000 ppm Y.....	89
Fig. 5.4 BSE/SEM microstructures of the studied intermetallics (a) β, (b) β _{300Y} and (c) β _{5000Y} . .	90
Fig. 5.5 Microstructure of the β _{5000Y} (a) BSE image and (b) EDS mapping of the respective region of a.	91
Fig. 5.6 Mg-Al-Y isotherm at (a) 450 °C and (b) at 25 °C with the terminal compositions shown with the dashed line. The diffusion path is shown with the solid line 1-2-3.	93
Fig. 5.7 Interface of the Mg ₁₇ Al ₁₂ /Y diffusion couple. (a-c) BSE micrographs at consecutive magnifications of squared and labeled regions, (d) EDS elements distribution map of c.	93
Fig. 5.8 (a) Profile of Mg, Al and Y distribution at the interface of Mg ₁₇ Al ₁₂ /Y, (b) EDS of Y rich precipitates on the Mg ₁₇ Al ₁₂ /Y interface.	94
Fig. 5.9 XRD patterns of the three samples.....	95
Fig. 5.10 Effect of (a) yttrium and (b) aluminum on the lattice parameter and e/a of the β-phase.	98

Fig. 5.11 Correlation between the lattice parameter and e/a of the β -phase.....	99
Fig. 6.1 SEM/BSE micrographs of as cast alloys (a) Mg-6Al, (b) Alloy 1 (60ppm Er), (c) Alloy 2 (880ppmEr), (d) Higher magnification of Alloy 2 showing the association between Er enriched phase and $Mg_{17}Al_{12}$	116
Fig. 6.2 EDS map analysis showing co-precipitated Er-enriched precipitates and $Mg_{17}Al_{12}$ in Alloy 2.	116
Fig. 6.3 APT plot of Mg and Al inside $Mg_{17}Al_{12}$ of Alloy 1 (60 ppm Er).	118
Fig. 6.4 Er peaks (pink) in α -Mg and $Mg_{17}Al_{12}$ of Alloy 1 (60 ppm Er).....	118
Fig. 6.5 XRD diffraction peaks of the 3 alloys.....	119
Fig. 6.6 (a) Phase diagram of Mg-(0-60) wt%Al-60 ppm Er. (b) Equilibrium isopleth for Mg-6wt% Al with different Er levels. The red lines show the solidification path for Alloy 1 (60 ppm Er) and Alloy 2 (880 ppm Er).	120
Fig. 6.7 Scheil cooling of Mg-6Al-Er (a)60ppmEr, (b)880ppmEr.....	121

LIST OF TABLES

Table 2.1 Correlation between elastic properties and ductility* of HCP metals [9] (reprinted/adapted by permission from [Springer Nature]: [Springer] [Metallurgical Transactions, A] by [M. H. Yoo] [1981]).	9
Table 2.2 Slip systems in magnesium [19] and the critical resolved shear stress for different deformation mechanisms in magnesium [25–27].	11
Table 2.3 Basal and prismatic CRSS and c/a for HCP Metals (25°C) [19,28,29].	11
Table 2.4 SFE values of common metals [38].	15
Table 2.5 Experimental estimated SFE of Mg[39].	15
Table 2.6 Calculated SFE for Mg and binary Mg alloys by DFT (values are in mJ/m ²) [39]. Reference of values from a: [52], b:[53], c:[54], d:[55], e:[56], f:[57], g:[41], h:[58], i:[59], j:[60], k:[61].	20
Table 2.7 Elements that change SFE [39].	20
Table 3.1 Studies on the Refinement of the $Mg_{17}Al_{12}$ Phase in Mg-Al Alloys.	43
Table 3.2 Chemical composition of the alloys.	45
Table 3.3 Room temperature average tensile properties.	47
Table 3.4 Room temperature average compression properties.	47
Table 3.5 Phases in the Alloys as determined via SEM/EDS.	48
Table 3.6 Effect of Y addition on the size and area fraction of second phases.....	50
Table 3.7 Average lattice parameter of $Mg_{17}Al_{12}$ after XRD pattern refinement.....	53
Table 3.8 Phases observed in FIB and TEM analysis.	54
Table 4.1 EDS on the precipitates after matrix extraction.	75
Table 4.2 Precipitates size and α -Mg grain size as measured with ImageJ.	76
Table 4.3 Tensile properties of as cast samples at room temperature.	77
Table 4.4 Compression properties of as cast samples at room temperature.	77
Table 4.5 Equilibrium and non-equilibrium (Scheil) thermodynamic calculations.....	77

Table 5.1 Compositions of the Intermetallics (ICP).	86
Table 5.2 EPMA/WDS chemical analysis of the matrix (solid solution).	91
Table 5.3 EPMA/WDS chemical analysis of the Y enriched precipitates in β_{5000Y}	91
Table 5.4 Lattice parameter as per XRD results.	95
Table 5.5 Microhardness and measured moduli values of the three intermetallic samples.	96
Table 5.6 Radii and Valence of Elements [37]	97
Table 5.7 Lattice parameter as per XRD results and calculated e/a ratio.	97
Table 6.1 Chemical composition of the alloys using ICP.	112
Table 6.2 Mechanical properties of the as cast samples at room temperature.	114
Table 6.3 Effect of Er addition on the size and morphology of second phases.	115
Table 6.4 Composition of α -Mg matrix and $Mg_{17}Al_{12}$ of Alloy 1 (60 ppm Er).....	117
Table 6.5 Average lattice parameter of β - $Mg_{17}Al_{12}$ after Rietveld refinement.....	119
Table 6.6 Formation temperature and amount of each phase predicted by Scheil cooling.....	122
Table 7.1 Summary of the investigated alloys and their main characteristics.	139

CHAPTER 1

Introduction

1.1 Introduction

Within the last decades, the governments have been making efforts to reduce greenhouse gases (e.g. CO₂) which are responsible for the climate change. Automotive industry is one of the largest sources of CO₂ emissions globally. A typical passenger vehicle emits approximately 4.6 metric tons of CO₂ annually [1]. Reducing the weight of vehicles constitutes a viable solution to this problem and it also can help to increase fuel economy [2]. Ten percent saving in vehicle's weight leads to 6-8% fuel economy improvement [3]. Considering that 1L of gasoline produces about 2.3 kg of CO₂ and an average Canadian car burns 2000 L of gasoline annually (4600 kg of CO₂) [4], 160L of fuel per year (368 kg of CO₂) can be saved per 10% weight reduction. Lightweight materials such as magnesium (Mg) alloys have the potential to reduce the weight of some vehicle's components by 75% and vehicle's chassis by up to 50% increasing the fuel efficiency. Particularly, this is important for electric vehicles which are equipped with advanced electronics, safety sensors and navigation systems which increase the vehicle's weight [3,5]. Twenty percent weight reduction translates to 14% range increase (i.e., of electric vehicles) due to the lower energy consumption [6]. However, the weight is not the only consideration as the car components should meet the safety standards, adequate mechanical properties and being cost effective [3].

Mg alloys can be grouped as cast and wrought alloys which are largely based either on the Mg-Al or on the Mg-rare earth (RE) systems. Mg-RE based alloys have been traditionally

developed for aerospace use [7]. Mg-Al based alloys are used in consumer products or automotive applications as non-structural components such as covers, housings and brackets or as structural components such as steering wheel armatures, instrument panel beams and seat structures [8,9]. There is a current interest in using Mg-Al casting alloys for structural car-body applications such as front-end carrier, pillars and door panels. Such usage requires improved ductility and crashworthiness which cannot be met by the current commercial Mg-Al-Mn (AM) alloys. Crashworthiness is the ability of the material to absorb energy and to deform plastically before fracture. When translated to material property requirements crashworthiness can be assessed mainly by the tensile ductility, tensile toughness and impact resistance [10]. Since the automotive industry is cost sensitive, replacing the Mg-Al alloys with the costly Mg-RE aerospace alloys is not a viable option. However, trace additions of RE alloying elements to the Mg-Al alloys is acceptable. The main question that is the driving force for this research is “Can we improve the ductility and toughness of the AM60 casting alloy while maintaining its strength, corrosion, castability and the cost range via alloy modification?” This requires a systematic study of the parameters influencing the ductility of Mg in general and of the Mg-Al alloys specifically.

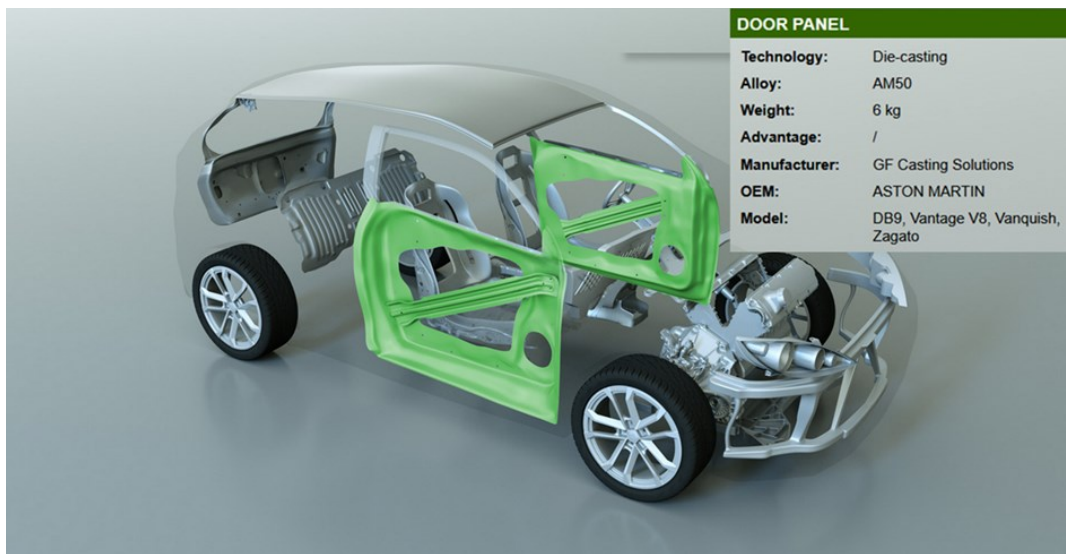


Fig. 1.1 Example of vehicle's door panel using Mg-Al-Mn based alloy (AM50) [11].

The factors that influence ductility range from crystal structure (lattice parameters, axial ratio), elastic properties (shear modulus, G , bulk modulus, B , surface energy, Γ_{sv}) to microstructure (grain size, second phases) and their effects on plastic deformation (slip, twinning, strain hardening) [12–17].

1.2 Research objectives

The long-term objective of this research is to develop a cast Mg-6wt%Al based alloy (AM60) with improved ductility without compromising the strength at room temperature. It is hypothesized that the addition of trace (ppm level) rare earth elements such as Y and Er will modify the main second phase i.e., β -Mg₁₇Al₁₂, without forming new phases. A similar effect has been observed before in Al-Si based alloys where ppm additions have successfully modified the eutectic silicon phase improving dramatically the mechanical properties [18–20]. The main objectives can be summarized as follow:

- a. Investigate the effect of trace Y addition in the Mg-6wt%Al based alloy using mechanical testing, microstructural investigation techniques and thermodynamic calculations to better understand the mechanism of microstructure refinement
- b. Study the modification of Mg₁₇Al₁₂ intrinsic properties (i.e., the nature of the intermetallic such as but not limited to the elastic moduli, lattice constant, electron to atom ratio, bonding) after adding trace Y additions to elaborate the mechanism of its modification in Mg-Al alloys.
- c. Investigate the effect of other trace alloying additions (i.e., Er) on the modification of Mg₁₇Al₁₂ phase and α -Mg.

1.3 Thesis outline and chapters description

This is a manuscript-based PhD thesis which presents the research work on the development of high ductility Mg-Al alloys through second phases modification. It comprises 8 chapters including the current introduction (Chapter 1). Chapter 2 includes the literature review on the potential mechanisms that can be employed to improve the ductility of Mg alloys with a summary of the research progress up to date. Chapter 3 presents the positive effect of trace Y additions on the mechanical properties of the binary Mg-6%Al through the refinement of β -Mg₁₇Al₁₂ and its underlying mechanism. Chapter 4 discusses the effect of higher Y addition on the mechanical properties of Mg-6%Al alloy reinforcing the concept that trace Y addition is better in refining the microstructure of these alloys. Chapter 5 focuses on the effect of Y on the intrinsic properties of Mg₁₇Al₁₂ intermetallic using different experimental and theoretical techniques. Chapter 6 evaluates the effect of trace Er addition on the modification of β phase and the result on the mechanical properties of Mg-Al-Er alloys. The main conclusions and the future work are presented in Chapter 7 and contributions to original knowledge are stated in Chapter 8.

1.4 References

- [1] Greenhouse Gas Emissions from a Typical Passenger Vehicle, (n.d).
[https://www.epa.gov/greenvehicles/greenhouse-gas-emissions-typical-passenger-vehicle#:~:text=typical passenger vehicle%3F-,A typical passenger vehicle emits about 4.6 metric tons of,around 11%2C500 miles per year.](https://www.epa.gov/greenvehicles/greenhouse-gas-emissions-typical-passenger-vehicle#:~:text=typical%3F-,A%20typical%20passenger%20vehicle%20emits%20about%204.6%20metric%20tons%20of%20around%2011%20C500%20miles%20per%20year.) (accessed October 5, 2020).
- [2] S. Kulkarni, D.J. Edwards, E.A. Parn, C. Chapman, C.O. Aigbavboa, R. Cornish, Evaluation of vehicle lightweighting to reduce greenhouse gas emissions with focus on magnesium substitution, J. Eng. Des. Technol. (2018).
- [3] Shannon Brescher Shea, 54.5 MPG and Beyond: Materials Lighten the Load for Fuel

- Economy, (2012). <https://www.energy.gov/articles/545-mpg-and-beyond-materials-lighten-load-fuel-economy> (accessed October 5, 2020).
- [4] N.R. Canada, Learn the facts: Fuel consumption and CO₂, 2014. (n.d). https://www.nrcan.gc.ca/sites/www.nrcan.gc.ca/files/oeef/pdf/transportation/fuel-efficient-technologies/autosmart_factsheet_6_e.pdf (accessed October 5, 2020).
- [5] P. Gao, R. Hensley, A. Zielke, A road map to the future for the auto industry, McKinsey Quarterly, Oct. (2014).
- [6] M. Bull, Mass Reduction Performance of PEV and PHEV Vehicles, in: Proc. 22nd Int. Tech. Conf. Enhanc. Saf. Veh., National Highway Traffic Safety Administration Washington, DC, 2011.
- [7] M. Pekguleryuz, Alloying behavior of magnesium and alloy design, Fundam. Magnes. Alloy Metall. (2013) 152–196.
- [8] P.K. Mallick, Advanced materials for automotive applications: An overview, in: Adv. Mater. Automot. Eng., Elsevier, 2012: pp. 5–27.
- [9] M. Avedesian, H. Baker, ASM specialty handbook: magnesium and magnesium alloys., ASM International, Ohio, 1998.
- [10] W.D. Callister, Materials science and engineering an introduction, John Wiley, 2007.
- [11] Magnesium Automotive Applications Demonstrator, (2020). <https://www.intlimg.org/page/3d-demonstrator-2020> (accessed October 5, 2020).
- [12] D. Shin, C. Wolverton, The effect of native point defect thermodynamics on off-stoichiometry in β -Mg₁₇Al₁₂, Acta Mater. 60 (2012) 5135–5142.

- [13] A.M.B. Correa, Effect of Solute Elements on the Lattice Parameters of Magnesium, ProQuest, 2008.
- [14] Z. Yu, A. Tang, Q. Wang, Z. Gao, J. He, J. She, K. Song, F. Pan, High strength and superior ductility of an ultra-fine grained magnesium–manganese alloy, *Mater. Sci. Eng. A.* 648 (2015) 202–207.
- [15] A. Becerra, M. Pekguleryuz, Effects of lithium, indium, and zinc on the lattice parameters of magnesium, *J. Mater. Res.* 23 (2008) 3379–3386.
- [16] M. Pekguleryuz, M. Celikin, M. Hoseini, A. Becerra, L. Mackenzie, Study on edge cracking and texture evolution during 150 C rolling of magnesium alloys: the effects of axial ratio and grain size, *J. Alloys Compd.* 510 (2012) 15–25.
- [17] N. Wang, W.-Y. Yu, B.-Y. Tang, L.-M. Peng, W.-J. Ding, Structural and mechanical properties of Mg₁₇Al₁₂ and Mg₂₄Y₅ from first-principles calculations, *J. Phys. D. Appl. Phys.* 41 (2008) 195408. doi:10.1088/0022-3727/41/19/195408.
- [18] A. Knuutinen, K. Nogita, S.D. McDonald, A.K. Dahle, Modification of Al–Si alloys with Ba, Ca, Y and Yb, *J. Light Met.* 1 (2001) 229–240.
- [19] S.C. Flood, J.D. Hunt, Modification of Al–Si eutectic alloys with Na, *Met. Sci.* 15 (1981) 287–294.
- [20] A.K.P. Rao, K. Das, B.S. Murty, M. Chakraborty, On the modification and segregation behavior of Sb in Al–7Si alloy during solidification, *Mater. Lett.* 62 (2008) 2013–2016.

CHAPTER 2

Literature Review

2.1 Introduction

Fuel economy and greenhouse emission control can be achieved by reducing the vehicle's weight. Steel is the main material, which is widely used to manufacture cars, but its high density (7.9 g/cm^3) cannot satisfy the strategy of weight reduction. Light metals with lower densities such as magnesium (1.8 g/cm^3), aluminum (2.7 g/cm^3) and titanium (4.4 g/cm^3) could be proper candidates for weight reduction[1]. However, the price of titanium ($\sim \$ 4.2/\text{lb}$) [2] is 17 times higher than that of steel ($\sim \$0.24/\text{lb}$)[3] rendering it a very expensive material for automotive manufacturers. Aluminum is the predominant candidate during the automotive material selection to replace steel with a lower cost ($\sim \$1/\text{lb}$) [2] than titanium. Despite this, only the use of magnesium (Mg) can further decrease the weight of a vehicle due to its lower density and higher specific strength [4] even though it is more expensive ($\$2.35/\text{lb}$)[2]. New promising technologies for magnesium production could decrease its price to $\$0.64/\text{lb}$ - $\$1.09/\text{lb}$ helping to expand its application to automotive industry [5]. However, the ductility and strength of magnesium alloys should be enhanced before their widely use as structural components [6].

This literature review focuses on the fundamentals of the following points:

1. The inherent ductility of hexagonal close-packed metals in general and of Mg specifically.
2. Special considerations with respect to the ductility of cast Mg-Al alloys used in automotive applications.

3. The factors that can influence and potentially improve the ductility and toughness of Mg-Al alloys.

4. Research conducted to improve the ductility of Mg-Al alloys.

2.2 The inherent ductility of hexagonal close-packed metals and of magnesium

Ductility of engineering alloys is a function of microstructure and loading conditions as well as the inherent ductility of the matrix crystals. While the microstructure can be modified by changing the process parameters, the inherent ductility of single crystals only depends on the chemistry (electronic structure). Pugh [7] introduced the quotient of elastic bulk modulus to shear modulus, B/G , as a measure of the inherent malleability of a pure metal. High value of B/G indicates a malleable metal contrary to a low B/G value which relates to brittleness. Malleability is associated with ductility [8]. The B/G ratio for HCP metals was obtained from the values of elastic constants at room temperatures [9]. Table 2.1 shows a good correlation between this ratio and the relative ductility values. In another study by Rice and Thomson[10] it was shown that crystals with wide dislocation cores and small Ga/Γ_{sv} values (< 7.5 to 10) are ductile; contrarily brittleness is promoted when the dislocations' cores are narrow and the Ga/Γ_{sv} value is large. Here Γ_{sv} is the surface energy and a is the lattice constant. Easier plastic flow at the crack tip can occur when dislocations have larger core width as they are more mobile. The generation of dislocations in the vicinity of crack tips determines the ductile vs brittle behavior of metals [11]. A blunt crack propagates slower and requires larger loads to induce dislocation emission [12]. According to the Ga/Γ_{sv} criterion, Be is still the most brittle metal and Ti and Zr the most ductile. Mg has fair ductility with a B/G of 2.03 and Ga/Γ_{sv} of 8.10 [9]. It is noted in Table 2.1 that the good ductility in general is related to axial ratio c/a in the range of 1.571 to 1.599 (Hf, Ti, Zr, Tl) with some

exceptions (Sc, Ru, Os). It seems that both crystal structure (c/a), elastic constants and microstructural factors govern ductility in hexagonal metals.

Table 2.1 Correlation between elastic properties and ductility* of HCP metals [9] (reprinted/adapted by permission from [Springer Nature]: [Springer] [Metallurgical Transactions, A] by [M. H. Yoo] [1981]).

Metal	c/a	B/G	Ductility	Ga/ Γ sv
Cd	1.886	2.21	Fair	10.24
Zn	1.856	1.73	Poor	11.73
Mg	1.624	2.03	Fair	8.10
Co	1.623	2.31	Fair	9.27
Re	1.615	2.05	Fair	15.73
Tl	1.599	6.52	Good	-
Zr	1.593	2.65	Good	6.90
Sc	1.592	1.94	Poor [13]	9.27
Ti	1.588	2.47	Good	7.31
Ru	1.583	1.63	Poor	19.45
Hf	1.571	1.95	Good	9.16
Os	1.579	1.64 [14]	Poor	-
Y	1.572	1.63	Fair	11.59
Be	1.568	0.74	Poor	26.12

* poor ductility = elongation < 15% and good ductility = elongation > 40

2.3 Crystal structure and plastic deformation behaviour of pure magnesium

2.3.1 Slip

Magnesium has HCP crystal structure (...ABABAB... stacking of atoms) with $c/a = 1.624$ (ideal $c/a = 1.633$) [15]. The basic slip in Mg is the basal slip (0001) due to the low c/a ratio which leads to lower critical resolved shear stress (CRSS) on the basal plane at room temperature but it provides only two independent slip systems [16]. Other slip systems are activated at higher stresses or at higher temperatures (Fig. 2.1, Table 2.2 & 2.3) [17,18]. Within the HCP metals, the slip behavior (Table 2.3) at room temperature is related to the axial ratio (c/a) due to the change in the critical resolved shear stress (CRSS) with c/a , on the basal plane. The CRSS for basal slip increases as c/a decreases (eg. Ti) and other slip systems such as prismatic and/or pyramidal are activated to accommodate the slip. The CRSS on the basal plane for Mg is low because of its relatively higher

c/a ratio (1.624 at 25 °C). The c/a ratio decrease (either 0001 planes decrease, or $10\bar{1}0$ planes increase) results to increase of the interplanar distance d and thus the shear stress required to move dislocations becomes lower. This relationship is described by Peierls-Nabarro stress, $\tau = P \cdot e^{-2\pi d/b(1-\mu)}$ where P is a factor depending on G (shear modulus), and μ (Poisson's ratio); b stands for the Burger's vector; and d is the interplanar distance [19,20]. Furthermore, Taylor [21] following Von Mises [22] formulated that five independent slip systems are required for homogenous deformation of polycrystalline metals. Groves and Kelly [23] analyzed the independent modes of possible HCP slip systems (Fig. 2.1) with a , and $c + a$, dislocations (Table 2.2). Slip system with $c + a$ Burgers vectors alone provides five independent modes sufficient to fulfill von Mises criterion.

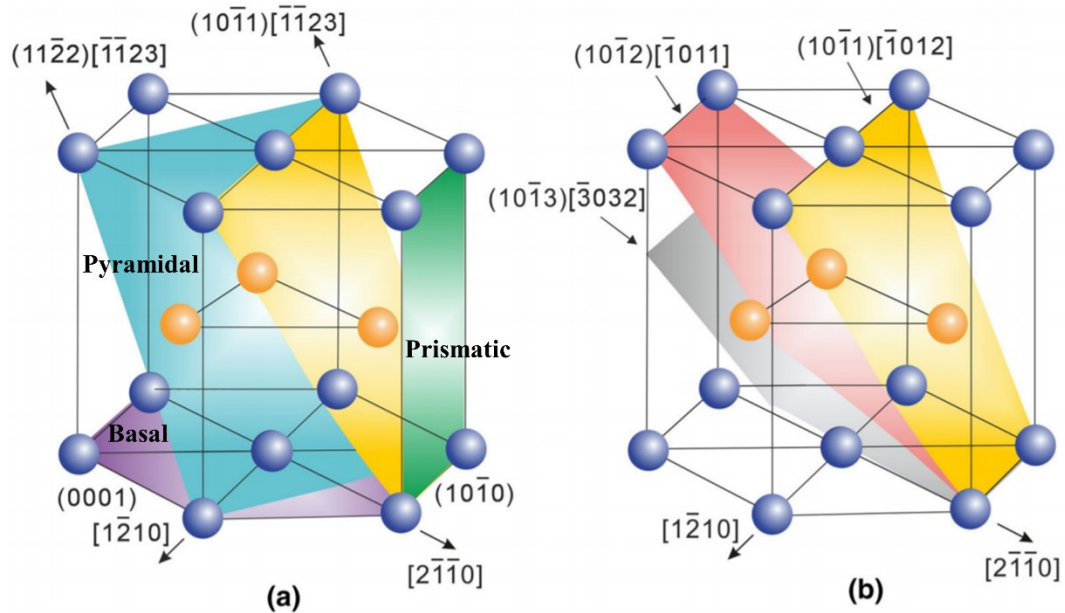


Fig. 2.1 The HCP structure of magnesium with (a) the basal, prismatic and pyramidal planes, (b) extension and contraction deformation twins [24] (reprinted/adapted by permission from [Springer Nature]:[Springer][Metallurgical and Materials Transactions A] by [J. F. Nie et al] [2020]).

Table 2.2 Slip systems in magnesium [19] and the critical resolved shear stress for different deformation mechanisms in magnesium [25–27].

Slip system	Slip plane and direction	Independent systems	Deformation mechanism	CRSS (MPa)
Basal (α)	$\{0001\}\langle 11\bar{2}0\rangle$	2	Basal slip	0.45-0.81
Prismatic (α)	$\{10\bar{1}0\}\langle 11\bar{2}0\rangle$	2	Prismatic $\langle a \rangle$ slip	~39.2
Pyramidal type II ($c + \alpha$)	$\{11\bar{2}2\}\langle 11\bar{2}3\rangle$	5	Pyramidal $\langle a + c \rangle$ slip	45-81
Pyramidal type I (α)	$\{10\bar{1}1\}\langle 11\bar{2}0\rangle$	4		
Twins		0-5	Extension twinning Contraction twinning	2-3 76-153

Table 2.3 Basal and prismatic CRSS and c/a for HCP Metals (25°C) [19,28,29].

Metal	c/a	Basal CRSS (MPa) $\{0001\}\langle 11\bar{2}0\rangle$	Prismatic CRSS (MPa) $\{10\bar{1}0\}\langle 11\bar{2}0\rangle$
Cd	1.886	0.57	-
Mg	1.624	0.43	39.2
Zn	1.856	0.4	6-15
Ti	1.588	110	48.95

2.3.2 Twinning

Twinning is the other deformation mechanism in Mg, and it compensates for the limited slip systems at room temperature. It is known that the twinning shear is related to the axial ratio in HCP crystals [15,30,31] as presented in Fig.2.2 [9]. Tension twins (extension along c-axis) show negative slopes and compression twins (contraction towards c-axis) show positive slope (Fig. 2.2). Additionally, the twinning mode of $\{10\bar{1}2\}\langle \bar{1}011\rangle$ changes from tension to compression for axial ratio of $\sqrt{3}$. Thus, metals with c/a ratio less than 1.73 (Be, Ti, Zr, Re, Mg) present extension twins and those with c/a more than 1.73 (Zn, Cd) present contraction twins [15]. Generally, the frequency of specific twinning mode occurrence depends on the value of twinning shear according to Fig. 2.2 and experiments in which the axial ratio changes by alloying (i.e., lower the shear value, higher the frequency). Other factors that affect the twinning mode are the ease of atomic shuffling and

gliding. Thus, metals such as Re, Zr and Ti exhibit high ductility as they profusely twin in both tensile and compressive modes. However, brittle metals such as Be and Zn twin only by $\{10\bar{1}2\}$ tension twin [9].

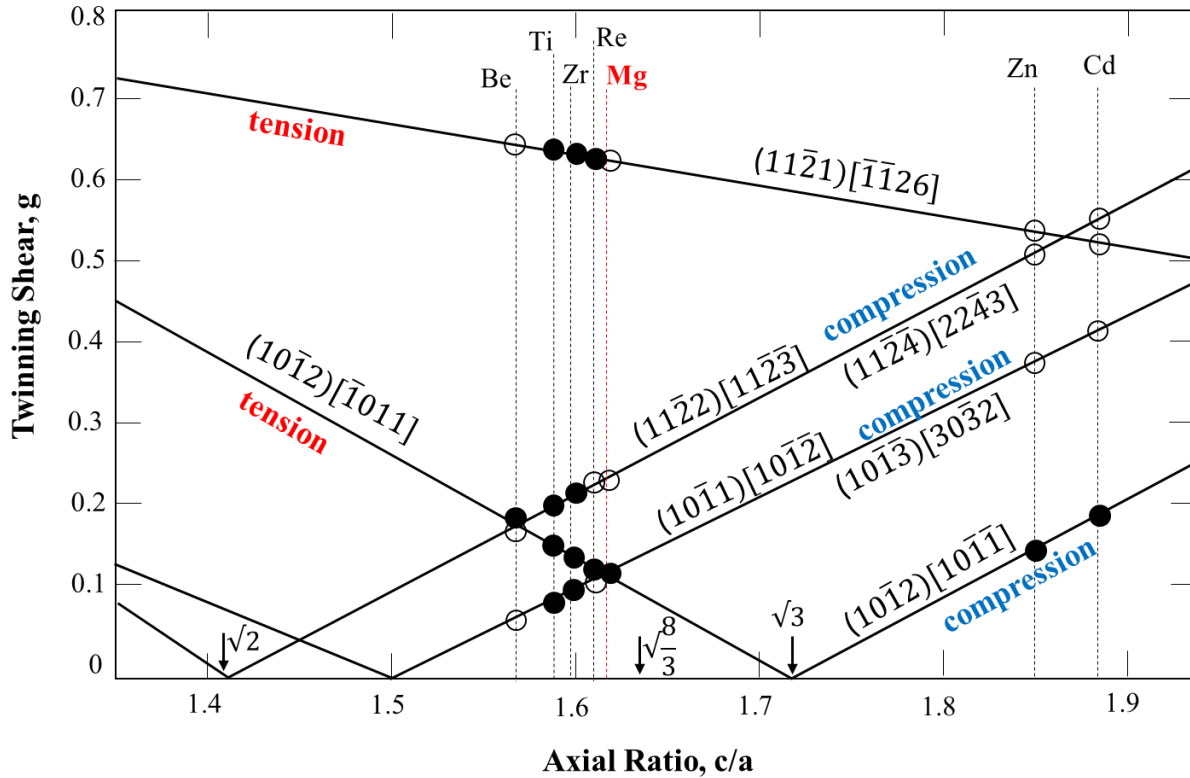


Fig. 2.2 Twinning shear versus axial ratio (twin mode is active at filled circles). Redrawn from [9,15].

During homogeneous straining of a polycrystalline material, the internal stress of some grains can be tensile and for some others can be compressive along c-axis. A single twin system can provide zero to five independent modes (Table 2.2) where the latter is assured in the case that both tension and compression twins are active, provided that the local stress state is favorable [9]. The ductility of HCP metals that undergo twinning is affected by the slip-twin interactions: the twin boundaries act as sinks for gliding dislocations then the metal may exhibit higher ductility. However, if the dislocations pile-up at the interface of twin boundaries, crack nucleation occurs. Pure Mg with c/a

=1.624 exhibits the usual $\{10\bar{1}2\}$ tension twins. In Mg, edge cracking occurs due to the pile-up of basal dislocations which are repelled by $\{10\bar{1}2\}$ tension twins [9]. One possible way to improve the ductility of Mg is by reducing the frequency of tension twinning by altering the c/a ratio.

2.3.3 Strain hardening curve of Mg under tensile loading

Single crystal: Crystal structure and SFE largely determine the three stages of dislocation activity in metallic single crystals (Fig.2.3) [20]. Stage I is easy glide (dislocation glide on a single slip system) and is characterized by a slow rate of strain hardening. This stage is governed by the crystal structure and the number of slip systems; it is seen in metals such as the HCP Mg with limited slip systems[32]. FCC and BCC metals which have high number of slip systems activated from the beginning of the plastic deformation and do not show Stage I easy glide [33]. In Stage II (dislocation pile-up stage) dislocation pile-up at obstacles causes high back stress; the stress to push dislocations increases resulting in a high rate of strain hardening. This stage is governed by stacking fault energy (SFE); FCC metal aluminum (Al) with high SFE and narrow stacking faults (SF) can exhibit easy cross slip of partial dislocations and prevent dislocation pile-up; they do not show Stage II behavior. Copper, on the other hand, also FCC but with low SFE and wide SF, cannot easily cross slip its partial dislocations and its stress-strain curve is characterized by Stage II and high rate of strain hardening. Stage II dislocation pile-up stage which leads to early crack initiation is detrimental to ductility and tensile toughness. Stage III involves dislocation-intersection activity which creates jogs that slow down dislocation mobility (dynamical recovery). This stage strongly depends on temperature. Strain hardening rate here decreases with increasing strain. BCC metals and FCC Al (high SFE and narrow SF) can cross slip their extended dislocation and their strain hardening curve is dominated by Stage III [11,20].

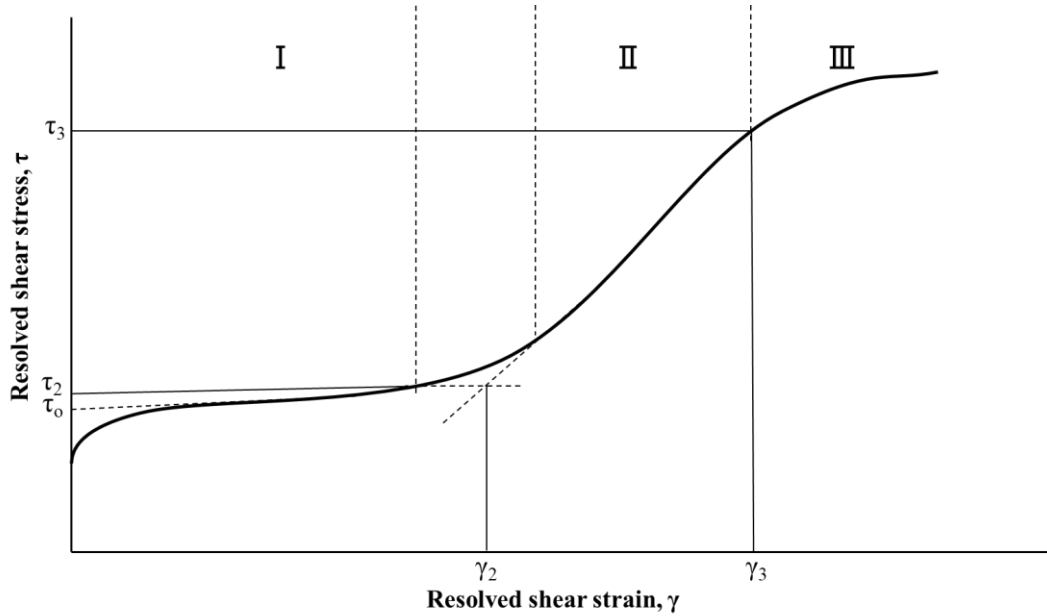


Fig. 2.3 Three stages of strain hardening in metallic single crystals. Redrawn from [20].

Polycrystalline Mg: Polycrystalline metals usually do not exhibit Stage I behavior because easy glide does not occur due the differing crystal orientations of the grains. Recent research [34,35] has shown that coarse-grained polycrystalline Mg does exhibit easy glide and Stage I behavior. The strain hardening exponent, n , in the Hollomon equation $\sigma_t = K\varepsilon_t^n$ where K =stress coefficient; σ_t =true stress, and ε_t =true strain, is largely determined by the type of strain hardening the metal exhibits. With a low value of $n \sim 0.16$ for the polycrystalline Mg, the tensile toughness (energy absorption during plastic deformation) which is determined by the area under the $\sigma_t - \varepsilon_t$ curve can be low [8]. Fine grained Mg would not show Stage I easy glide; and its Stage II behavior would be governed by its ability to cross slip (SFE), twinning and non-basal slip activation.

2.3.4 Stacking Fault (SF)

Stacking faults are planar defects in the crystal structure of close-packed structures stemming from the introduction or removal of atomic layers. These faults carry energy per unit area called the stacking fault energy (SFE) which influences the plastic deformation of metals. The SF is created

by the faults in the ABAB stacking of the HCP crystal structure on the basal plane. The SF can form during slip from the creation of partial dislocations through dissociation reactions. The partial dislocations having the same sign repel each other and additional rows of atoms can add to the SF pushing the partials apart and increasing the SF width. The energy of the SF governs the width of the fault [11]. High SFE metals such as Al (Table 2.4) have narrow SFs and the two partials with the fault in between (called an extended dislocation) [11] can slip and cross slip through, but the process is thermally, or stress activated as it requires vacancy creation or atom reshuffling to cause the dislocation reactions needed. Metals with low SFE such as Mg, Cu, Ag and stainless steel have wide faults and the ability of the dislocations to cross slip the partials is limited [36]. Experimental estimates of SFE for Mg differ widely ranging from 50mJ/m² to 280mJ/m² [37].

Table 2.4 SFE values of common metals [38].

Metal	SFE (mJ/m²)
cobalt	15
stainless steel 304	21
silver	22
gold	45
copper	78
nickel	128
aluminum	166

Table 2.5 Experimental estimated SFE of Mg[39].

Basal Stacking Fault	SFE (mJ/m²)
Experimental	50-280
<i>DFT calculations</i>	
Growth fault intrinsic, I ₁	16-30
Extrinsic fault, E	53-90
Deformation fault, I ₂	33-60
Twin-like fault, T ₂	38-60

Recently, density functional theory (DFT) calculations have been used to estimate SFE for Mg as shown in Table 2.5 [39]. DFT calculations distinguish between stable and unstable SFs. The SFE evolves during slip deformation from stable SFE to unstable SFE. Vitek [40] introduced the terminology of generalized stacking fault energy (GSFE) to describe the evolution of stacking faults during slip. The difference of two supercells can be used to describe the GSFE where the stable position is described by a burger vector $b=0$ and the unstable position by $b\neq 0$.

The stable SFE was calculated to be 36mJ/m^2 by Smith and the GSFE in slip was calculated to range between 86 mJ/m^2 (unstable growth and deformation faults) and 181mJ/m^2 (unstable twin-like faults) [39]. Hence, the stable and unstable stacking faults have a low SFE (GSFE) in Mg (i.e., the faults are wide; only the twin-like fault evolves into a narrower fault with higher SFE during slip). Recently, the role of SFE in the activation of non-basal slip was suggested by Sandlobes et al[41] . It is possible to change the SFE via solute additions; this will be treated in a subsequent section.

2.3.5 Effect of solutes on crystal structure and plastic deformation of Mg

Solute atoms can affect the plastic deformation behavior of Mg by influencing the crystal structure parameters and the axial ratio, c/a by distorting the lattice spacing due to the different size or number of valence electrons [19]. Electron-to-atom ratio (e/a) factor affects the lattice spacing and it changes with the valence electrons of the solute element [42]. The electronic structure of Mg and its Brillouin zones (BZ) can be used to explain this relationship. The first BZ is described as a Wigner-Seitz primitive cell in the reciprocal space (k -space) and it consists of a set of planes which form a closed volume and they are equivalent to the planes in the real crystal. BZ contains the valence electrons, and the surfaces are energy discontinuities which satisfy the Bragg's law. Because of these discontinuities, the electrons cannot change their states from inside to outside the

closed volume without excitation [16,43,44]. In Mg, the planes $\{0002\}$, $\{1\bar{1}00\}$ and $\{10\bar{1}1\}$ bound the 1st BZ [16]. The properties of Mg and its alloys and the effect of e/a on lattice spacing can be determined by the manner in which overlap of electrons occurs. With solutes of higher valency than Mg, e/a increases leading to overlap from the 1st Brillouin zone. These excess electrons cause an internal stress to the crystal and the lattice is distorted [16,44]. Furthermore, the reciprocal space plane will be pushed toward the center by the increased number of electrons and as a result the lattice parameter a in the real crystal expands. Conversely, solutes with lower valency contract parameter a in the real lattice. The c -spacing, on the other hand is not affected by alloying until a critical value that affects the overlap across the basal plane $\{0002\}$ is reached. This overlap expands the c -axis and it occurs at ~ 0.75 at% for a three valent solute and at 0.375 at.% for a four valent solute [16].

Hume-Rothery et al. found that the c/a of Mg decreases slightly with the addition of 0.496 at. % Al and then increases. They found that a small addition (0.63 at.%) does not change the c/a ratio but higher additions do [45]. It is also known that one-valent Li can change the crystal structure of Mg from HCP to BCC [16,19]. Similarly, it was shown that Y addition in Mg increases its lattice parameters as the e/a ratio increases and the c/a ratio follows a ‘V’ trend [46]. However, Sandlöbes et al. do not observe any essential change to the c/a ratio with the addition of Y in the binary Mg-Y alloy [47]. Becerra and Pekguleryuz [48] have studied Li, In and Zn and reported that Li decrease the c/a ratio from 1.624 to 1.6068 in the 0-16at%Li range due to decrease of e/a from 2 to 1.84 causing electron overlap from the 2nd Brillouin zone to the 1st Brillouin which leads to a contraction of the c -spacing in real space and a decrease in c/a . Three-valent In increased the c/a of Mg to 1.6261 as In increased towards 3.3at%. The changes in a - and c -spacing were related to changes in e/a as well as the atom size effect through Vegard’s law [49]. Becerra et al.

have also determined the change in the interplanar spacing of basal, prismatic and pyramidal planes in Mg-Li alloys in the range 0-16at%Li [19]. The spacing of basal planes presents larger reduction than the interplanar spacing of non-basal planes. As the interplanar spacing decreases, the stress to move the dislocations in the basal plane is higher (Peierls stress §2.3.1). Experimentally, the prismatic slip is set in the range 1.624-1.610 and extensive prismatic slip has been observed at Mg-16at%Li alloys [19]. Becerra et al [48] have generated an empirical relationship between c/a and e/a using experimentally determined axial ratio (c/a) and valence electron concentration (e/a) of binary and multi-component alloys. The c/a vs. electron concentration relationship here is given as $c/a = -15.6(e/a)^2 + 60(e/a) - 55.8$. Interestingly, it is found that an e/a of ~ 1.83 and 2.03 would give an axial ratio of 1.58 . Ti is a metal with similar axial ratio and good ductility as it does not present basal slip at room temperature due to high CRSS (Table 2.3). Mg could present this axial ratio at 20 at% Li addition and theoretically for ~ 3 -5at% In. This could be an interesting approach to improve the formability of Mg alloys. Future first principles simulations could elucidate the possible additions in Mg which could change the e/a ratio and change the unit cell towards a BCC structure.

2.3.6 Effect of solutes on axial ratio and twinning

Both tension and compression twins (§ 2.3.2., Fig. 2.2) are involved in HCP metals with high ductility. Pure Mg usually presents $\{10\bar{1}2\}$ tension twins but solute additions can change c/a and thereby the twinning mode. In Mg, the $\{10\bar{1}2\}$ tension twins can be followed by $\{10\bar{1}1\}$ compression twins as its c/a is where these twin shears are very close [15]. Pekguleryuz et al. [18] have investigated the edge cracking in 150 °C rolling of AZ31 and Mg-2wt%Li-1wt%Zn alloy with different c/a (1.6247 and 1.6190 respectively). The Mg-Li-Zn alloy which had low tendency to edge cracking showed tension/compression double twins, while the AZ31 with tension twins

showed severe edge cracking. Pure Mg with $c/a=1.6240$ exhibits $\{10\bar{1}2\}$ tension twins. With Li addition, the c/a ratio decreases, and this c/a promotes tension/compression twins (Fig. 2.2). Notably, AZ31 with c/a higher than pure Mg exhibits mostly $\{10\bar{1}1\}$ tension twin (lower shear stress). Thus, the ductility of AZ31 is low due to the dislocation pile-up at tension twins and the crack initiation. It can be deduced that twinning related ductility can be increased in Mg via alloying that decreases the c/a from 1.6240 towards 1.588.

2.3.7 Effect of solutes on stacking fault energy in magnesium

High SFE eliminates Stage II dislocation pile-up stage via enhanced cross-slip of partial dislocations. Increasing the SFE would enable cross-slip in Mg and delay fracture thereby increasing ductility. On the other hand, recent studies [50] stress the importance of lowering the SFE which results in the generation of pyramidal $c+a$ dislocations. The effects of alloying elements on the SFE of Mg have been recently estimated via DFT calculations and are shown in Table 2.6 [39]. The elements that increase the SFE for the various SFs in Mg are few and the effects are limited to certain types of faults (Table 2.7) [39]. If the unstable SFE for twin-like fault is taken as 111 mJ/m^2 rather than 181 mJ/m^2 , then few other elements can be added to the table. Elements that decrease the SFE are also listed in Table 2.7 [39]. Thornton [51] showed that electron to atom ratio significantly affects the SFE and it is determined by the composition of the alloy.

Table 2.6 Calculated SFE for Mg and binary Mg alloys by DFT (values are in mJ/m²) [39].
Reference of values from a: [52], b:[53], c:[54], d:[55], e:[56], f:[57], g:[41], h:[58], i:[59], j:[60],
k:[61].

System	Growth fault (I ₁)		Deformation fault (I ₂)		Extrinsic fault (E)		Twin-like fault (T ₂)	
	Stable SFE	Unstable SFE	Stable SFE	Unstable SFE	Stable SFE	Unstable SFE	Stable SFE	Unstable SFE
Mg	21 ^a , 18 ^b , 16 ^c , 30 ^e , 17.98 ^d , 20 ^g , 17.1 ^h , 17.8 ⁱ , 18 ^k	86.2 ^h	44 ^a , 36 ^b , 34 ^c , 36 ^d , 60 ^e , 33.84 ^f , 33.8 ^h , 38.3 ⁱ , 33 ^k	97 ^c , 92 ^d , 87.6 ^h	69 ^a , 58 ^b , 59 ^c , 90 ^e , 52.57 ^f	-	51 ^a , 40 ^b , 38 ^c , 39 ^d , 60 ^e , 40.55 ^f	181 ^c , 111 ^d
Mg-Li	16.7 ⁱ , 28 ^k	-	47 ^d , 48.2 ⁱ , 46 ^k	95 ^d	-	-	56 ^d , 63.5 ^j	119 ^d
Mg-Na	15.7 ⁱ	-	46.8 ⁱ	-	66.7 ⁱ	-	-	-
Mg-Al	12.5 ⁱ	-	21 ^d , 33.6 ⁱ	78 ^d	55.7 ⁱ	-	32 ^d	96 ^d
Mg-K	13.5 ⁱ	-	32.5 ⁱ	-	47.5 ⁱ	-	-	-
Mg-Ca	13.8 ⁱ	-	33.5 ⁱ	-	49.6 ⁱ	-	-	-
Mg-Ti	-	-	36 ^d	112 ^d	-	-	47 ^d	137 ^d
Mg-Mn	13.5 ⁱ	-	38 ^d , 40.3 ⁱ	103 ^d	81.4 ⁱ	-	83 ^d	149 ^d
Mg-Fe	3.3 ⁱ	-	52 ^d , 40.3 ⁱ	110 ^d	79.8 ⁱ	-	80 ^d	146 ^d
Mg-Ni	-	-	55 ^d	99 ^d	-	-	81 ^d	135 ^d
Mg-Cu	16.6 ⁱ	-	53 ^d , 40.1 ⁱ	97 ^d	66.4 ⁱ	-	68 ^d	126 ^d
Mg-Zn	18.2 ^h , 8.5 ⁱ	91.0 ^h	37 ^d , 35.1 ^h , 30.8 ^j	86 ^d , 94.2 ^h	58.8 ⁱ	-	43 ^d	195 ^d
Mg-Sr	15.6 ⁱ	-	33.2 ⁱ	-	46.3 ⁱ	-	-	-
Mg-Y	3.7 ^h , 1.8 ^j	61.2 ^h	25 ^d , 15.7 ^h , 32.9 ^j	71 ^d , 62.1 ^h	47.1 ⁱ	-	21 ^d	85 ^d
Mg-Zr	9.8 ^j	-	26 ^d , 35.3 ⁱ	99 ^d	67.5 ⁱ	-	32 ^d	119 ^d
Mg-Ag	-	-	49 ^d	101 ^d	-	-	62 ^d	127 ^d
Mg-Nd	10.8 ^j	-	32.3 ⁱ	-	51.9 ⁱ	-	-	-
Mg-Sn	13.8 ^j	-	2 ^d , 37.2 ^j	64 ^d	50.1 ⁱ	-	25 ^d	79 ^d
Mg-Pb	-	-	4 ^d	55 ^d	-	-	32 ^d	80 ^d

Table 2.7 Elements that change SFE [39].

	Growth Fault		Deformation Fault		Extrinsic Fault	Twin-like Fault	
	Stable	Unstable	Stable	Unstable	Stable	Stable	Unstable
Increase SFE	Li	Zn	Li, Na, Mn, Fe, Ni, Cu, Zn, Ag	Li, Ti, Mn, Fe, Ni, Cu, Zr, Ag	Mn, Fe,	Li, Ni, Ti, Mn, Fe, Ni, Cu, Zn, Ag	Li, Ti, Mn, Fe, Ni, Cu, Zn, Zr, Ag
Decrease SFE	Na, Al, K, Ca, Mn, Fe, Cu, Sr, Y, Zr, Nd, Sn	Y	Al, K, Ca, Sr, Y, Zr, Nd, Sn, Pb	Al, Y, Sn, Pb	Na, Al, K, Ca, Sr, Y, Nd, Sn	Y, Zr, Sn, Pb	Al, Y, Sn, Pb

2.4 Ductility in Mg-Al casting alloys

2.4.1 Mg-Al based cast alloys (AM)

Mg-Al based casting alloys are based on binary Mg-Al system with 2-10% Al content (Fig. 2.4a). Aluminum is soluble in Mg up to 2% (at room temperature) at equilibrium and the excess forms the $Mg_{17}Al_{12}$ intermetallic second phase which has a wide composition range (not a stoichiometric line compound) [52]; it contains both covalent and metallic bonding. It presents homopolar bonds among Al atoms, heteropolar bonds between Mg and Al and metallic bond among Mg atoms and it can be written as $(Al_2)_{12}^{-2} Mg_{24}^{+} Mg_{10}$. Its crystal structure is cubic, isomorphous with the α -Mn (cI58). Its unit cell consists of 34 Mg atoms which occupy 3 different positions namely Mg(I), Mg(II) and Mg(III) and 24 Al atoms [15,53]. Due to its wide chemical composition the lattice parameters can vary significantly. Zhang et al.[54] report that the lattice parameter can vary from 1.050 nm to 1.069 nm affected by the different orientation relationship with the magnesium matrix. There are different types of orientation relationships between the Mg matrix and the $Mg_{17}Al_{12}$ precipitate with the most predominant to be the $(0001)_{Mg} \parallel (011)_{\beta}$ and $[2\bar{1}\bar{1}0]_{Mg} \parallel [1\bar{1}1]_{\beta}$ [55–58].

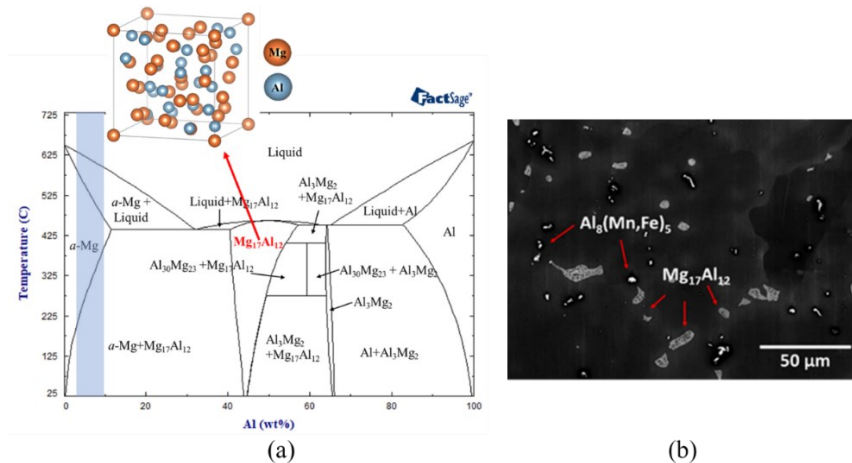


Fig. 2.4 (a) Calculated Mg-Al phase diagram with the structure of $Mg_{17}Al_{12}$ using FactSage (FTlite database) [59]. The light blue area represents the Al range (wt%) of the commercial Mg-Al system. (b) BSE-SEM micrograph showing the as-cast microstructure of a commercial Mg-Al based alloy (AM60B) synthesized and cast at McGill.

Mg-Al-Mn based alloys, such as AM60B (~6% Al and ~0.3% Mn) are commonly used for die casting automotive components. These alloys offer a good combination of strength, ductility and castability. Al ensures the good castability due to the increase of freezing range and Mn removes the Fe and Ni impurities with additional melt treatments leading to a better corrosion resistance. Mn also contributes to grain refinement. AM cast alloy microstructure consists of α -Mg solid solution (~2% Al), the $Mg_{17}Al_{12}$ and $Al_8(Mn,Fe)_5$ intermetallic phases in the interdendritic regions (Fig.2.4b) . The $Mg_{17}Al_{12}$ precipitates present different morphologies (i.e., lamellar, fibrous, granular, divorced or partially divorced) which are affected by the amount of Al and the cooling rate of the alloy. As aluminum increases the β -phase becomes less divorced [52,60–62].

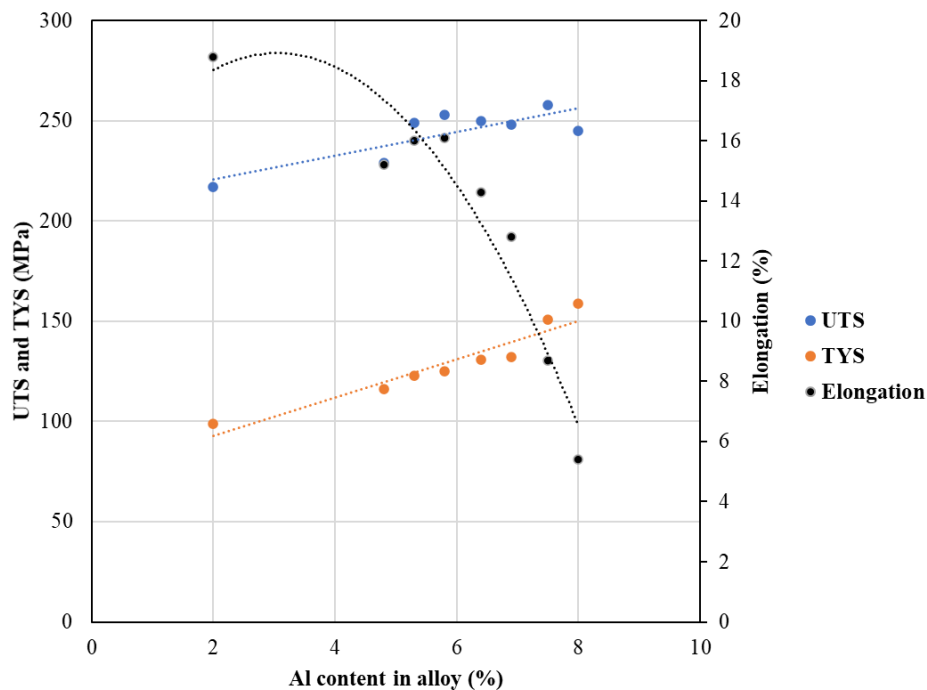


Fig. 2.5 (a) Effect of Al content on ultimate tensile strength, yield strength (0.2% offset) and elongation in AM series alloys. Redrawn from [35,63].

The amount of β -Mg₁₇Al₁₂ phase (Fig. 2.5) and its morphology determine the strength and ductility of cast AM alloys. As the amount of the phase increases strength increases and ductility decreases. AM alloy compositions have been developed mainly to obtain certain combinations of strength and ductility by controlling the amount of β -Mg₁₇Al₁₂ in the alloy. By lowering the amount of Al, the ductility increases due to the lower volume fraction of Mg₁₇Al₁₂; however the strength decreases. The AM60 (Mg-6%Al-0.3%Mn) alloy offers the best combination of strength and ductility [52,62,64,65].

2.4.2 Ductility improvement of Mg-Al based cast alloys

Mg-Al based alloys were developed by Norsk Hydro to help expanding Mg application in structural automotive components which need high energy absorption. Alloys with 2-6wt%Al are good candidates for such applications due to their high ductility [66]. There is a current interest to expand the use of Mg-Al alloys in critical automotive structural applications. As a result, the further increase in ductility without compromising strength is important. As described in the previous sections, there are different mechanisms that can affect the mechanical properties such as the intrinsic properties of Mg matrix and the microstructure. The following sections describe three different mechanisms that could affect the ductility of cast Mg-Al based alloys. The current thesis mainly focuses on the effect of trace additions on the refinement of the microstructure and more specifically that of β -Mg₁₇Al₁₂ and α -Mg.

2.4.2.1 Modification of AM alloys with trace additions

Previous knowledge on Al-Si cast alloys has shown that trace additions can refine the eutectic silicon morphology which can significantly improve the ductility [67]. The eutectic silicon can be refined with low additions such as Sr[68], Na[69], Sb[70], Y, and Yb [71]. For instance, ppm Sr addition co-segregates with Al and Si inside the eutectic precipitates causing growth poisoning;

hence refinement of the eutectic phase [72]. However, this modification can be lost if it does not occur at the optimum addition range which is around 100ppm level for Al-Si alloys. When the alloying addition is less than the optimum level, the Si is under modified and for higher additions than the optimum new phases form and the alloy is over-modified [67,73]. A similar approach can be used for Mg-Al cast alloys. Koubichek [74] has first identified the refining effect of trace Sr and Ca additions on the grain size and the $Mg_{17}Al_{12}$ phase in Mg-Al alloys in 1959. Knowledge exists on the grain refinement of Mg-9%Al-1%Zn (AZ91) alloy with ppm Sr additions due to the poisoning of α -Mg grains by a thin layer of Sr which leads to growth restriction [75]. Recent investigations focus on the addition of RE in Mg alloys which improve the mechanical properties. Rare earths are surface active and they tend to segregate to defects such as grain boundaries and interfaces leading to their modification [76,77]. Minor additions of Gd in AZ91 forms Al_8Mn_4Gd precipitates which refine the $Mg_{17}Al_{12}$ phase and the α -Mg grains because they act as nucleation sites [78]. Wang et al.[79] examined the effect of yttrium addition to AZ91 alloy. The volume fraction of β - $Mg_{17}Al_{12}$ decreases with Y addition and it becomes fine after the formation of Al_2Y . Nd addition improves the ductility of the alloy by decreasing the amount of $Mg_{17}Al_{12}$ due to the higher affinity of Al to create Al_2Nd intermetallics [80]. Furthermore, similar effects have been observed with the addition of Ce in the as cast Mg-4Al based alloy where the ductility increased due to the refinement of the microstructure and the suppression of β -phase. However, high amounts of Ce (6wt%) form coarse and brittle Al_2Ce intermetallics which deteriorate the ductility [81,82]. Additionally, Er seems to increase the ductility of Mg-Al based alloys [83,84]. Trace Er addition formed Al_3Er intermetallics which refined the microstructure improving the mechanical properties [83]. Trace Er in AZ31 was observed to be beneficial for the strength and ductility due to grain size refinement; however higher additions reduce the strength due to Al_2Er formation which leads

to grain coarsening and reduction of $Mg_{17}Al_{12}$ [85]. Er can also present beneficial effect on the $Mg_{17}Al_{12}$ intermetallic as it can refine it and increase its microhardness [86]. Studies on Mg-Si alloys have shown that Nd and Gd can refine the Mg_2Si precipitate by poisoning it but higher additions can be potentially detrimental as other second phases form [87,88]. It was previously observed [89] that Sn addition in Mg-Al-Zn alloys can modify the morphology of $Mg_{17}Al_{12}$ which changes from lamellar into fully divorced. This transformation improved the ductility of the alloy. Additionally, Candan et al. results show that the addition of Ti in AZ91 decreases the amount of $Mg_{17}Al_{12}$ but without any effect on ductility [90].

Ductility of Mg castings is affected by the morphology, distribution, and nature (stoichiometry, bonding, hardness, ductility) of the second phases. In Mg-Al cast alloys the $Mg_{17}Al_{12}$ intermetallic is present as a divorced or partially divorced eutectic. The ductility of $Mg_{17}Al_{12}$ seems to be a controversial issue in literature as it is considered a brittle [53,91,92] or ductile [93,94] phase according to first principle calculations. These calculations are based on the calculated elastic constants of $Mg_{17}Al_{12}$; namely the ratio of the shear modulus over the bulk modulus where a ratio less than 0.57 indicates a ductile intermetallic (β - $Mg_{17}Al_{12}$ shows a range from 0.46 to 0.68). The dissolution of an alloying addition inside $Mg_{17}Al_{12}$ or the formation of a new phase depend on the amount and type of alloying addition[95]. The alloying additions can occupy different positions in $Mg_{17}Al_{12}$ (i.e., Mg (I, II, III) or Al positions) depending on the minimization of the occupational energy. It has been shown that Ca, Zr and La substitute the Mg atoms and Zn, Cu and Ni substitute the Al atoms. Mn and Sn show positive occupation energies and it is not investigated what positions they occupy [95]. The substitution of Mg and/or Al leads to structural stability and distortion of the lattice changing the lattice parameter of $Mg_{17}Al_{12}$ [96–98].

2.4.2.2 Ductility of the α -Mg matrix

Another important factor influencing the ductility of Mg-Al based alloys is the plastic deformation behavior of the α -Mg matrix. To avoid easy glide where dislocations accumulate quickly at the intermetallics leading to an early fracture, high SFE that promotes cross slip is desirable. High plastic work capacity (high tensile toughness) is important in delaying fracture in the presence of stress concentrators [36]. Dislocation mobility is also important in blunting the crack tips during growth, hence smaller dislocation cores and high SFE are desirable [11,12]. On the other hand, new research does show that a low SFE can lead to the activation of pyramidal $c+a$ dislocations which can contribute to ductility [41,47,50]. Casting alloys develop their properties mainly via liquid metal processing and if possible, via subsequent heat treatments. Due to cost sensitivity, automotive parts are cast by high-productivity processes such as high pressure die casting (HPDC). The α -Mg in HPDC AM alloys is supersaturated in Al (i.e., the Al > 2wt% Al equilibrium value) due to the rapid HPDC solidification rates. Al decreases the SFE [39] and slightly decreases the c/a ratio of Mg up to 0.496 at% Al (0.55% Al) and then increases [45]. Supersaturation of the α -Mg matrix of the HPDC AM alloy may result in further increase in c/a . Increased c/a favors tension twinning decreasing the ductility of the alloy. Rare earths (RE) can improve the ductility of pure Mg by decreasing the SFE [50] or by forming long period stacking ordered phases (LPSO) when a transition metal is present [99]. However, the presence of Al decreases the solubility of RE in α -Mg solid solution forming brittle intermetallics with them [100–103] counteracting the effect of the above mechanisms.

2.4.2.3 Role of dispersoid in tensile toughness

Limited slip systems in HCP Mg and inability to activate non-basal slip systems can lead to dislocation pile-up at obstacles. Celikin et al. [104] have seen that dislocations can pile up at

intermetallics leading to early crack initiation during creep; the failure could be delayed when nano-scale dispersoids could pin dislocations within the grains. In AJ62 (Mg-6Al-2Sr-0.3Mn) [105] alloy produced by HPDC, α -Mg matrix supersaturated in Al-Mn led to the precipitation of nano-dispersoids during thermal exposure which delayed cracking and failure. The design of nano-scale dispersoids is challenging but seems to require the presence of peritectic slow diffusing solutes to be combined with eutectic solutes in a supersaturated matrix. The effect would be increase in strength as well as a delay in failure which could increase tensile toughness.

2.5 References

- [1] P.K. Mallick, Advanced materials for automotive applications: An overview, in: Adv. Mater. Automot. Eng., Elsevier, 2012: pp. 5–27.
- [2] D. Bernhardt, J. Reilly II, Mineral Commodity Summaries 2020, 2020. <https://pubs.usgs.gov/periodicals/mcs2020/mcs2020.pdf>.
- [3] Projected hrc steel prices worldwide between 2018-2020, (2020). <https://www.statista.com/statistics/214246/world-steel-prices/> (accessed October 7, 2020).
- [4] T. Mukai, H. Watanabe, K. Higashi, Application of superplasticity in commercial magnesium alloy for fabrication of structural components, Mater. Sci. Technol. 16 (2000) 1314–1319.
- [5] G. Kardys, Magnesium Car Parts: Cost Factors (Part 2), (2017). <https://insights.globalspec.com/article/7250/magnesium-car-parts-cost-factors-part-2> (accessed October 7, 2020).
- [6] R. Ahmad, B. Yin, Z. Wu, W.A. Curtin, Designing high ductility in magnesium alloys, Acta Mater. 172 (2019) 161–184.

- [7] S.F. Pugh, XCII. Relations between the elastic moduli and the plastic properties of polycrystalline pure metals, London, Edinburgh, Dublin Philos. Mag. J. Sci. 45 (1954) 823–843.
- [8] W.D. Callister, Materials science and engineering an introduction, John Wiley, 2007.
- [9] M.H. Yoo, Slip, twinning, and fracture in hexagonal close-packed metals, Metall. Trans. A. 12 (1981) 409–418.
- [10] J.R. Rice, R. Thomson, Ductile versus brittle behaviour of crystals, Philos. Mag. A J. Theor. Exp. Appl. Phys. 29 (1974) 73–97.
- [11] D. Hull, D.J. Bacon, Introduction to dislocations, Elsevier, 2011.
- [12] G.E. Beltz, D.M. Lipkin, L.L. Fischer, Role of crack blunting in ductile versus brittle response of crystalline materials, Phys. Rev. Lett. 82 (1999) 4468.
- [13] D. Geiselman, The metallurgy of scandium, J. Less Common Met. 4 (1962) 362–375. doi:[https://doi.org/10.1016/0022-5088\(62\)90005-X](https://doi.org/10.1016/0022-5088(62)90005-X).
- [14] Supplier Data - Osmium (Os) (Goodfellow), (n.d). <https://www.azom.com/properties.aspx?ArticleID=1842> (accessed October 12, 2020).
- [15] A.A. Kaya, M.O. Pekguleryuz, K.U. Kainer, Fundamentals of magnesium alloy metallurgy, Woodhead Publishing, Cambridge, 2013.
- [16] G.V. Raynor, The physical metallurgy of magnesium and its alloys, Pergamon, 1959.
- [17] Z. Yu, A. Tang, Q. Wang, Z. Gao, J. He, J. She, K. Song, F. Pan, High strength and superior ductility of an ultra-fine grained magnesium–manganese alloy, Mater. Sci. Eng. A. 648 (2015) 202–207.

- [18] M. Pekguleryuz, M. Celikin, M. Hoseini, A. Becerra, L. Mackenzie, Study on edge cracking and texture evolution during 150 C rolling of magnesium alloys: the effects of axial ratio and grain size, *J. Alloys Compd.* 510 (2012) 15–25.
- [19] A. Becerra, M. Pekguleryuz, Effects of lithium, indium, and zinc on the lattice parameters of magnesium, *J. Mater. Res.* 23 (2008) 3379–3386.
- [20] G.E. Dieter, D.J. Bacon, *Mechanical metallurgy*, McGraw-hill New York, 1986.
- [21] G.I. Taylor, H. Quinney, The plastic distortion of metals, *Philos. Trans. R. Soc. London. Ser. A, Contain. Pap. a Math. or Phys. Character.* 230 (1931) 323–362.
- [22] R. von Mises, Mechanik der plastischen Formänderung von Kristallen, *ZAMM-Journal Appl. Math. Mech. Für Angew. Math. Und Mech.* 8 (1928) 161–185.
- [23] G.W. Groves, A. Kelly, Independent slip systems in crystals, *Philos. Mag.* 8 (1963) 877–887.
- [24] J.F. Nie, K.S. Shin, Z.R. Zeng, Microstructure, Deformation, and Property of Wrought Magnesium Alloys, *Metall. Mater. Trans. A.* (2020) 1–65.
- [25] B.S. Wang, R.L. Xin, G.J. Huang, Q. Liu, Strain rate and texture effects on microstructural characteristics of Mg-3Al-1Zn alloy during compression, *Scr. Mater.* 66 (2012) 239–242.
- [26] G. Wan, B.L. Wu, Y.D. Zhang, G.Y. Sha, C. Esling, Anisotropy of dynamic behavior of extruded AZ31 magnesium alloy, *Mater. Sci. Eng. A.* 527 (2010) 2915–2924.
- [27] J. Koike, Enhanced deformation mechanisms by anisotropic plasticity in polycrystalline Mg alloys at room temperature, *Metall. Mater. Trans. A.* 36 (2005) 1689–1696.
- [28] R. Abbaschian, R.E. Reed-Hill, *Physical metallurgy principles*, Cengage Learning, 2008.

- [29] D.H. Lassila, M.M. LeBlanc, J.N. Florando, Zinc single-crystal deformation experiments using a “6 degrees of freedom” apparatus, *Metall. Mater. Trans. A.* 38 (2007) 2024–2032.
- [30] M.H. Yoo, J.K. Lee, Deformation twinning in hcp metals and alloys, *Philos. Mag. A.* 63 (1991) 987–1000.
- [31] J. Wang, J.P. Hirth, C.N. Tomé, ($1\bar{1}012$) Twinning nucleation mechanisms in hexagonal-close-packed crystals, *Acta Mater.* 57 (2009) 5521–5530.
- [32] H. Yoshinaga, R. Horiuchi, Work hardening characteristics of the basal slip of magnesium single crystals, *Trans. Japan Inst. Met.* 3 (1962) 220–226.
- [33] W.F. Hosford, *Mechanical behavior of materials*, Cambridge university press, 2010.
- [34] L. Xiao, G. Yang, H. Qin, J. Ma, W. Jie, Asymmetric tension-compression mechanical behavior of the as-cast Mg-4.58 Zn-2.6 Gd-0.16 Zr alloy, *Mater. Sci. Eng. A.* (2020) 140439.
- [35] T. Wang, J.J. Jonas, S. Yue, Easy Glide in a Coarse-Grained Mg-2Zn-2Nd Alloy, *Metall. Mater. Trans. A.* 47 (2016) 4795–4799.
- [36] R.W. Hertzberg, R.P. Vinci, J.L. Hertzberg, *Deformation and fracture mechanics of engineering materials*, John Wiley & Sons, 1996.
- [37] S.L. Shang, W.Y. Wang, B.C. Zhou, Y. Wang, K.A. Darling, L.J. Kecskes, S.N. Mathaudhu, Z.K. Liu, Generalized stacking fault energy, ideal strength and twinnability of dilute Mg-based alloys: A first-principles study of shear deformation, *Acta Mater.* 67 (2014) 168–180. doi:<https://doi.org/10.1016/j.actamat.2013.12.019>.
- [38] B. Verlinden, J. Driver, I. Samajdar, R.D. Doherty, Thermo-mechanical processing of

- metallic materials, Elsevier, 2007.
- [39] Z. Ding, S. Li, W. Liu, Y. Zhao, Modeling of Stacking Fault Energy in Hexagonal-Close-Packed Metals, *Adv. Mater. Sci. Eng.* 2015 (2015) 639519. doi:10.1155/2015/639519.
- [40] V. Vitek, Intrinsic stacking faults in body-centred cubic crystals, *Philos. Mag.* 18 (1968) 773–786.
- [41] S. Sandlöbes, M. Friák, S. Zaefferer, A. Dick, S. Yi, D. Letzig, Z. Pei, L.-F. Zhu, J. Neugebauer, D. Raabe, The relation between ductility and stacking fault energies in Mg and Mg–Y alloys, *Acta Mater.* 60 (2012) 3011–3021.
- [42] H. Jones, LIX. The effect of electron concentration on the lattice spacings in magnesium solid solutions, London, Edinburgh, Dublin *Philos. Mag. J. Sci.* 41 (1950) 663–670.
- [43] C. Kittel, P. McEuen, P. McEuen, *Introduction to solid state physics*, Wiley New York, 1996.
- [44] W.B. Pearson, *A handbook of lattice spacings and structures of metals and alloys: International series of monographs on metal physics and physical metallurgy*, Vol. 4, Elsevier, 2013.
- [45] W. Hume-Rothery, G.V. Raynor, The apparent sizes of atoms in metallic crystals with special reference to aluminium and indium, and the electronic state of magnesium, *Proc. R. Soc. London. Ser. A. Math. Phys. Sci.* 177 (1940) 27–37.
- [46] Q. Peng, J. Meng, Y. Li, Y. Huang, N. Hort, Effect of yttrium addition on lattice parameter, Young’s modulus and vacancy of magnesium, *Mater. Sci. Eng. A.* 528 (2011) 2106–2109.
- [47] S. Sandlöbes, S. Zaefferer, I. Schestakow, S. Yi, R. Gonzalez-Martinez, On the role of non-

- basal deformation mechanisms for the ductility of Mg and Mg–Y alloys, *Acta Mater.* 59 (2011) 429–439.
- [48] A.M.B. Correa, *Effect of Solute Elements on the Lattice Parameters of Magnesium*, ProQuest, 2008.
- [49] L. Vegard, Die konstitution der mischkristalle und die raumfüllung der atome, *Zeitschrift Für Phys.* 5 (1921) 17–26.
- [50] S. Sandlöbes, Z. Pei, M. Friák, L.-F. Zhu, F. Wang, S. Zaeferrer, D. Raabe, J. Neugebauer, Ductility improvement of Mg alloys by solid solution: Ab initio modeling, synthesis and mechanical properties, *Acta Mater.* 70 (2014) 92–104.
- [51] P.R. Thornton, T.E. Mitchell, P.B. Hirsch, The dependence of cross-slip on stacking-fault energy in face-centred cubic metals and alloys, *Philos. Mag.* 7 (1962) 1349–1369.
- [52] M. Avedesian, H. Baker, *ASM specialty handbook: magnesium and magnesium alloys.*, ASM International, Ohio, 1998.
- [53] W.-C. Hu, Y. Liu, X.-W. Hu, D.-J. Li, X.-Q. Zeng, X. Yang, Y.-X. Xu, X. Zeng, K.-G. Wang, B. Huang, Predictions of mechanical and thermodynamic properties of Mg₁₇Al₁₂ and Mg₂Sn from first-principles calculations, *Philos. Mag.* 95 (2015) 1626–1645. doi:10.1080/14786435.2015.1040098.
- [54] M.X. Zhang, P.M. Kelly, Crystallography of Mg₁₇Al₁₂ precipitates in AZ91D alloy, *Scr. Mater.* (2003) 647-652. doi:10.1016/S1359-6462(02)00555-9.
- [55] A. Bobby, U.T.S. Pillai, B.C. Pai, Investigation on Lead and Yttrium Addition on the Microstructure and Mechanical Properties of AZ91 Magnesium Alloy, *J. Solid Mech.*

- Mater. Eng. 7 (2013) 273–280.
- [56] A.A. Kaya, P. Uzan, D. Eliezer, E. Aghion, Electron microscopical investigation of as cast AZ91D alloy, Mater. Sci. Technol. 16 (2000) 1001–1006.
- [57] J.F. Nie, X.-L. Xiao, C.P. Luo, B.C. Muddle, Characterisation of precipitate phases in magnesium alloys using electron microdiffraction, Micron. 32 (2001) 857–863.
- [58] M.-X. Zhang, P.M. Kelly, Edge-to-edge matching and its applications: Part II. Application to Mg–Al, Mg–Y and Mg–Mn alloys, Acta Mater. 53 (2005) 1085–1096.
- [59] C.W. Bale, P. Chartrand, S.A. Degterov, G. Eriksson, K. Hack, R. Ben Mahfoud, J. Melançon, A.D. Pelton, S. Petersen, FactSage thermochemical software and databases, Calphad. 26 (2002) 189–228.
- [60] T. Zhu, P. Fu, L. Peng, X. Hu, S. Zhu, W. Ding, Effects of Mn addition on the microstructure and mechanical properties of cast Mg–9Al–2Sn (wt%) alloy, J. Magnes. Alloy. 2 (2014) 27–35. doi:<https://doi.org/10.1016/j.jma.2014.01.003>.
- [61] K. Korgiopoulos, M. Pekguleryuz, The significant effect of trace yttrium level on the mechanical properties of cast Mg–6Al alloy through a refinement mechanism, Mater. Sci. Eng. A. 775 (2020) 138966.
- [62] M.D. Nave, A.K. Dahle, D.H. StJohn, Eutectic growth morphologies in magnesium-aluminium alloys, in: TMS Annu. Meet., 2000: pp. 233–242. doi:10.1002/9781118808962.ch33.
- [63] H.E. Friedrich, B.L. Mordike, Magnesium technology, Springer, 2006.
- [64] J.W. Edington, K.C.T. Russell, Practical electron microscopy in materials science,

Macmillan International Higher Education, 1977.

- [65] K. Korgiopoulos, M. Pekguleryuz, Towards the Development of High Ductility Mg-Al Based Alloys Through Second-Phase Refinement with Trace Yttrium Additions, in: *Magnes. Technol.* 2020, 2020.
- [66] T.K. Aune, H. Westengen, T. Ruden, Mechanical properties of energy absorbing magnesium alloys, SAE Technical Paper, 1993.
- [67] J.E. Gruzleski, B.M. Closset, The treatment of liquid aluminum-silicon alloys, Amer Foundry Society, Illinois, 1990.
- [68] A.K. Dahle, K. Nogita, S.D. McDonald, C. Dinnis, L. Lu, Eutectic modification and microstructure development in Al-Si Alloys, *Mater. Sci. Eng. A.* 413 (2005) 243–248.
- [69] S.C. Flood, J.D. Hunt, Modification of Al-Si eutectic alloys with Na, *Met. Sci.* 15 (1981) 287–294.
- [70] A.K.P. Rao, K. Das, B.S. Murty, M. Chakraborty, On the modification and segregation behavior of Sb in Al-7Si alloy during solidification, *Mater. Lett.* 62 (2008) 2013–2016.
- [71] A. Knuutinen, K. Nogita, S.D. McDonald, A.K. Dahle, Modification of Al-Si alloys with Ba, Ca, Y and Yb, *J. Light Met.* 1 (2001) 229–240.
- [72] M. Timpel, N. Wanderka, R. Schlesiger, T. Yamamoto, N. Lazarev, D. Isheim, G. Schmitz, S. Matsumura, J. Banhart, The role of strontium in modifying aluminium-silicon alloys, *Acta Mater.* 60 (2012) 3920–3928.
- [73] S. Nafisi, R. Ghomashchi, Effects of modification during conventional and semi-solid metal processing of A356 Al-Si alloy, *Mater. Sci. Eng. A.* 415 (2006) 273–285.

- [74] L. Koubichek, Effect of small additions of elements on grain size and the refinement of the Mg₄Al₃ [Mg₁₇Al₁₂] phase in Mg alloy. *Izv. Vyschikh. Outebnykh Za Vedeny, Metall. Non-Ferrous Met.* 6 (1959).
- [75] C.A. Aliravci, J.E. Gruzleski, F.C. Dimayuga, Effect of strontium on the shrinkage microporosity in magnesium sand castings, *AFS Trans.* 100 (1992) 353–362.
- [76] X. Tong, L. Zai, G. You, H. Wu, H. Wen, S. Long, Effects of bonding temperature on microstructure and mechanical properties of diffusion-bonded joints of as-cast Mg–Gd alloy, *Mater. Sci. Eng. A.* 767 (2019) 138408.
- [77] D. Rossouw, B. Langelier, A. Scullion, M. Danaie, G.A. Botton, Multivariate-aided mapping of rare-earth partitioning in a wrought magnesium alloy, *Scr. Mater.* (2016) 174–178. doi:10.1016/j.scriptamat.2016.07.022.
- [78] J. Wang, X. Li, Simultaneously improving strength and ductility of AZ91-type alloys with minor Gd addition, *J. Alloys Compd.* (2019).
- [79] S.-R. Wang, P.-Q. Guo, L.-Y. Yang, Y. Wang, Microstructure and mechanical properties of AZ91 alloys by addition of yttrium, *J. Mater. Eng. Perform.* 18 (2009) 137–144. doi:10.1007/s11665-008-9255-z.
- [80] J. Zhang, J. Wang, X. Qiu, D. Zhang, Z. Tian, X. Niu, D. Tang, J. Meng, Effect of Nd on the microstructure, mechanical properties and corrosion behavior of die-cast Mg-4Al-based alloy, *J. Alloys Compd.* (2008) 556–564. doi:10.1016/j.jallcom.2007.10.056.
- [81] J. Zhang, Z. Leng, M. Zhang, J. Meng, R. Wu, Effect of Ce on microstructure, mechanical properties and corrosion behavior of high-pressure die-cast Mg-4Al-based alloy, *J. Alloys*

- Compd. (2011) 1069–1078. doi:10.1016/j.jallcom.2010.09.185.
- [82] A.K. Chaubey, S. Scudino, K.G. Prashanth, J. Eckert, Microstructure and mechanical properties of Mg-Al-based alloy modified with cerium, *Mater. Sci. Eng. A.* (2015) 46–49. doi:10.1016/j.msea.2014.11.081.
- [83] S. Seetharaman, C. Blawert, B.M. Ng, W.L.E. Wong, C.S. Goh, N. Hort, M. Gupta, Effect of erbium modification on the microstructure, mechanical and corrosion characteristics of binary Mg-Al alloys, *J. Alloys Compd.* (2015) 759–770. doi:10.1016/j.jallcom.2015.05.284.
- [84] S. Sankaranarayanan, B.M. Ng, S. Jayalakshmi, M.G. Kumar, Q.B. Nguyen, M. Gupta, Microstructure and Mechanical Properties of a Magnesium-Aluminium-Erbium Alloy, in: *Magnes. Technol.* 2015, Springer, 2015: pp. 445–449. doi:10.1007/978-3-319-48185-2_82.
- [85] Y. Ma, X. Zhang, H. Liu, L. Meng, Effects of Er on the microstructure and properties of AZ31 magnesium alloy prepared via the EMS process, *Rare Met.* 29 (2010) 339–345.
- [86] L.I. Yonggang, W.E.I. Yinghui, H.O.U. Lifeng, G.U.O. Chunli, H.A.N. Pengju, Effect of erbium on microstructures and properties of Mg-Al intermetallic, *J. Rare Earths.* 32 (2014) 1064–1072.
- [87] J. Hu, C. Tang, X. Zhang, Y. Deng, Modification of Mg₂Si in Mg-Si alloys with neodymium, *Trans. Nonferrous Met. Soc. China.* 23 (2013) 3161–3166.
- [88] L. Ye, J. Hu, C. Tang, X. Zhang, Y. Deng, Z. Liu, Z. Zhou, Modification of Mg₂Si in Mg–Si alloys with gadolinium, *Mater. Charact.* 79 (2013) 1–6.
- [89] Y. Turen, Effect of Sn addition on microstructure, mechanical and casting properties of

- AZ91 alloy, *Mater. Des.* (2013) 1009–1015. doi:10.1016/j.matdes.2013.02.037.
- [90] S. Candan, M. Unal, E. Koc, Y. Turen, E. Candan, Effects of titanium addition on mechanical and corrosion behaviours of AZ91 magnesium alloy, *J. Alloys Compd.* (2011) 1958–1963. doi:10.1016/j.jallcom.2010.10.100.
- [91] D. Zhou, J. Liu, S. Xu, P. Peng, First-principles investigation of the binary intermetallics in Mg-Al-Sr alloy: Stability, elastic properties and electronic structure, *Comput. Mater. Sci.* (2014) 24-29. doi:10.1016/j.commatsci.2014.01.007.
- [92] Z.W. Huang, Y.H. Zhao, H. Hou, P.D. Han, Electronic structural, elastic properties and thermodynamics of Mg₁₇Al₁₂, Mg₂Si and Al₂Y phases from first-principles calculations, *Phys. B Condens. Matter.* (2012) 1075–1081. doi:10.1016/j.physb.2011.12.132.
- [93] N. Wang, W.-Y. Yu, B.-Y. Tang, L.-M. Peng, W.-J. Ding, Structural and mechanical properties of Mg₁₇Al₁₂ and Mg₂₄Y₅ from first-principles calculations, *J. Phys. D. Appl. Phys.* 41 (2008) 195408. doi:10.1088/0022-3727/41/19/195408.
- [94] Y.-H. Duan, Y. Sun, M.-J. Peng, Z.-Z. Guo, First principles investigation of the binary intermetallics in Pb–Mg–Al alloy: stability, elastic properties and electronic structure, *Solid State Sci.* 13 (2011) 455–459. doi:10.1016/j.solidstatesciences.2010.12.011.
- [95] J. Dai, Y. Song, R. Yang, Influences of alloying elements and oxygen on the stability and elastic properties of Mg₁₇Al₁₂, *J. Alloys Compd.* 595 (2014) 142–147.
- [96] J. Su, F. Guo, H. Cai, L. Liu, Study on alloying element distribution and compound structure of AZ61 magnesium alloy with yttrium, *J. Phys. Chem. Solids.* 131 (2019) 125–130.

- [97] D. Zhou, P. Peng, J. Liu, Energetics, electronic structure, and structure stability of the calcium alloying Mg₁₇Al₁₂ phase from first principles calculations, *Mater Sci Pol.* 25 (2007) 145–153.
- [98] D.W. Zhou, P. Peng, H. Zhuang, Y.J. Hu, J.S. Liu, First-principle study on structural stability of Ca alloying Mg₁₇Al₁₂ phase, *Zhongguo Youse Jinshu Xuebao/Chinese J. Nonferrous Met.* 15 (2005) 546–551.
- [99] Y. Kawamura, M. Yamasaki, Formation and mechanical properties of Mg₉₇Zn₁RE₂ alloys with long-period stacking ordered structure, *Mater. Trans.* 48 (2007) 2986–2992.
- [100] B. Pourbahari, M. Emamy, H. Mirzadeh, Synergistic effect of Al and Gd on enhancement of mechanical properties of magnesium alloys, *Prog. Nat. Sci. Mater. Int.* 27 (2017) 228–235.
- [101] C. Wang, J. Dai, W. Liu, L. Zhang, G. Wu, Effect of Al additions on grain refinement and mechanical properties of Mg–Sm alloys, *J. Alloys Compd.* 620 (2015) 172–179.
- [102] M. Faruk, A. OzDEMIR, K.U. Kainer, H. Norbert, Influence of Ce addition on microstructure and mechanical properties of high pressure die cast AM50 magnesium alloy, *Trans. Nonferrous Met. Soc. China.* 23 (2013) 66–72.
- [103] L. Wang, Y. Feng, E. Guo, L. Wang, Y. Fu, S. Zhao, G. Cao, Comparative study on microstructure and mechanical properties of Mg-3Nd-3Al and Mg-3Nd-0.5 Zr alloys under different heat treatment conditions, *JOM.* 71 (2019) 2194–2201.
- [104] M. Çelikin, The creep behaviour of Magnesium-Manganese based alloys, (2012).
- [105] M. Pekguleryuz, P. Labelle, D. Argo, Magnesium die casting alloy AJ62x with superior

creep resistance, ductility and die castability, SAE Trans. (2003) 24–29.

CHAPTER 3

The significant effect of trace Yttrium level on the mechanical properties of cast Mg-6Al alloy through a refinement mechanism

According to the literature review, rare earths are promising in improving the mechanical properties by refining the microstructure of Mg-Al based alloys. However, the high cost can be prohibitive in using them at high levels in Mg automotive applications. Using the knowledge of eutectic Si refinement in Al-Si alloys with low alloying additions (ppm level), this chapter discusses the mechanism of Mg₁₇Al₁₂ refinement with ppm Y additions and the improvement of Mg-6wt%Al mechanical properties. Thermodynamic simulations, microstructural investigation and mechanical testing are employed to better understand the role of low Y additions in the refinement of Mg-Al based alloys. This chapter has been published as a journal article: *Korgiopoulos, K., & Pekguleryuz, M. (2020). The significant effect of trace yttrium level on the mechanical properties of cast Mg-6Al alloy through a refinement mechanism. Materials Science and Engineering: A, 775, 138966.*

ABSTRACT

It was observed that low level of yttrium (Y) has a modifying effect on the $Mg_{17}Al_{12}$ phase in the binary Mg-6wt%Al casting alloy. Scanning/transmission electron microscopy, mechanical testing and thermodynamic calculations were employed to understand the modification mechanism. It is found that Y at *trace* level refines the β - $Mg_{17}Al_{12}$ phase leading to increased tensile elongation and compressive strain to fracture. The refinement effect is lost with further increase in the Y level. Thermodynamic calculations (Scheil cooling) indicate that the formation temperature of the Al_4MgY phase changes with the Y level. At *trace* levels, its nucleation temperature is the same as that of $Mg_{17}Al_{12}$, producing a co-precipitation/nucleation effect. As Y increases, Al_4MgY forms at increasingly higher temperatures than β - $Mg_{17}Al_{12}$ with a loss of the refinement due to the disappearance of co-precipitation.

Keywords: Magnesium; $Mg_{17}Al_{12}$ refinement; Mg-Al alloys; Tensile Ductility; Compressive strain; Thermodynamic calculations

3.1 Introduction

Magnesium-aluminum based casting alloys (Mg-Al-Mn, Mg-Al-Zn) are the most widely used automotive alloys utilized in interior, under-the-hood and wheel components for vehicle lightweighting, resulting in fuel economy, reduced emissions and performance improvement [1,2]. There is current interest in further developing these alloys for improved ductility and stiffness in order to extend their use in cast structural body applications such as pillars, closures and panels.

In Mg-Al based alloys, the β - $Mg_{17}Al_{12}$ intermetallic phase has a major effect on mechanical properties; it improves strength but also reduces ductility. The β - $Mg_{17}Al_{12}$ phase reduces ductility in various ways. Dislocation pileup at the interface between α -Mg and β -phase can lead to crack

initiation both in the α -Mg and in the $\text{Mg}_{17}\text{Al}_{12}$ phase. Crack propagation through the $\text{Mg}_{17}\text{Al}_{12}$ precipitates can be detrimental if the phase is a continuous network or it has coarse divorced eutectic morphology [3,4]. Lamellar, fibrous and granular morphology is more beneficial for ductility as the crack propagates a short distance before it is stopped at the interface with the ductile α -Mg matrix. It is also expected that strain accumulation leading to crack initiation in the α -Mg phase would be accentuated if the phase morphology is one of sharp edges and the size scale is sufficient to accumulate dislocations at its interface. In commercial alloys, the Al level is kept at 6wt% to attain an optimum combination of ductility and strength. New structural applications in crashworthy automotive components require further improvement of ductility while maintaining the strength levels of Mg-6wt%Al alloys [2,5,6]. The refining of the β - $\text{Mg}_{17}\text{Al}_{12}$ phase can therefore partially prevent its adverse effect on the ductility of Mg-Al alloys.

The beneficial effects of morphological refining are well known in Al-Si alloys [7] where the *trace* additions of Na and Sr can refine the eutectic silicon morphology and greatly improve the ductility. It is also known that the effect occurs only at the optimum addition range that is usually in the 100-200 ppm levels; below the optimum level, the Si phase is under-modified and above the optimum level the modification effect is lost, and the alloy is over-modified. Over-modification is considered to coincide with the formation of a new phase between the addition element (e.g., Sr) and Al. The mechanism of phase modification via Sr is attributed to growth poisoning of the silicon phase by the surface-active Sr segregating to the growth surfaces or the habit planes of the silicon [7].

The refining effect of *trace* additions of Sr and Ca on the grain size and the $\text{Mg}_{17}\text{Al}_{12}$ phase in Mg-Al alloys has been first identified by Koubichek [8] in 1959. Previous work supports the

grain refining effect of ppm Sr additions in AZ91 due to the poisoning of α -Mg grains by a thin layer of Sr which retards the growth [9].

In recent years, more work has been carried out on the refining of Mg alloys via Sr or Sb [10]. Table 3.1 summarizes work carried out in the last decade on the modification of the $Mg_{17}Al_{12}$; none of the studies include a systematic investigation to determine optimum addition level for phase refinement without the formation of new detrimental phases.

Table 3.1 Studies on the Refinement of the $Mg_{17}Al_{12}$ Phase in Mg-Al Alloys.

Addition/Alloy	Effect on $Mg_{17}Al_{12}$	Optimum level	Ref.
Y /AZ91	Dispersed but also formed Al_2Y		[11]
Y /AZ91	Refined with formation of Al_2Y ; Ductility improvement		[12]
Y/AZ80	Refinement of continuous network; Formation of Al_2Y		[13]
Y/AZ91	Mass fraction decrease with formation of coarse Al_2Y ; enhanced ductility	0.6wt%	[14]
Sn/AZ91	Change from lamellar into fully divorced; enhanced tensile elongation	0.5wt%	[15]
Nd/Mg-4Al	Reduces volume fraction but forms Al_2Nd ; improves ductility		[16]
Ce/Mg-Al	General refinement of the alloy microstructure; Reduced volume fraction of $Mg_{17}Al_{12}$; improves ductility	below 6wt%	[17,18]
Ti/AZ91	Suppression of partially divorced $Mg_{17}Al_{12}$; no effect on ductility		[19]
Er/Mg-Al	Improves ductility		[20,21]

The inherent ductility of the intermetallic second phase is also important. For example, electron compounds with an electron/atom ratio of 3/2 are non-stoichiometric and exist over a composition range; they have partial metallic bonding and exhibit plasticity governed by dislocation core structures and metastable stacking-fault energies as well as grain-boundary deformation mechanisms [22]. The $Mg_{17}Al_{12}$ phase has a cubic crystal A-12 type structure

isomorphous with the α -Mn (cI58) with space group I-43m. Its unit cell consists of 34 Mg atoms and 24 Al atoms and it combines three different types of bonds[23,24]. It presents homopolar bonds among Al atoms, heteropolar bonds between Mg and Al and metallic bond among Mg atoms, $(Al_2)_{12}^{-2} Mg_{24}^{+} Mg_{10}$ [23]. In the literature, the inherent ductility of the $Mg_{17}Al_{12}$ intermetallic is a controversial issue, as on the one hand, researchers consider it as a brittle phase [24–30] according to first principle calculations and experimental results and, on the other hand, this intermetallic is considered to be ductile [31,32]. This is based on a ratio of calculated elastic constants, namely the ratio of the shear modulus (G-resistance to plastic deformation) over the bulk modulus (B-resistance to fracture) where a ratio less than 0.57 indicates a ductile intermetallic (β - $Mg_{17}Al_{12}$ shows a range from 0.46 to 0.68).

In the present study, low level Y additions were made to Mg-6wt%Al (Mg-6Al) alloy based on its potential effect for $Mg_{17}Al_{12}$ phase refinement. Microstructural investigation using scanning and transmission electron microscopy (SEM, TEM) was carried out to understand β -phase modification with *trace* levels of Y. Thermodynamic calculations and experiments were performed to study phase selection and solidification paths in Mg-6Al-(Y) alloys. The effect β -phase modification on the mechanical properties of the Mg-6Al-(Y) alloys was determined.

3.2 Experimental Procedures

Four different alloys (Table 3.2) were synthesized using commercial purity (99.98%) Mg ingot (Magnesium Electron), 99.9% pure Al granules (Alfa Aesar) and 99.9% pure Y rods (Hefa Rare Earth Canada). Pure Mg was heated to 700 °C inside a graphite crucible in a Norax Canada Induction Furnace under a protective atmosphere of CO_2/SF_6 gas (0.553% SF_6 and balanced CO_2); the alloying elements were added at 720 °C and held for 20 minutes at temperature; the molten

metal was then stirred and skimmed and the alloys were poured under protective atmosphere into a preheated (400 °C) steel mold to produce flat plates (6mm thickness).

Inductively coupled plasma atomic-emission spectroscopy (ICP-AES) was used to determine the chemical composition (Table 3.2). The Alloy 1 where Y actual level was very low was also analyzed with laser ablation inductively coupled plasma mass spectrometry (LA-ICP-MS) as it was challenging to detect *trace* level Y likely due to its partitioning to defects, an effect also seen in rare earth additions to Mg [33].

Table 3.2 Chemical composition of the alloys.

Target Alloy*	Al (wt%)	Y (ppm)	Mn*** (wt%)	Fe*** (wt%)	Si*** (wt%)
Mg-6Al	6.23	-	0.015	0.027	0.004
Alloy 1	6.28	0.2-1.5**	0.015	0.023	0.004
Alloy 2	6.18	130	0.004	0.009	0.003
Alloy 3	6.16	280	0.014	0.010	0.005

*Mg: balance **Average from LA & ICP AES*** Impurities from the raw materials

Tensile test specimens with a gauge length of 25 mm were machined from the cast samples according to the ASTM E8 standard. The elongation was measured by an extensometer. Compressive test samples with a diameter of 5 mm and a height of 7.5 mm were also machined from the castings. Tensile and compression testing (MTS 810-100kN servo-hydraulic machine) were conducted at room temperature with a strain rate of 0.001 s⁻¹. Boron nitride was used as lubricant on mica sheets for the compression test.

Specimens for microstructural analysis were prepared by manual grinding with a series of SiC papers and then polishing with colloidal silica. Hitachi SU3500 scanning electron microscope (SEM,) with an energy dispersive X-ray spectroscopy (EDS) detector was used for microstructural investigation. A Nikon-Epiphot 200 optical microscope was used to measure

the grain size of the alloys after etching at room temperature. The etchant contained 4.2 gr picric acid, 10 ml acetic acid, 10 ml distilled water and 70 ml ethanol. Crystallographic information of the cast alloys was obtained by X-Ray Diffraction (XRD) using a Bruker D8 Discovery X-Ray Diffractometer (Cu source) after stress annealing at 260 °C for 1 hour as described in [2]. The samples were prepared by grinding and polishing before the heat treatment to create a flat surface.

For the transmission electron microscopy (TEM), a diamond saw was used to cut thin foils from the tensile samples gauge length that were mechanically ground with a series of SiC paper to reduce the thickness to 100 µm. A hole-punch was used to obtain 3 mm discs that were jet-polished in a Struers Tenupol 3 jet polisher. A solution of 10% perchloric acid at -30 °C was used for jet polishing. To investigate the correlation between the Al-Mg-Y and Mg₁₇Al₁₂ precipitates another TEM sample was prepared using focused ion beam (FEI Helios Nanolab 660 DualBeam-FIB) cutting the two phases at the same time. The TEM images were acquired using a FEI Tecnai G² F20 Cryo-STEM microscope operating at 200 kV.

3.3 Results and Discussion

3.3.1 Mechanical Properties

Tensile tests at room temperature were conducted on as-cast alloys to investigate the effect of the Y additions on mechanical properties. Compression tests were also conducted at room temperature to eliminate the effect of these defects such as porosity and inclusions on tensile ductility.

The average tensile ductility (EI) of Mg-6Al increases ~63% with the *trace* addition of Y (Alloy 1) however, it decreases for higher additions of Y (Table 3.3). The same trend is followed in the ultimate tensile strength (UTS) which increases 14% while the yield strength (YS) remains almost constant.

Table 3.3 Room temperature average tensile properties.

	Mg-6Al	Alloy 1	Alloy 2	Alloy 3
UTS (MPa)	206 ± 5	235 ± 13	185±8	207 ± 8
YS (MPa)	74 ± 6	72 ± 11	64±2	71 ± 8
El (%)	8 ± 2	13 ± 3	8±1	9 ± 1

Table 3.4 Room temperature average compression properties.

	Mg-6Al	Alloy 1	Alloy 2	Alloy 3
UCS (MPa)	276 ± 8	271 ± 3	233±6	263 ± 4
CYS (MPa)	105 ± 8	97 ± 5	86±2	103 ± 4
Strain (%)	23 ± 1	28 ± 2	21±3	22 ± 2

The effect of *trace* Y is also seen on compressive properties (Table 3.4). The strain to fracture increases 22% with the *trace* Y addition and it decreases with higher Y levels following the same trend as the elongation in the tensile test. The results reveal the significantly positive effect of only a *trace* level of Y (which is 0.2-1.5 ppm as per ICP analysis) on the ductility of the Mg-6Al alloy. It is also noted that the beneficial effect of Y is lost when Y content increases to 100 ppm. The tensile and compression stress-strain curves in terms of strain to fracture are shown in Fig. 3.1.

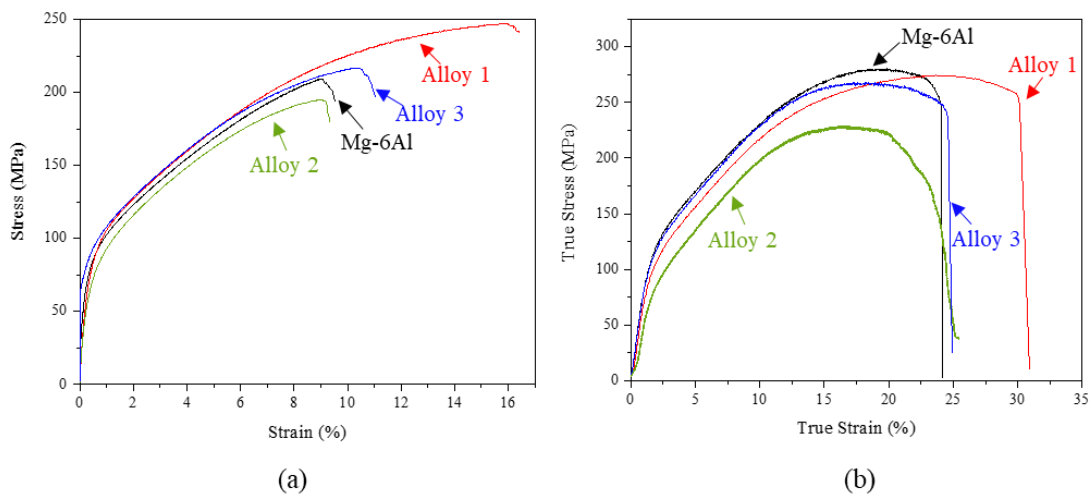


Fig. 3.1 (a) Tensile and (b) compression stress-strain curves for the best performing samples. The best performing samples were considered to have the effects of casting defects removed.

3.3.2 Alloy Microstructures, Phase Selection and Mg₁₇Al₁₂ Refinement

The SEM micrographs of the four alloys in the as-cast condition are shown in Fig. 3.2. The findings are summarized in Table 3.5. Mg-6Al and Alloy 1 possess divorced Mg₁₇Al₁₂ eutectic and Mg-Al-Fe-Mn phases. Alloy 2 and Alloy 3 contain divorced Mg₁₇Al₁₂ eutectic, Mg-Al-Mn-Fe-Y and Mg-Al-Y precipitates.

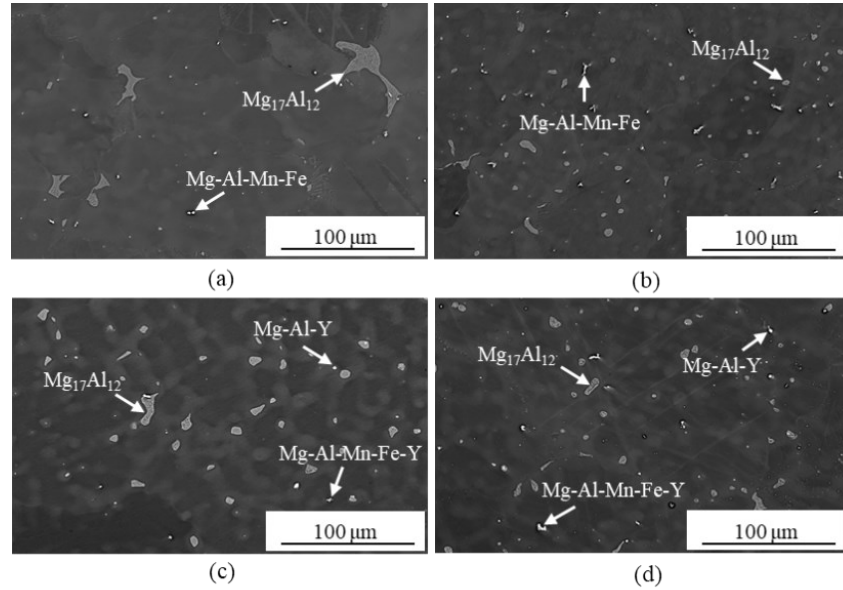


Fig. 3.2 As-cast microstructures of (a) Mg-6Al, (b) Alloy 1, (c) Alloy 2, (d) Alloy 3.

Table 3.5 Phases in the Alloys as determined via SEM/EDS.

Alloy	Phases
Mg-6Al	α -Mg, β -Mg ₁₇ Al ₁₂ partially divorced, Mg-Al-Fe-Mn, Al enriched interdendritic regions
Alloy 1	α -Mg, β -Mg ₁₇ Al ₁₂ partially divorced, Mg-Al-Fe-Mn, Al enriched interdendritic regions
Alloy 2	α -Mg, β -Mg ₁₇ Al ₁₂ , Mg-Al-Mn-Fe-Y, Mg-Al-Y, Al enriched interdenditic regions
Alloy 3	α -Mg, β -Mg ₁₇ Al ₁₂ , Mg-Al-Mn-Fe-Y, Mg-Al-Y, Al enriched interdenditic regions

Alloy 1:

The alloy microstructure (Fig. 3.2b) exhibits significant refinement of the Mg₁₇Al₁₂ compared to the base alloy. Neither the α -Mg matrix nor any of the phases give Y signal in SEM/EDS analysis.

Alloys 2 and 3:

Alloy 2 and Alloy 3 microstructures (Fig. 3.2 c, d) are more refined than the base alloy, but the $Mg_{17}Al_{12}$ is slightly coarser in Alloy 2. Yttrium is not detected in the α -Mg matrix in these alloys (Fig. 3.3). Yttrium is found as Mg-Al-Y phase or in the Mg-Al-Mn-Fe precipitates. Some but not all of the Mg-Al-Y and Mg-Al-Mn-Fe precipitates (with or without Y) are associated with β - $Mg_{17}Al_{12}$ (Fig. 3.3). The close association may be an indication that they have a nucleating or a co-precipitation role in the formation of $Mg_{17}Al_{12}$. These particles can be coarse or fine, but it is expected that only the finer particles can function as effective nucleants for the $Mg_{17}Al_{12}$ phase.

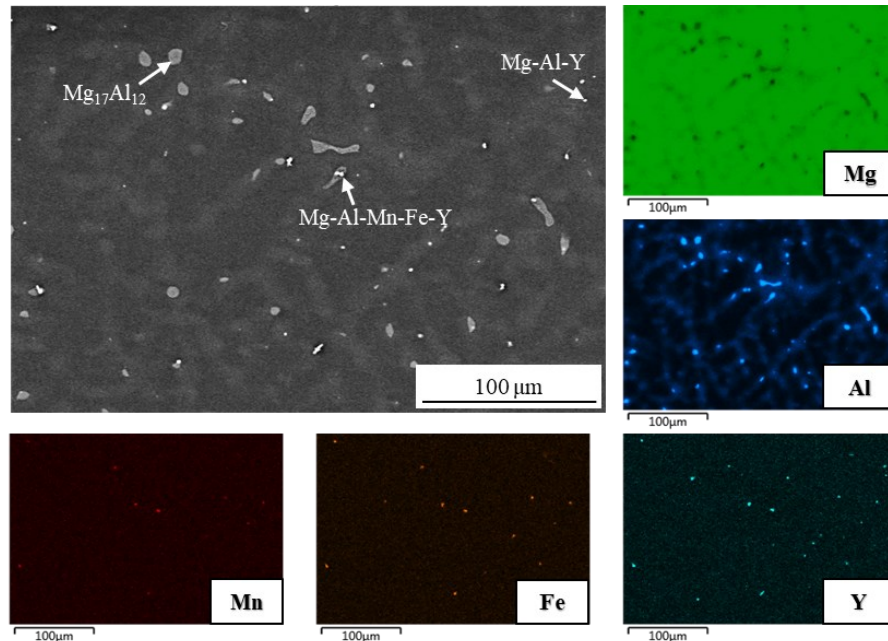


Fig. 3.3 EDS mapping analysis in Alloy 2 (100ppmY). Alloy 3 (300ppmY) has similar microstructure.

The SEM images of Fig. 3.2 were analyzed with the ImageJ software [34] (~ 1000 $Mg_{17}Al_{12}$ and ~ 300 Mg-Al-Mn-Fe-(Y) particles analyzed) to determine the effect of Y on the size of the second phases (Table 3.6). The area fraction of β - $Mg_{17}Al_{12}$ slightly increases in Alloy 1 and decreases with high Y additions (Alloy 2&3). Additionally, the β - $Mg_{17}Al_{12}$ size decreases 47% for

trace Y addition (Alloy 1) and then it increases again with higher Y amounts. The standard deviation of the size also decreases with *trace* Y showing that the morphology of the island-like β -phase becomes more regular. It is observed that the area fraction of Mg-Al-Mn-Fe phase also increases with *trace* Y addition (Alloy 1) and then decreases again with higher Y amounts. Its size follows similar trend with $Mg_{17}Al_{12}$ phase where it decreases in Alloy 1, and it becomes coarser with higher amounts of Y amount. Mg-Al-Y forms only in Alloy 2 & 3 which becomes coarser as Y level increases. The α -Mg grain size of Alloy 1 decreases 11% compared to the binary Mg-6Al and it increases with higher additions of Y. The grain coarsening with Y addition has been reported previously [35,36] and has been related to the coarsening of the pro-peritectic Al_2Y phase [37]. The present results show that the effect of *trace* Y is different from the effect of higher levels of Y additions. There is a refining effect of *trace* level of Y on the β -phase, Mg-Al-Mn-Fe precipitates and α -Mg matrix. Importantly the refining effect is lost as the Y level increases from *trace* levels (Alloy 1) to higher Y amounts (Alloy 2 & 3). This effect is very similar to the grain refining effect of Sr on AZ91 alloy [9] where a loss of grain refining occurs at levels higher than 200 ppm Sr.

Table 3.6 Effect of Y addition on the size and area fraction of second phases.

Alloys	$Mg_{17}Al_{12}$ Area fraction (%)	$Mg_{17}Al_{12}$ Size (μm^2)	Mg-Al- Mn-Fe- (Y)* Area fraction (%)	Mg-Al- Mn-Fe- (Y)* Size (μm^2)	Mg-Al-Y Area fraction (%)	Mg-Al-Y Size (μm^2)	α -Mg Grain Size (μm)
Mg-6Al	0.97 \pm 0.40	32 \pm 15	0.09 \pm 0.05	1.56 \pm 0.06	-	-	96 \pm 13
Alloy 1	1.44 \pm 0.66	17 \pm 5	0.12 \pm 0.03	1.41 \pm 0.20	-	-	85 \pm 15
Alloy 2	1.22 \pm 0.35	24 \pm 5	0.04 \pm 0.01	1.97 \pm 0.56	0.04 \pm 0.02	2.74 \pm 0.68	104 \pm 14
Alloy 3	0.7 \pm 0.40	22 \pm 12	0.08 \pm 0.02	4.01 \pm 0.62	0.03 \pm 0.02	3.47 \pm 0.74	98 \pm 8

*Y is present in Mg-Al-Mn-Fe phase only in Alloy 2 & 3

3.3.3 The Effect of Mg₁₇Al₁₂ Refinement on Ductility

One of the questions that can be raised at this time is whether the improvement in the ductility of Mg-6Al is due to the refinement of the β -phase, the Mg-Al-Mn-Fe, or the grain size. To assess the effect of the microstructure on ductility, polynomial regression analysis was conducted with the Minitab software. The statistical coefficients calculated by the software are: the standard error S which shows the standard deviation between the data and the fitted values; the $R^2_{(adj)}$ which represents the modified R^2 and it shows how close the data are to the fitted line from the regression; the P value is the probability that shows the evidence against the null hypothesis (lower probability means stronger evidence against the null hypothesis) [38]. According to the analysis of variance (ANOVA), for the tensile ductility, the only significant factor is the size of Mg₁₇Al₁₂ ($R^2_{(adj)}$ =99.98% with standard error S= 0.0351012 and P=0.009). The resulted equation showing the relationship of %El with Mg₁₇Al₁₂ size is: $\%El = 44.38 - 2.648 Mg_{17}Al_{12} Size + 0.04724 Mg_{17}Al_{12} Size^2$.

For the other variables, i.e., α -Mg grain size, the area fraction of Mg₁₇Al₁₂ and Mg-Al-Mn-Fe-(Y) and the size of the latter, the R^2 is lower, and the P value is much higher than the significance level (=0.05) that prove that only the size of Mg₁₇Al₁₂ has a significant effect on ductility. However, the regression on compression strain to fracture shows that again the size of Mg₁₇Al₁₂ has significant effect ($R^2_{(adj)}$ = 99.84%, S=0.122854, P=0.023) but also the area fraction of Mg-Al-Mn-Fe-(Y) ($R^2_{(adj)}$ = 99.99%, S=0.0225992, P=0.004) and α -Mg grain size ($R^2_{(adj)}$ = 94.04%, S=0.759051, P=0.020) can significantly affect the strain to fracture. It is likely that the latter has an effect on shear deformation.

3.3.4 The Role of Y on Mg₁₇Al₁₂ Refinement

Several other questions can be asked with respect to the role of Y on β -Mg₁₇Al₁₂ refinement. What is the mechanism of β -Mg₁₇Al₁₂ refinement with Y? Why is the *trace* level Y more effective than 100-300ppm levels? Are the same mechanisms involved in all three alloys? Both experimental investigation and thermodynamic calculations were performed to understand the role of Y on β -Mg₁₇Al₁₂ refinement.

3.3.4.1 Experimental Study

The Effect of Y on β -Mg₁₇Al₁₂ Lattice Parameters

XRD was used to investigate if there was any crystallographic change of the β -phase (Fig.3.4). Five bulk samples from different areas of each alloy were analyzed after stress annealing at 260 °C for 1 hour to reduce internal stresses. The XRD patterns were refined at 2θ : 35.6°-45° (the only strong peaks for Mg₁₇Al₁₂) using Rietveld refinement with the GSAS II software [39] to obtain information about the lattice parameter a and cell volume of Mg₁₇Al₁₂ (Table 3.7). No Mg-Al-Mn-Fe-(Y) was detected. Mg₁₇Al₁₂ presents a large range of lattice parameters due to its wide chemical composition range [2]. Zhang et al. report that the range varies from 1.050nm to 1.069 nm and it is associated with the different orientation relationships of the phase with the Mg matrix [40]. The lattice parameter and by extension the cell volume of Mg₁₇Al₁₂ show an increasing trend for Alloy 1 and Alloy 2, but with further Y addition (Alloy 3) they decrease. It is likely that at low Y levels, Y incorporates into the crystal structure of β - phase changing slightly the lattice parameter, but when it is added in higher amount, then there is a preferential reaction to form Y-enriched secondary phases.

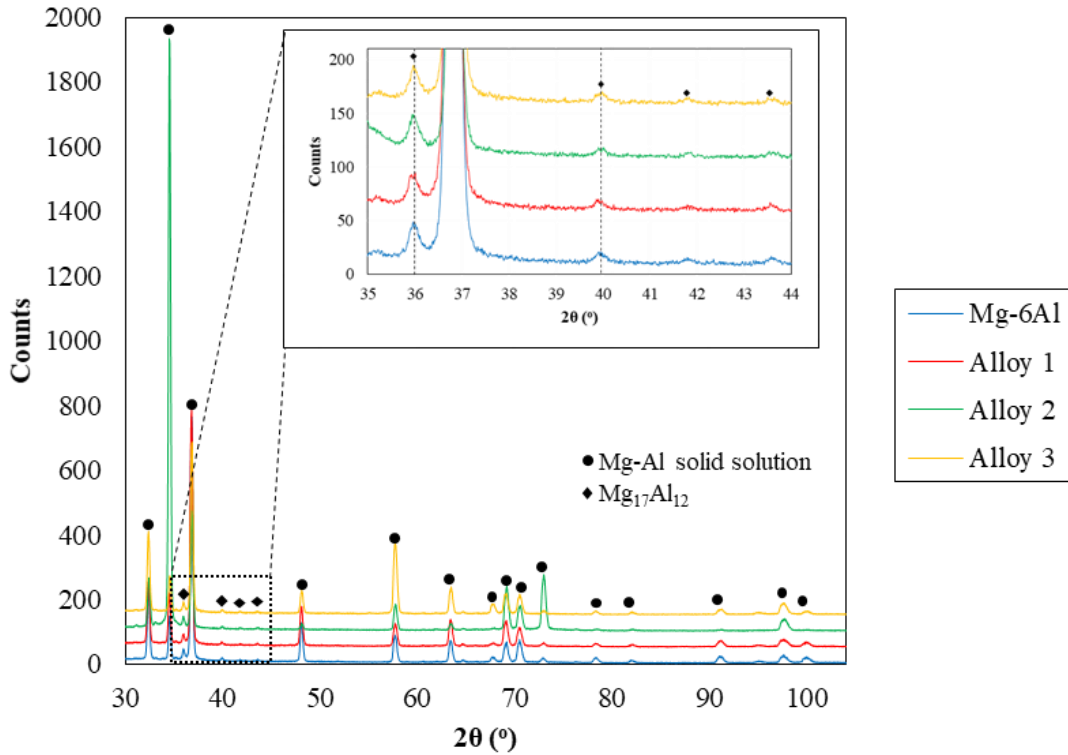


Fig. 3.4 XRD diffraction peaks.

Table 3.7 Average lattice parameter of $Mg_{17}Al_{12}$ after XRD pattern refinement

Alloys	a (Å)	Cell Volume (Å ³)	Weight fraction
Mg-6Al	10.5841 ± 0.0014	1185.68	0.034 ± 0.003
Alloy 1	10.5856 ± 0.0019	1186.18	0.036 ± 0.002
Alloy 2	10.5871 ± 0.0025	1186.67	0.039 ± 0.006
Alloy 3	10.5849 ± 0.0018	1185.92	0.033 ± 0.002

Yttrium in the Microstructure

TEM analyses were conducted to further investigate the role of Y in the microstructure. TEM/EDS analyses were performed on Mg-6Al, Alloy 1 and Alloy 3. Table 3.8 summarizes the phases observed via TEM. Further details are discussed below.

Table 3.8 Phases observed in FIB and TEM analysis.

Alloys	Mg ₁₇ Al ₁₂ size (FIB) (μm^2)	Mg ₁₇ Al ₁₂ depth in matrix (TEM cross section) (μm)	Mn enriched phase (μm^2)	MgAlY phase (μm^2)
Mg-6Al	31	2	0.009-0.5	-
Alloy 1	18.5	0.8	-	-
Alloy 3	11	2.7	1.3	0.3

Alloy 1 (0.2-1.5 ppm Y): TEM/EDS was not able to determine the location of Y either the α -Mg matrix or in any of the precipitates of Alloy 1 even though the bulk chemical analysis of Alloy 1 gives Y in the composition, albeit at very low levels. It is recently reported via atom probe tomography [33] and SEM/EDS [41] that rare earth elements segregate to defects (surfaces, interfaces, grain boundaries, dislocations, stacking faults due to their surface active nature where the solute decreases the energy of the defect. The Density Functional Theory defines this as the change in Gibbs energy relative to the concentration gradient between the bulk alloy and the surface. Yamauchi [42] model defines that when the Wigner-Seitz radius (r) of the solute element is larger than the host (r_Y : 0.2 nm [43], r_{Mg} : 0.14 nm [44]), then surface segregation occurs because of the accompanying reduction in surface energy. Yamauchi showed that when $\rho = r_{\text{solute}}/r_{\text{host}}$ is above 1 surface segregation is likely. Surface segregation is not seen only for rare earth solutes. D. Aydin et al [45] have shown the surface activity of Sr in Mg and its role in oxidation and ignition of Mg.

Alloy 3 (280 ppm Y): TEM analysis of the alloy (Fig. 3.5a & b) shows dislocations pile-up at the interface of Mg-Al-Mn-Fe-Y (the chemistry identified by spot EDS analysis) that may lead eventually to crack initiation. The TEM image (Fig. 3.6) shows the association of Mg₁₇Al₁₂ with AlMgY precipitate. The two precipitates as well as the matrix were cut with FIB (Fig.3.6a) in order

to examine this specific area under TEM (Fig.3.6b). The scanning transmission electron microscopy (STEM) mapping of the precipitates (Fig.3.7) shows a polygonal (nearly square) precipitate close to the edge of $Mg_{17}Al_{12}$ phase where Y, Al and Mg exist. The diffraction pattern of the phase (Fig.3.6 b) was indexed with ImageJ and CrystTBox [46] softwares that show that the phase matches the hexagonal $AlMgY$ precipitate [47]. The diffraction pattern also shows spot splitting and satellite spots which can occur due to the presence of dislocations inside the precipitate [48].

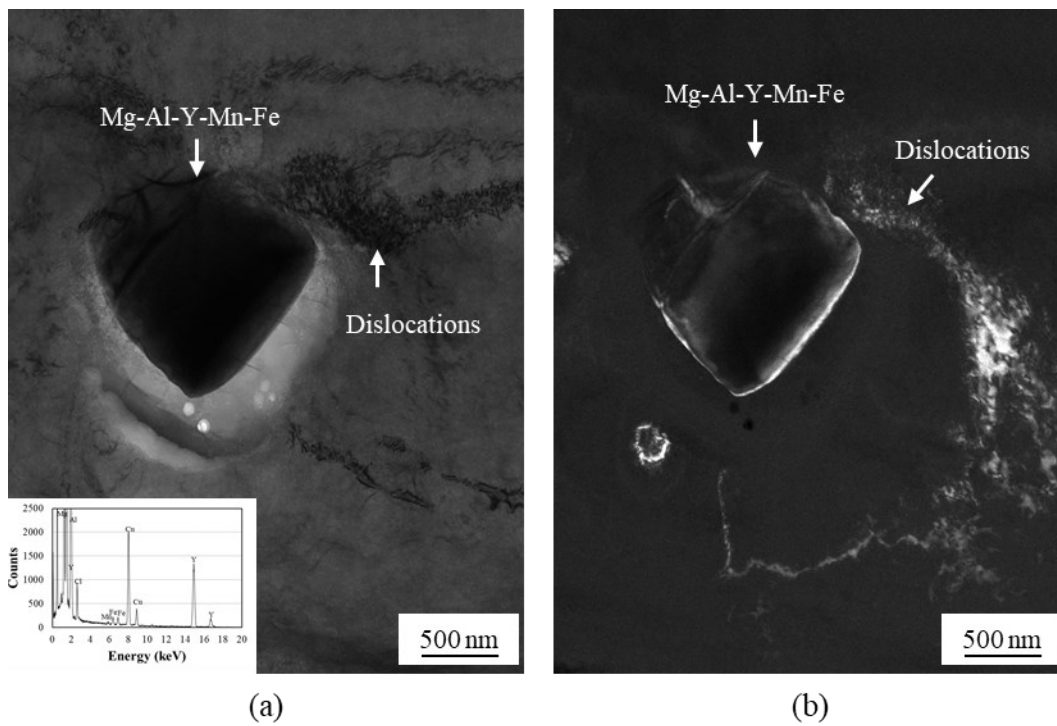


Fig. 3.5 TEM investigation on Alloy 3 (300 ppmY) with Mg-Al-Y-Mn-Fe precipitate as per EDS (Cu signal is coming from the holder and Cl is impurity from the sample preparation) (a) Bright field (b) Dark field imaging.

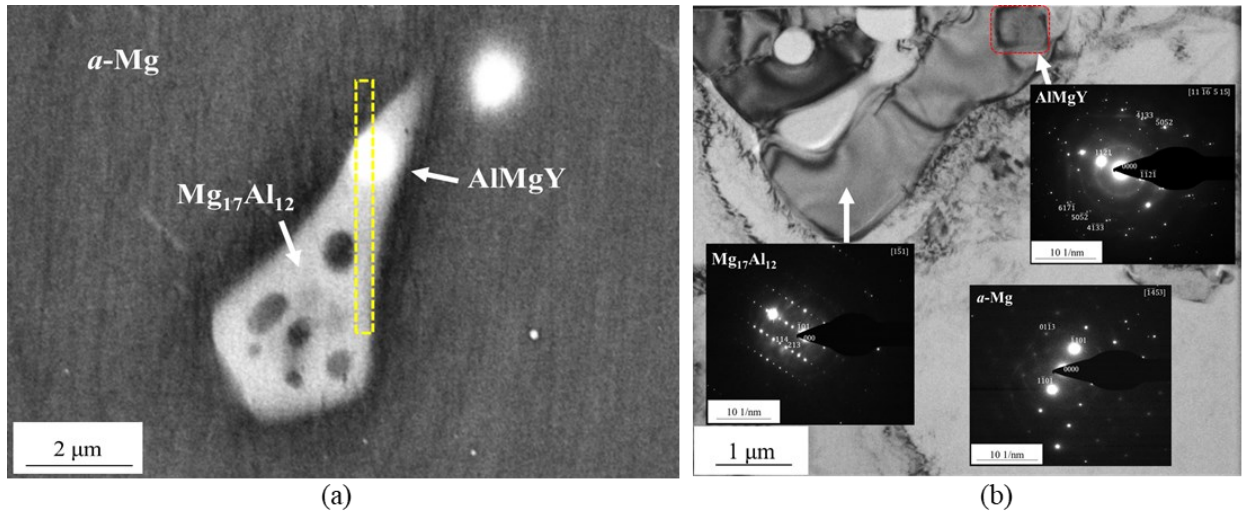


Fig. 3.6 (a) SEM-BSE (Alloy 3) image showing the association of AlMgY particle with Mg₁₇Al₁₂. The yellow square dot line shows the area where the TEM cross section sample was extracted. (b) TEM bright field imaging. In red dot line is the AlMgY precipitate.

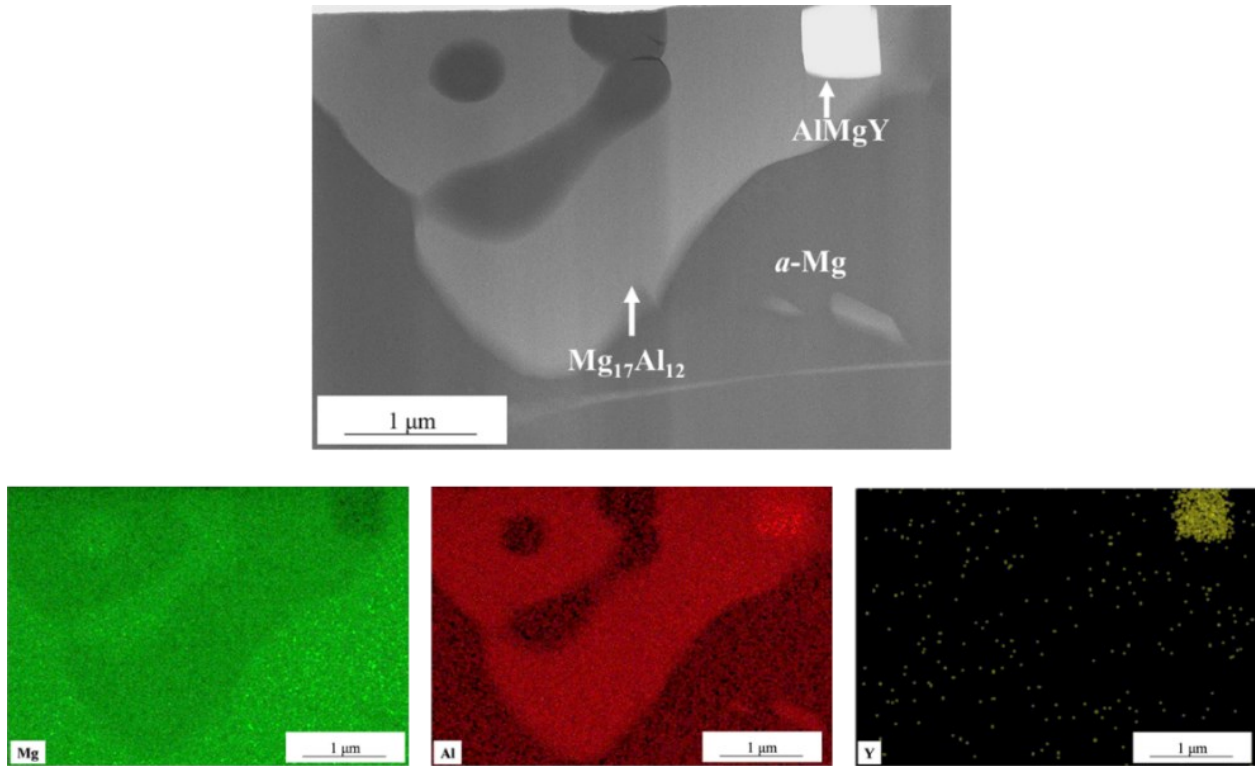


Fig. 3.7 HAADF image with the 3 elemental maps for Mg, Al and Y.

High resolution TEM (HRTEM) imaging was obtained at the interface of $Mg_{17}Al_{12}$ and AlMgY precipitates (Fig. 3.8a). Fast Fourier Transformation (FFT) was applied to the acquired image using the Digital Micrograph software and then by applying a mask and inverse FFT, the contrast was enhanced making visible the details of the interface (Fig. 3.8b). The interface between the two precipitates is semi-coherent, with misfit dislocations relaxing the interfacial strain. Some dislocations appear inside the AlMgY phase as also observed in the diffraction pattern but none in the $Mg_{17}Al_{12}$. The near-coherency of the interface strongly suggests that AlMgY phase acted as nucleation point of the β -phase. As it is known [49] from aging precipitation sequence that precipitates lose coherence with the matrix or the associated phases as they grow, it can be suggested that when finer, the AlMgY could have increased coherency with the β -phase.

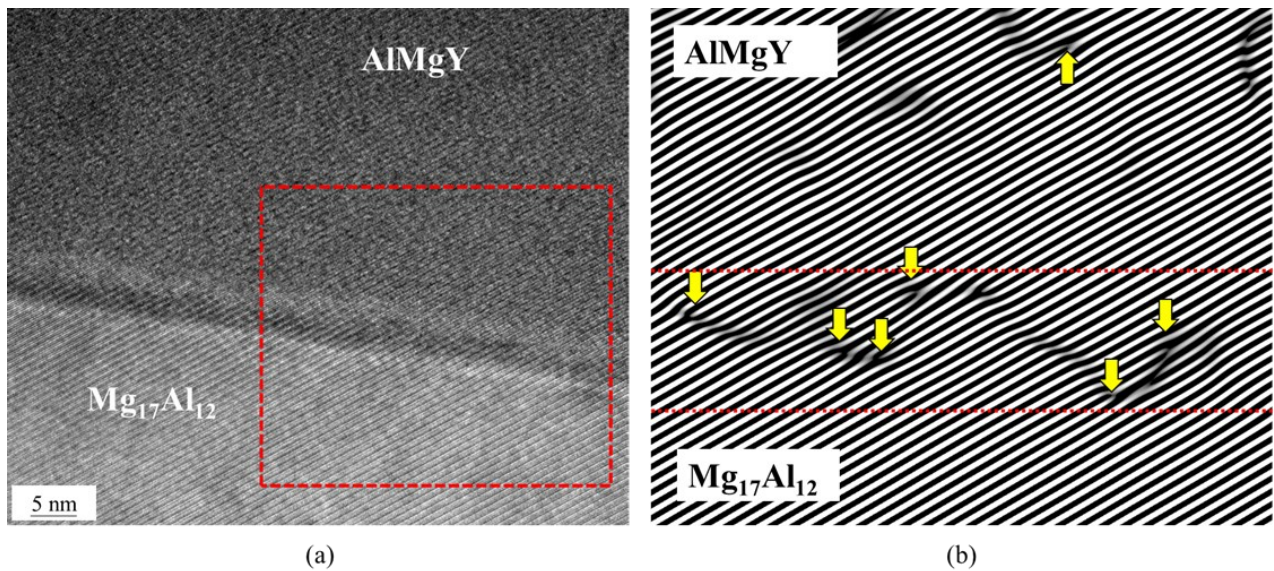


Fig. 3.8 (a) HRTEM of the AlMgY/ $Mg_{17}Al_{12}$ interface with the corresponding FFT. The region where further analysis was conducted appears in the red dotted square. (b) Inverse FFT imaging of the interface. The area in the square depicts the interface and the yellow.

3.3.4.2 Thermodynamic Simulations

Thermodynamic calculations based on the CALPHAD method (FactSage with FTlite database) [50] have been performed in equilibrium and non-equilibrium conditions (Scheil cooling) for Mg-

6Al binary system and Mg-6Al-xY alloys with Fe, Si and Mn impurities using the compositions of ICP (Table 3.2), to predict the formation of second phases in the Mg matrix. Scheil cooling assumes that no solute back diffusion occurs in the solid phase and that the local concentration of the solid remains constant during the solidification.

The equilibrium isopleth of the Mg-6Al-(0-0.1) Y system given in Fig. 3.9 indicates that, at room temperature, alloys 1, 2 and 3 possess α -Mg, $\text{Al}_{13}\text{Fe}_4$, Mg_2Si , $\text{Mg}_{17}\text{Al}_{12}$ and Al_4MgY . The solidification path for Alloys 1, 2 and 3 is similar with the main two differences:

- 1) At $\sim 540^\circ\text{C}$ the Al_8Mn_5 phase forms in Alloy 1 and Alloy 2 instead of the Al_3Y which forms in Alloy 3 (Fig. 3.9, #12 and #7 respectively) and
- 2) At 525°C where the Al_3Y forms earlier in the Alloy 2 and Alloy 3 (Fig. 3.9, #14).

Al_4MgY starts to form in Alloy 1, Alloy 2 and Alloy 3 as a result of the solid-state reaction of Al_3Y with α -Mg at temperatures $\sim 470^\circ\text{C}$. Notably, as shown in Fig. 10, the aluminum range of Al_4MgY phase coincides with the aluminum range of $\text{Mg}_{17}\text{Al}_{12}$ ($\sim 43\text{-}45\text{ wt}\%$). Al_4MgY phase was first detected by Zarechnyuk et al [51] as having MgZn_2 structure with lattice parameters of $a=0.533\text{nm}$ and $c=0.857\text{ nm}$.

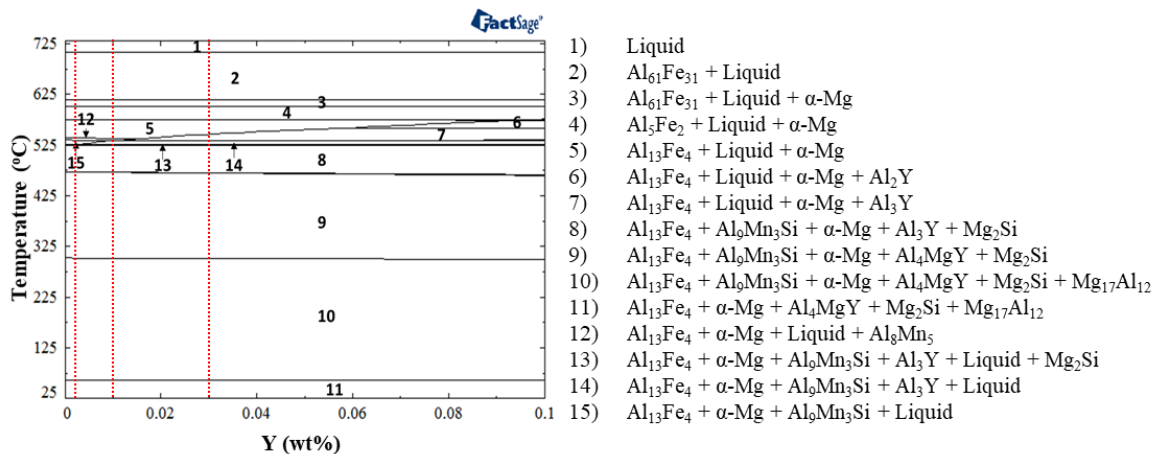


Fig. 3.9 Equilibrium isopleth for Mg-6Al-(0-0.1) Y showing the solidification path for alloys 1, 2, 3 (round dot vertical lines).

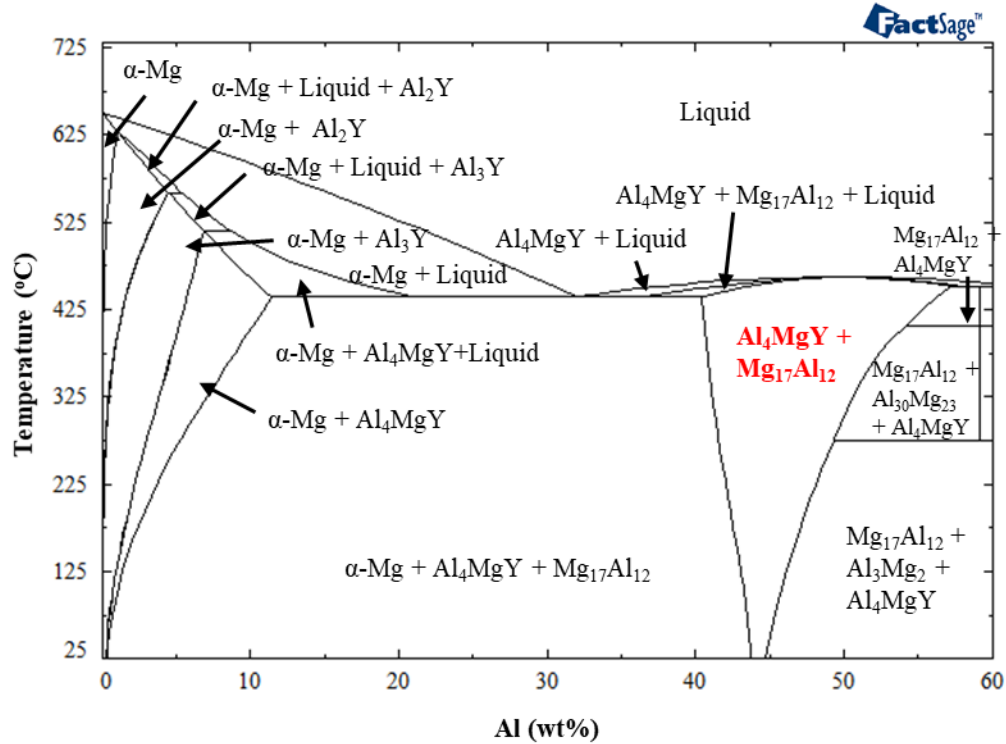
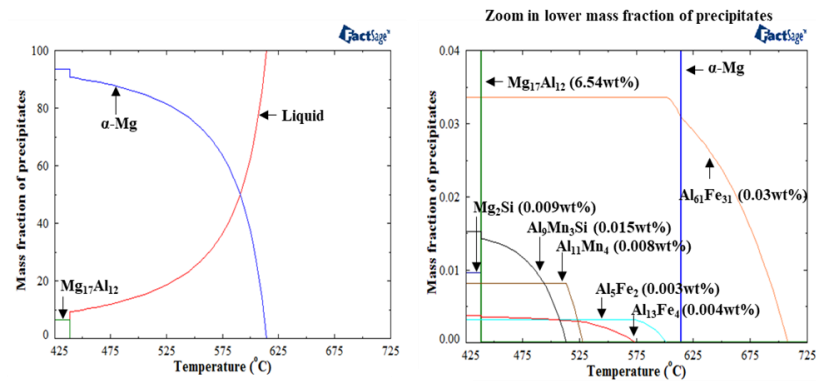


Fig. 3.10 Equilibrium phase diagram of Mg-Al-Y with 0.03wt%Y showing the aluminum range of Al_4MgY and $\text{Mg}_{17}\text{Al}_{12}$ (~ 43-45 wt% Al).

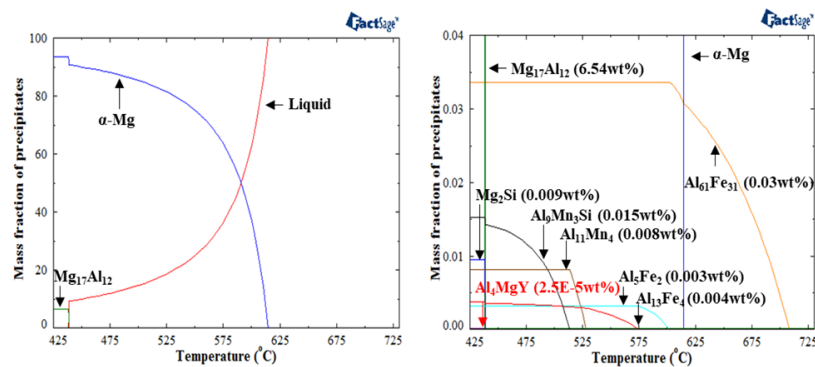
Non-equilibrium (Scheil) calculations were also performed for different Y compositions (Fig. 3.11) using the ICP results for Al, Fe, Mn and Si. The amount of Al_4MgY increases and $\text{Mg}_{17}\text{Al}_{12}$ does not change significantly with increasing Y in the alloy (up to 300ppmY). The Al_4MgY starts to precipitate at very low Y levels (Fig. 3.11b) and for higher additions (Fig. 3.11.c&d) its mass fraction increases.

It is noted that SEM, XRD and thermodynamic simulation results indicate that the mass fraction of $\text{Mg}_{17}\text{Al}_{12}$ does not change significantly but there is a trend in the area fraction (from the SEM results). Area fraction is not always the same as volume fraction and the differences can be accentuated by morphology. The β -phase is not a spherical phase; it has usually a long and bulky morphology but with the *trace* level of yttrium addition, it assumes a mixture of long/bulky and nodular/dispersed morphologies (Fig.3.2). The area we see in SEM images is the cross section

of these phases; when the area fraction increases, we likely have a finer and more dispersed phase that demonstrates increased area fraction values in 2D images. Hence, area fraction can be associated with refinement and it is that parameter that was used in the regression analysis. The most significant result of the thermodynamic calculations with respect to the mechanism of β -phase refinement in Alloy 1 is related to the precipitation temperatures of Al_4MgY and $Mg_{17}Al_{12}$. The precipitation temperatures of Al_4MgY and $Mg_{17}Al_{12}$ coincide at 438 °C for low Y levels e.g., Alloy 1 (Fig. 3.11b) and as Y level increases e.g., Alloy 3 (Fig. 3.11d) the Al_4MgY precipitates at higher temperatures (~ 500 °C) before the solid-state formation of the $Mg_{17}Al_{12}$ phase at 438 °C which is the end of the solidification. The stoichiometry of the precipitate from the TEM analysis is not the same as the one predicted from thermodynamic calculations. That could be attributed to the metastable state of the $AlMgY$ precipitate which may be a precursor to Al_4MgY .



(a)



(b)

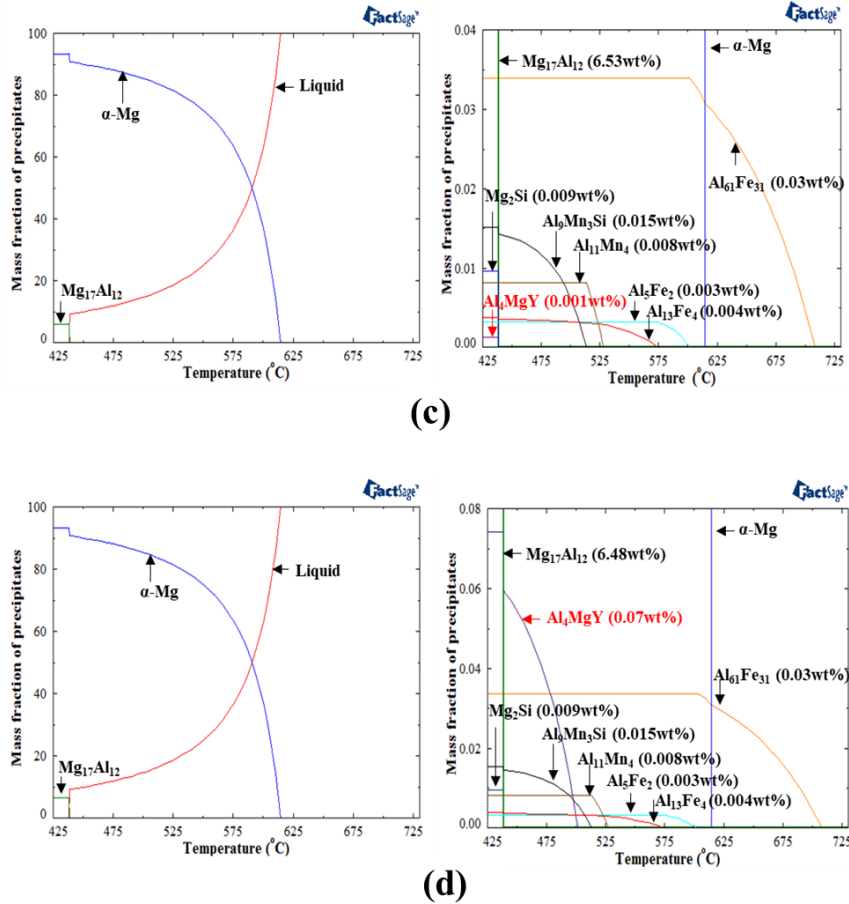


Fig. 3.11 Non-equilibrium calculations with (a) 0ppmY, (b) 0.1ppmY, (c) 5ppmY, (d) 300ppmY. The wt% in the parentheses present the amount of each precipitate in the end of solidification.

In Mg-6Al, $Mg_{17}Al_{12}$ phase forms through a eutectic reaction $L \rightarrow \alpha-Mg + \beta-Mg_{17}Al_{12}$. A similar effect was reported by Wang et al [10] who have observed the refinement of the $\beta-Mg_{17}Al_{12}$ phase via Sb addition through an inoculation mechanism wherein Mg_2Si precipitates refined by Sb act as nuclei for the $Mg_{17}Al_{12}$ phase. In our work, fine Al_4MgY precipitates would act as nuclei for the $Mg_{17}Al_{12}$ phase which precipitates. Hence, when low Y is present, the likelihood for the nucleation of the $Mg_{17}Al_{12}$ phase and its refinement by Al_4MgY is strong. This mechanism may

not occur when the Y level is higher where the Al_4MgY may be too coarse (size of MgAlY is $3.47 \mu\text{m}^2$ from Table 3.6) to substantially refine the $\text{Mg}_{17}\text{Al}_{12}$.

3.4 Conclusions

- 1) Low level of yttrium (Y) additions made to Mg-6Al reveals that *trace* level (0.2-1.5 ppm) of Y bulk value lead to 47% refinement of the $\beta\text{-Mg}_{17}\text{Al}_{12}$ phase and a refinement in the Mg-Al-Mn-Fe phase. The refinement is lost, and the trends reverse for higher values of bulk Y content (100-300 ppm).

Trace level bulk Y causes increase in the area fractions of $\beta\text{-Mg}_{17}\text{Al}_{12}$ and Mg-Al-Mn-Fe phases; the trends reverse for higher bulk Y levels.

- 2) Sixty three percent (63%) increase in tensile ductility and fourteen percent (14%) increase in ultimate tensile strength are obtained at the *trace* level of Y addition. There is also more than 20% increase in compressive strain to fracture. Higher values of bulk Y content (100-300 ppm) result in loss of the ductility and strength improvements obtained at the *trace* level of Y.
- 3) The grain size of $\alpha\text{-Mg}$ decreases in Alloy 1 but increases for higher Y additions.
- 4) A significant relationship is obtained between $\beta\text{-Mg}_{17}\text{Al}_{12}$ phase refinement and tensile ductility yielding the equation $\%El = 44.38 - 2.648 \text{ Mg}_{17}\text{Al}_{12} \text{ Size} + 0.04724 \text{ Mg}_{17}\text{Al}_{12} \text{ Size}^2$ with $R_{(\text{adj})}^2=99.98\%$. Other changes in the microstructure do not show a strong relationship to tensile ductility.
- 5) Compressive strain to fracture has strong relationships with the refinement of the $\beta\text{-Mg}_{17}\text{Al}_{12}$, Mg-Al-Mn-Fe phases and $\alpha\text{-Mg}$ grain size, but it is not affected by the weight fraction of $\beta\text{-Mg}_{17}\text{Al}_{12}$ phase.
- 6) XRD analysis indicated a slight increase in the lattice parameter of $\beta\text{-Mg}_{17}\text{Al}_{12}$ phase which forms at the *trace* level of bulk Y. This change in lattice parameter is lost at the higher Y levels.

- 7) TEM results show that the AlMgY precipitate has a semi-coherent interface with the Mg₁₇Al₁₂ with misfit dislocations.
- 8) Thermodynamic calculations indicate that the alloys contain α -Mg, Mg₁₇Al₁₂ and Al₄MgY and Al-Mn (Si, Fe) phases.
- 9) Non-equilibrium Scheil calculations show that precipitation temperatures of Al₄MgY and Mg₁₇Al₁₂ coincide at 438 °C for *trace* Y levels (e.g., Alloy 1) and as Y increases (e.g., Alloy 3), Al₄MgY precipitates at higher temperature (~500 °C) before the solid-state formation of the Mg₁₇Al₁₂ phase at 438 °C at the end of the solidification. This strongly suggests that, at low Y, the likelihood for the nucleation of the Mg₁₇Al₁₂ phase and its refinement by Al₄MgY is strong, which explains the refinement of Mg₁₇Al₁₂ in Alloy 1. At higher Y, the early precipitation of Al₄MgY phase which may have coarsened when Mg₁₇Al₁₂ forms, can account for the loss of refinement in Alloys 2 & 3.

3.5 Acknowledgements

This project was conducted under the financial support of the Natural Sciences and Engineering Research Council of Canada (NSERC) Discovery Grant (G210358NSERC/RGPIN-2016-05121). The authors thank Pierre Vermette, Dr. Amir Farkoosh, Luis A. Villegas-Armenta for their assistance in alloy casting and discussions as well as the Centre de Métallurgie du Québec-CMQ. Konstantinos Korgiopoulos gratefully acknowledges McGill Engineering Doctoral Award program (MEDA). We are also grateful for the help and assistance of Dr. Xue-Dong Liu (TEM), Dr. Longbo Yang (LA-ICP) and Ms. Weawkamol Leelapornpisit (FIB).

3.6 References

- [1] H.E. Friedrich, B.L. Mordike, Magnesium technology, Springer, 2006.
- [2] M. Avedesian, H. Baker, ASM specialty handbook: magnesium and magnesium alloys.,

- ASM International, Ohio, 1998.
- [3] M.D. Nave, A.K. Dahle, D.H. StJohn, Eutectic growth morphologies in magnesium-aluminium alloys, in: TMS Annu. Meet., 2000: pp. 233–242. doi:10.1002/9781118808962.ch33.
- [4] S. Kleiner, O. Beffort, A. Wahlen, P.J. Uggowitzer, Microstructure and mechanical properties of squeeze cast and semi-solid cast Mg-Al alloys, *J. Light Met.* (2002) 277–280. doi:10.1016/S1471-5317(03)00012-9.
- [5] F. Kaiser, K.U. Kainer, Magnesium alloys and technology, John Wiley & Sons, Weinheim, 2003.
- [6] J. Rowe, *Advanced materials in automotive engineering*, Elsevier, Cambridge, 2012.
- [7] J.E. Gruzleski, B.M. Closset, *The treatment of liquid aluminum-silicon alloys*, Amer Foundry Society, Illinois, 1990.
- [8] L. Koubichek, Effect of small additions of elements on grain size and the refinement of the mg₄al₃ [mg₁₇al₁₂] phase in ml5 alloy. *Izv. Vyschikh. Outchebnykh Za Vedeny, Metall. Non-Ferrous Met.* 6 (1959).
- [9] C.A. Aliravci, J.E. Gruzleski, F.C. Dimayuga, Effect of strontium on the shrinkage microporosity in magnesium sand castings, *AFS Trans.* 100 (1992) 353–362.
- [10] Z. Wang, H. Wang, J. Gong, M. Li, W. Cheng, W. Liang, Modification and refinement effects of Sb and Sr on Mg₁₇Al₁₂ and Mg₂Si phases in Mg-12Al-0.7Si alloy, *China Foundry.* 13 (2016) 310–315. doi:10.1007/s41230-016-5112-0.
- [11] S.-R. Wang, P.-Q. Guo, L.-Y. Yang, Y. Wang, Microstructure and mechanical properties of AZ91 alloys by addition of yttrium, *J. Mater. Eng. Perform.* 18 (2009) 137–144. doi:10.1007/s11665-008-9255-z.

- [12] J. Zhang, X. Niu, X. Qiu, K. Liu, C. Nan, D. Tang, J. Meng, Effect of yttrium-rich misch metal on the microstructures, mechanical properties and corrosion behavior of die cast AZ91 alloy, *J. Alloys Compd.* 471 (2009) 322–330. doi:10.1016/j.jallcom.2008.03.089.
- [13] N. Kashefi, R. Mahmudi, The microstructure and impression creep behavior of cast AZ80 magnesium alloy with yttrium additions, *Mater. Des.* 39 (2012) 200–210. doi:10.1016/j.matdes.2012.02.036.
- [14] H. Cai, F. Guo, J. Su, L. Liu, B. Chen, Study on microstructure and strengthening mechanism of AZ91-Y magnesium alloy, *Mater. Res. Express.* 5 (2018) 36501. doi:10.1088/2053-1591/aab0b7.
- [15] Y. Turen, Effect of Sn addition on microstructure, mechanical and casting properties of AZ91 alloy, *Mater. Des.* (2013) 1009–1015. doi:10.1016/j.matdes.2013.02.037.
- [16] J. Zhang, J. Wang, X. Qiu, D. Zhang, Z. Tian, X. Niu, D. Tang, J. Meng, Effect of Nd on the microstructure, mechanical properties and corrosion behavior of die-cast Mg-4Al-based alloy, *J. Alloys Compd.* (2008) 556–564. doi:10.1016/j.jallcom.2007.10.056.
- [17] J. Zhang, Z. Leng, M. Zhang, J. Meng, R. Wu, Effect of Ce on microstructure, mechanical properties and corrosion behavior of high-pressure die-cast Mg-4Al-based alloy, *J. Alloys Compd.* (2011) 1069–1078. doi:10.1016/j.jallcom.2010.09.185.
- [18] A.K. Chaubey, S. Scudino, K.G. Prashanth, J. Eckert, Microstructure and mechanical properties of Mg-Al-based alloy modified with cerium, *Mater. Sci. Eng. A.* (2015) 46–49. doi:10.1016/j.msea.2014.11.081.
- [19] S. Candan, M. Unal, E. Koc, Y. Turen, E. Candan, Effects of titanium addition on mechanical and corrosion behaviours of AZ91 magnesium alloy, *J. Alloys Compd.* (2011) 1958–1963. doi:10.1016/j.jallcom.2010.10.100.

- [20] S. Sankaranarayanan, B.M. Ng, S. Jayalakshmi, M.G. Kumar, Q.B. Nguyen, M. Gupta, Microstructure and Mechanical Properties of a Magnesium-Aluminium-Erbium Alloy, in: *Magnes. Technol.* 2015, Springer, 2015: pp. 445–449. doi:10.1007/978-3-319-48185-2_82.
- [21] S. Seetharaman, C. Blawert, B.M. Ng, W.L.E. Wong, C.S. Goh, N. Hort, M. Gupta, Effect of erbium modification on the microstructure, mechanical and corrosion characteristics of binary Mg-Al alloys, *J. Alloys Compd.* (2015) 759–770. doi:10.1016/j.jallcom.2015.05.284.
- [22] R.W. Cahn, P. Haasen, *Physical Metallurgy*, Fourth revised and enhanced edition, 1996, Elsevier Science BV, n.d.
- [23] A.A. Kaya, M.O. Pekguleryuz, K.U. Kainer, *Fundamentals of magnesium alloy metallurgy*, Woodhead Publishing, Cambridge, 2013.
- [24] W.-C. Hu, Y. Liu, X.-W. Hu, D.-J. Li, X.-Q. Zeng, X. Yang, Y.-X. Xu, X. Zeng, K.-G. Wang, B. Huang, Predictions of mechanical and thermodynamic properties of Mg₁₇Al₁₂ and Mg₂Sn from first-principles calculations, *Philos. Mag.* 95 (2015) 1626–1645. doi:10.1080/14786435.2015.1040098.
- [25] A.K. Dahle, Y.C. Lee, M.D. Nave, P.L. Schaffer, D.H. StJohn, Development of the as-cast microstructure in magnesium-aluminium alloys, *J. Light Met.* (2001) 61-72. doi:10.1016/S1471-5317(00)00007-9.
- [26] D. Zhou, J. Liu, S. Xu, P. Peng, First-principles investigation of the binary intermetallics in Mg-Al-Sr alloy: Stability, elastic properties and electronic structure, *Comput. Mater. Sci.* (2014) 24-29. doi:10.1016/j.commatsci.2014.01.007.
- [27] Z.W. Huang, Y.H. Zhao, H. Hou, P.D. Han, Electronic structural, elastic properties and thermodynamics of Mg₁₇Al₁₂, Mg₂Si and Al₂Y phases from first-principles

- calculations, *Phys. B Condens. Matter.* (2012) 1075–1081.
doi:10.1016/j.physb.2011.12.132.
- [28] A. Munitz, C. Cotler, A. Stern, G. Kohn, Mechanical properties and microstructure of gas tungsten arc welded magnesium AZ91D plates, *Mater. Sci. Eng. A.* (2001) 68-73.
doi:10.1016/S0921-5093(00)01356-3.
- [29] K. Hagihara, K. Hayakawa, Plastic deformation behavior and operative slip systems in Mg17Al12 single crystals, *Mater. Sci. Eng. A.* 737 (2018) 393–400.
doi:10.1016/j.msea.2018.09.056.
- [30] H.N. Mathur, V. Maier-Kiener, S. Korte-Kerzel, Deformation in the γ -Mg17Al12 phase at 25–278° C, *Acta Mater.* 113 (2016) 221–229.
- [31] N. Wang, W.-Y. Yu, B.-Y. Tang, L.-M. Peng, W.-J. Ding, Structural and mechanical properties of Mg17Al12 and Mg24Y5 from first-principles calculations, *J. Phys. D. Appl. Phys.* 41 (2008) 195408. doi:10.1088/0022-3727/41/19/195408.
- [32] Y.-H. Duan, Y. Sun, M.-J. Peng, Z.-Z. Guo, First principles investigation of the binary intermetallics in Pb–Mg–Al alloy: stability, elastic properties and electronic structure, *Solid State Sci.* 13 (2011) 455–459. doi:10.1016/j.solidstatesciences.2010.12.011.
- [33] D. Rossouw, B. Langelier, A. Scullion, M. Danaie, G.A. Botton, Multivariate-aided mapping of rare-earth partitioning in a wrought magnesium alloy, *Scr. Mater.* (2016) 174-178. doi:10.1016/j.scriptamat.2016.07.022.
- [34] W.S. Rasband, Imagej, us national institutes of health, bethesda, maryland, usa, [Http//Imagej.Nih.Gov/Ij/](http://Imagej.Nih.Gov/Ij/). (2011).
- [35] H. Zou, X. Zeng, C. Zhai, W. Ding, The effects of yttrium element on microstructure and mechanical properties of Mg–5 wt% Zn–2 wt% Al alloy, *Mater. Sci. Eng. A.* 402 (2005)

- 142–148.
- [36] F.-S. Pan, M.-B. Chen, J.-F. Wang, P. Jian, A.-T. Tang, Effects of yttrium addition on microstructure and mechanical properties of as-extruded AZ31 magnesium alloys, *Trans. Nonferrous Met. Soc. China*. 18 (2008) s1–s6.
- [37] H.-W. Chang, D. Qiu, J.A. Taylor, M.A. Easton, M.-X. Zhang, The role of Al₂Y in grain refinement in Mg–Al–Y alloy system, *J. Magnes. Alloy*. 1 (2013) 115–121.
- [38] I. Minitab, Minitab 16 statistical software, URL[Computer Software]. State Coll. PA Minitab, Inc.(Www. Minitab. Com). (2010).
- [39] B.H. Toby, R.B. Von Dreele, GSAS-II: the genesis of a modern open-source all purpose crystallography software package, *J. Appl. Crystallogr.* 46 (2013) 544–549.
- [40] M.X. Zhang, P.M. Kelly, Crystallography of Mg₁₇Al₁₂ precipitates in AZ91D alloy, *Scr. Mater.* (2003) 647-652. doi:10.1016/S1359-6462(02)00555-9.
- [41] X. Tong, L. Zai, G. You, H. Wu, H. Wen, S. Long, Effects of bonding temperature on microstructure and mechanical properties of diffusion-bonded joints of as-cast Mg–Gd alloy, *Mater. Sci. Eng. A*. 767 (2019) 138408.
- [42] H. Yamauchi, Surface segregation in jellium binary solid solutions, *Phys. Rev. B*. 31 (1985) 7688. doi:<https://doi.org/10.1103/PhysRevB.31.7688>.
- [43] P. Politzer, R.G. Parr, D.R. Murphy, Approximate determination of Wigner-Seitz radii from free-atom wave functions, *Phys. Rev. B*. 31 (1985) 6809. doi:<https://doi.org/10.1103/PhysRevB.31.6809>.
- [44] P.-G. Reinhard, E. Suraud, Introduction to cluster dynamics, John Wiley & Sons, Weinheim, 2008.
- [45] D.S. Aydin, Z. Bayindir, M.O. Pekguleryuz, High Temperature Oxidation Behavior of

- Hypoeutectic Mg–Sr Binary Alloys: The Role of the Two-Phase Microstructure and the Surface Activity of Sr, *Adv. Eng. Mater.* 17 (2015) 697–708.
doi:<https://doi.org/10.1002/adem.201400191>.
- [46] M. Klinger, More features, more tools, more CrystTBox, *J. Appl. Crystallogr.* 50 (2017) 1226–1234.
- [47] T.-S. You, M.-K. Han, G.J. Miller, On the “coloring problem” in YMgZn and related phases, *Inorganica Chim. Acta.* 361 (2008) 3053–3062.
- [48] J.W. Edington, K.C.T. Russell, *Practical electron microscopy in materials science*, Macmillan International Higher Education, 1977.
- [49] G.C. Weatherly, R.B. Nicholson, An electron microscope investigation of the interfacial structure of semi-coherent precipitates, *Philos. Mag. A J. Theor. Exp. Appl. Phys.* 17 (1968) 801–831.
- [50] C.W. Bale, P. Chartrand, S.A. Degterov, G. Eriksson, K. Hack, R. Ben Mahfoud, J. Melançon, A.D. Pelton, S. Petersen, FactSage thermochemical software and databases, *Calphad.* 26 (2002) 189–228.
- [51] O.S. Zarechnyuk, M.E. Drits, R.M. Rykhal, V. V Kinzhibalo, Study of a Magnesium-Aluminum-Yttrium System at 400 in the Phase Containing 0–33.3 at.% Yttrium, *Izv. Akad. Nauk. SSSR Met.* 5 (1980) 242–244.

CHAPTER 4

The effect of Y on the microstructure and mechanical performance of an Mg-Al-Y casting alloy

Chapter 3 showed that trace Y additions refine the β -Mg₁₇Al₁₂ phase and improve the mechanical properties of Mg-6wt%Al based alloy. However, higher additions cause loss of the refinement effect and causes the formation of Y-rich second phases that decrease the mechanical properties. The current chapter focuses on higher Y additions where coarse Y-rich precipitates form. Microstructural investigation, mechanical testing and thermodynamic simulations are conducted to better understand the relationship between the Y-rich precipitates and the β phase. Compared to lower levels of Y discussed in the Chapter 3, the improvement in ductility and UTS with higher Y additions is less. This chapter identifies as its major contribution that Al₂Y precipitates are in close association with the Mg₁₇Al₁₂ phase indicating their role as nucleants. It also shows that the early formation of the Al₂Y in the liquid leads to the coarsening of Al₂Y particles, resulting in less significant improvement in mechanical properties compared to the alloy with trace level of Y. This chapter has been published as a journal article: *Korgiopoulos, K., & Pekguleryuz, M. (2021). The effect of Y on the microstructure and mechanical performance of an Mg-Al-Y casting alloy. Experimental Results, 2.*

ABSTRACT

Environmental gains of electric cars can be optimized with the use of lightweight and recyclable magnesium in the vehicle's structural components. Ductility improvement of low-density Mg-Al alloys will extend their use in automotive body applications. The authors achieved 63% ductility improvement in Mg-6wt%Al with trace Y (1.5 ppm) due to the β -phase refinement and predicted that higher levels would not perform as well. As predicted, 0.3wt% of Y addition investigated in this study led to lower mechanical performance and β -phase refinement than those obtained with trace additions. The tensile ductility and yield strength increased by \sim 13% and 16%, respectively, and the compression strain to fracture by \sim 22%. Scanning electron and optical microscopy, X-Rays diffraction, mechanical testing and thermodynamic calculations were used to investigate the effect of 0.3wt% Y on the microstructure of Mg-6wt%Al. The matrix dissolution revealed the close association of the Al_2Y and the $\beta\text{-Mg}_{17}\text{Al}_{12}$ phases.

Keywords: Magnesium; Mg-Al alloys; Matrix extraction; Tensile ductility; Compressive strain

4.1 Introduction

Future autonomous cars will rely on computer systems, sensors, and satellite navigation which require extensive electronics that increase the vehicle's weight [1]. Due to their high strength-to-weight-ratio, magnesium (Mg) structural alloys are a viable solution for vehicle-weight reduction in future cars. Mg-6wt%Al (Mg-6Al) casting alloys demonstrate the optimum level of strength and ductility for most automotive applications but further increase in their ductility will lead to their extended use in crashworthy car-body components [2]. The $\text{Mg}_{17}\text{Al}_{12}$ precipitate, the main second phase, improves strength but reduces ductility [2,3].

Studies have shown that yttrium (Y) additions can improve the ductility of Mg-Al alloys [4,5]. When Y is in the solid solution of α -Mg then it can improve its mechanical properties via: (1) decrease of the Stacking Fault Energy (SFE) activating the pyramidal $\langle c+a \rangle$ dislocations [6] or (2) forming long period stacking ordered (LPSO) phases when a transition metal is present [7]. However, with Al present, the solubility of rare earths in α -Mg is nil, instead brittle precipitates [8–10] form. Researchers have observed that the modification of β -Mg₁₇Al₁₂ in Mg-Al-Y alloys is responsible for improved mechanical properties [11–14]. Previous work [15] by the authors has shown that the refinement of β -Mg₁₇Al₁₂ improves the ductility of Mg-6Al cast alloys at trace Y additions. This has been attributed to co-precipitation (at close temperatures) of the Al₄MgY phase with the Mg₁₇Al₁₂ phase. Thermodynamics also predicted that the formation temperatures of the two phases deviate at higher Y levels leading to a loss in nucleant effectiveness.

4.2 Objective

The current work investigates the effect of Y additions (0.3 wt%) to see if β -phase refinement and ductility improvement seen in trace levels of Y are also observed at higher Y levels and to elucidate the role of Y on the mechanical properties of Mg-6Al based alloys.

4.3 Methods

Mg-6Al-0.3Y (in wt%) alloy was synthesized using commercial purity (99.98%) Mg, 99.9% pure Al granules and 99.9% pure Y rods. The total mass of the alloying additions was 617 gr using 95% recovery factor for Al and 60% for Y. The alloying additions were made at 720 °C in a graphite crucible under CO₂/SF₆ protective atmosphere. A graphite crucible was used because it is affordable, and it does not react with magnesium. The cleaning after casting is efficient and leaves no residuals that could possibly contaminate the subsequent castings. The molten alloy was then poured under protective atmosphere into a preheated (400°C) steel mold to produce a flat plate.

The actual composition (in wt%) of the alloy according to inductively coupled plasma atomic-emission spectroscopy is: 6.26% Al, 0.29% Y, 0.02% impurities (Fe, Mn) with Mg as balance. A scanning electron microscope (SEM-Hitachi SU3500) with an energy dispersive X-ray spectroscopy (EDS) detector was used for microstructural investigation. The grain size of α -Mg was measured with the intercept method using a Nikon-Epiphot 200 optical microscope after etching the samples with 4.2 gr picric acid, 10ml acetic acid, 10 ml distilled water and 70ml ethanol. The ImageJ software [16] was used to measure the precipitates and the grain size. The crystallographic information was obtained by XRD (Bruker D8 Discovery X-Ray Diffractometer-Cu source) in the bulk sample and after matrix extraction by using 5% acetic acid. The mechanical properties were evaluated by tensile and compression testing (MTS 810) at room temperature with a strain rate of 0.001s^{-1} . Thermodynamic calculations (FactSage with FTlite database) [17] based on the CALPHAD method have been performed in equilibrium and non-equilibrium conditions (Scheil cooling).

4.4 Results and Discussion

Mg-6Al-0.3Y alloy consists of partially divorced β - $\text{Mg}_{17}\text{Al}_{12}$, interdendritic Y-enriched precipitates and the Al enriched α -Mg phase as determined by EDS (Fig.4.1). Y is detected in Mg-Al-Y and Mg-Al-Mn-Fe-Y precipitates. Both precipitates are closely associated with $\text{Mg}_{17}\text{Al}_{12}$ suggesting that they act as nucleation sites. The Y-enriched precipitates range from fine to coarse and present in three different morphologies, namely, spherical, square and plate-like, with the expectation that only the finer precipitates can act as refiners for the β phase. Table 4.1 shows the composition of the β -phase and Al_2Y as per the EDS analysis. No Y was detected in the α -Mg solid solution. There is close association (Figs 4.1 & 4.2) of the Al_2Y precipitates with the $\text{Mg}_{17}\text{Al}_{12}$. Similar association has been observed before by the authors [15] in Mg-6%Al based

alloys for lower Y additions. XRD detects (Fig. 4.3a) Mg-Al solid solution and β - $Mg_{17}Al_{12}$ peaks in the bulk alloy. After the matrix extraction (Fig.4.3b), the matrix disappears and the peaks for Al_2Y and $Mg_{17}Al_{12}$ become stronger. The peak intensity of spectra b is lower due to the low amount and small size (average size ~ 10 -50 microns) of the extracted precipitates.

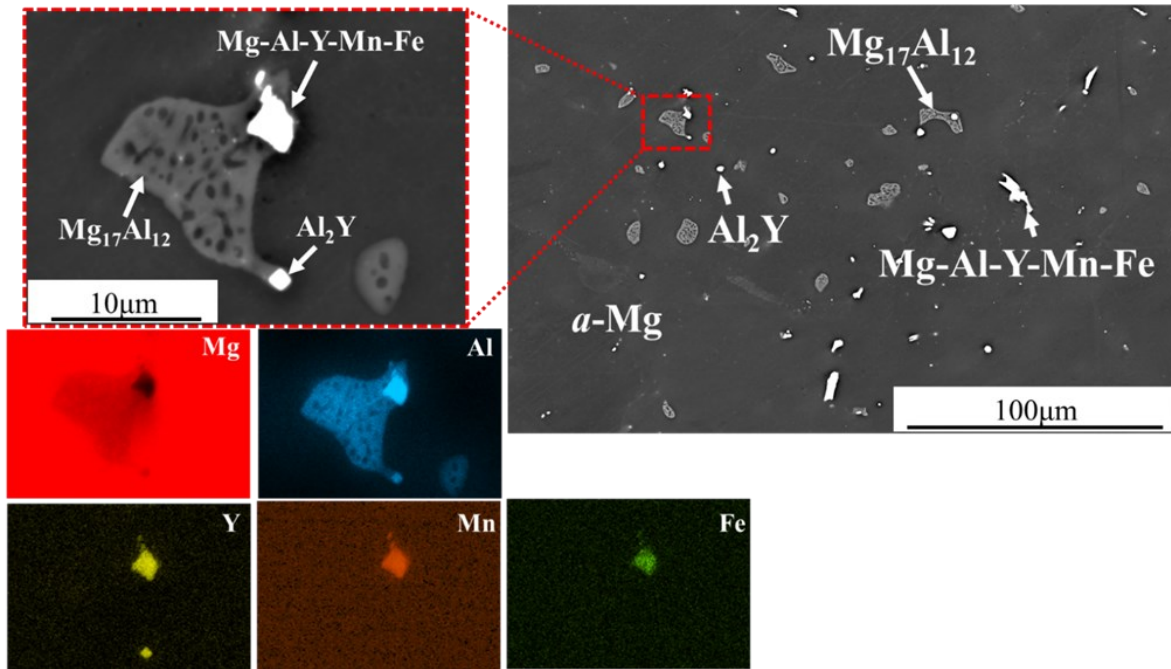


Fig. 4.1 SEM/BSE as-cast microstructure of Mg-6Al-0.3Y and EDS maps. The red square shows the close associations of Y enriched precipitates with $Mg_{17}Al_{12}$.

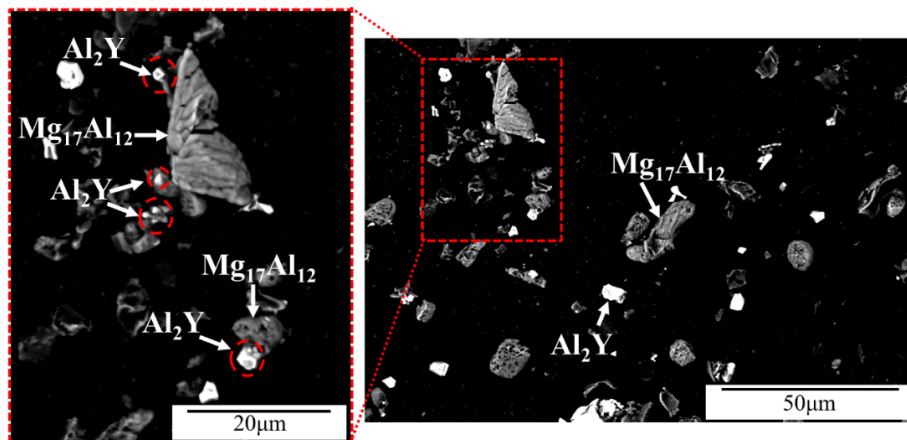


Fig. 4.2 Mg-Al-0.3Y alloy after matrix extraction. The red circles show the Al_2Y associated with the $Mg_{17}Al_{12}$ phase.

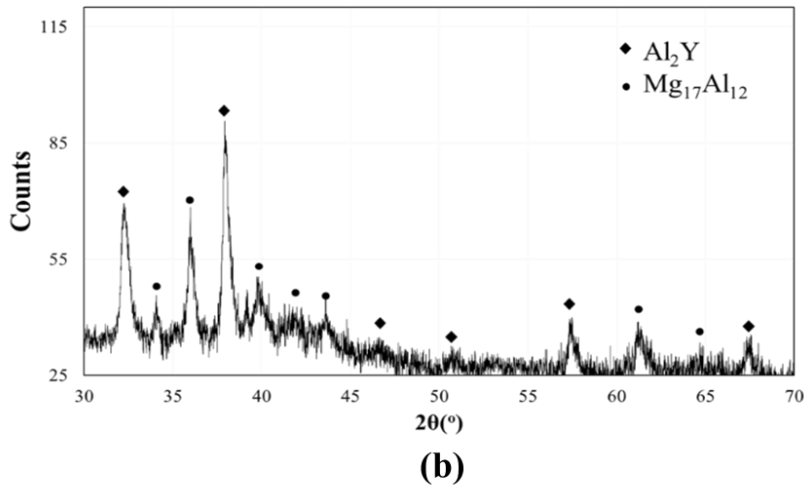
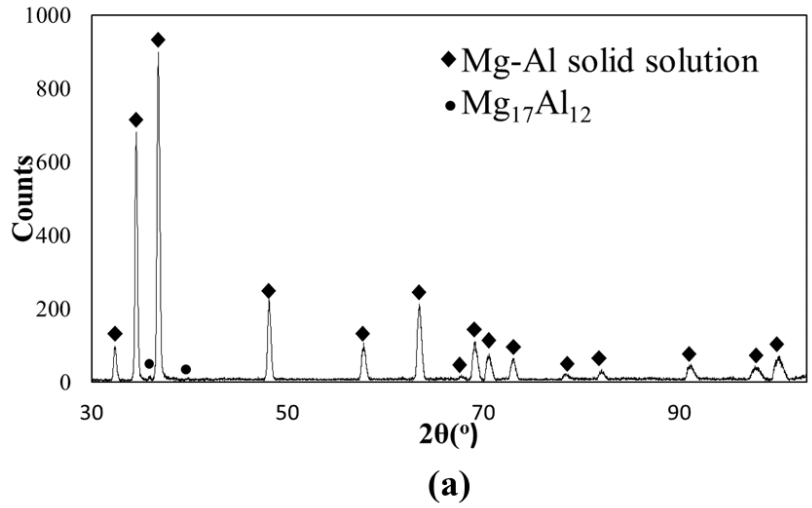


Fig. 4.3 XRD results (a) Bulk alloy, (b) after matrix extraction.

Table 4.1 EDS on the precipitates after matrix extraction.

Precipitate	Mg (at%)	Al (at%)	Y (at%)
Mg ₁₇ Al ₁₂	57.2±0.4	42.8±0.4	-
Al ₂ Y	2.3±1.2	61.5±1.9	36.2±0.7

The Mg₁₇Al₁₂ (Table 4.2) in Mg-6Al-0.3Y is 25% finer than that in the binary Mg-6Al, but 41% coarser than the alloy with trace Y amount. Additionally, high Y addition forms even coarser (~87 μm²) Mg-Al-Mn-Fe-(Y) and Mg-Al-Y precipitates. The grain size of the cast Mg-6Al-0.3Y

is also higher than the alloy with trace Y level as has been observed and attributed to the coarsening of the Al_2Y phase [18–20].

Table 4.2 Precipitates size and α -Mg grain size as measured with ImageJ.

Alloys	$Mg_{17}Al_{12}$ Size (μm^2)	Mg-Al-Mn-Fe-(Y) Size (μm^2)*	Mg-Al-Y Size (μm^2)	α -Mg Grain Size (μm)	Reference
Mg-6Al	32 ± 15	1.56 ± 0.06	-	96 ± 13	[6]
Mg-6Al with trace Y	17 ± 5	1.41 ± 0.20	-	85 ± 15	[6]
Mg-6Al-0.3Y	24 ± 6	7 ± 3	14 ± 10	105 ± 17	Current work

*Only precipitates in Mg-6Al-0.3Y alloy contain Y

Mg-6Al-0.3Y has the highest tensile yield strength (YS) of the three alloys (Table 4.3). Compared to the Mg-Al with trace Y, the tensile ductility (% El), ultimate tensile strength (UTS), and the compressive strength are lower (Tables 4.3 & 4.4). According to thermodynamic simulations conducted by the authors (Table 4.5), the solubility of Y in Mg-Al-Y is practically nil. Instead, Y forms precipitates (ordered intermetallics) with Al such as Al_4MgY , Al_3Y and Al_2Y . In Mg-Al-0.3Y, Al_2Y forms earlier (at higher temperature) than the β -phase (Table 4.5) and has time to coarsen losing its effectiveness as a nucleant of the β -phase and embrittling the alloy.

Table 4.3 Tensile properties of as cast samples at room temperature.

Alloy	UTS(MPa)	YS(MPa)	El(%)	Reference
Mg-6Al	206 ± 5	74 ± 6	8 ± 2	[15]
Mg-6Al with trace Y	235 ± 13	72 ± 11	13 ± 3	[15]
Mg-6Al-0.3Y	209 ± 17	86 ± 10	9 ± 2	Current work

Table 4.4 Compression properties of as cast samples at room temperature.

Alloy	CS(MPa)	CYS(MPa)	Strain(%)	Reference
Mg-6Al	276 ± 8	105 ± 8	23 ± 1	[15]
Mg-6Al with trace Y	271 ± 3	97 ± 5	28 ± 2	[15]
Mg-6Al-0.3Y	258±6	69±6	28±2	Current work

Table 4.5 Equilibrium and non-equilibrium (Scheil) thermodynamic calculations.

Alloy(wt%)	Equilibrium - Y solubility in α -Mg (wt%)	Scheil - Y solubility in α -Mg (wt%)	Y enriched phases	Scheil-Formation temperature of Mg ₁₇ Al ₁₂	Scheil-Formation temperature of Y enriched precipitates
Mg-0.01 Y	0.01	0.01	Y ₁₀ Mg ₂₄ Mg ₂₄	-	-
Mg-0.3Y	0.03	0.29	Y ₁₀ Mg ₂₄ Mg ₂₄	-	-
Mg-6Al-0.01Y	5.51E-21	0.00007	Al ₄ MgY	439 °C	460 °C
Mg-6Al-0.3Y	5.51E-21	0.0027	Al ₂ Y/Al ₃ Y (Scheil), Al ₄ MgY	439 °C	555 °C (Al ₃ Y), 610°C (Al ₂ Y), 510°C (Al ₄ MgY)

4.5 Conclusions

The addition of 0.3 wt% Y improves the tensile properties and the strain to fracture in compression of the binary cast alloys Mg-6 wt%Al. The improvement in ductility and UTS is not as significant as lower (trace level) Y additions. Al₂Y precipitates (determined via XRD and SEM/EDS) are in close association with the Mg₁₇Al₁₂ phase indicating their role as nucleants but the early formation of the Al₂Y in the liquid in Mg-Al-0.3Y leads to its coarsening, resulting in some loss in mechanical properties compared to the alloy with the trace level of Y.

4.6 Funding Information and Acknowledgements

This work was supported by the Natural Sciences and Engineering Research Council of Canada (NSERC) Discovery Grant (G210358NSERC/RGPIN-2016-05121). The authors thank Pierre Vermette and Dr. Amir Farkoosh for their assistance in alloy casting and discussions. Konstantinos Korgiopoulos gratefully acknowledges McGill Engineering Doctoral Award program (MEDA).

4.7 References

- [1] P. Gao, R. Hensley, A. Zielke, A road map to the future for the auto industry, McKinsey Quarterly, Oct. (2014).
- [2] H.E. Friedrich, B.L. Mordike, Magnesium technology, Springer, 2006.
- [3] M.D. Nave, A.K. Dahle, D.H. StJohn, Eutectic growth morphologies in magnesium-aluminium alloys, in: TMS Annu. Meet., 2000: pp. 233–242.
doi:10.1002/9781118808962.ch33.
- [4] G.-H. Su, L. Zhang, L.-R. Cheng, Y.-B. Liu, Z.-Y. Cao, Microstructure and mechanical properties of Mg-6Al-0.3 Mn-xY alloys prepared by casting and hot rolling, Trans. Nonferrous Met. Soc. China. 20 (2010) 383–389. doi:10.1016/S1003-6326(09)60150-3.

- [5] N. Tahreen, D.L. Chen, M. Nouri, D.Y. Li, Effect of Yttrium Addition on Texture Development in a Cast Mg-Al-Y Magnesium Alloy During Compression, in: M. Alderman, M. V Manuel, N. Hort, N.R. Neelameggham (Eds.), *Magnes. Technol.* 2014, Springer International Publishing, Cham, 2016: pp. 269–272. doi:10.1007/978-3-319-48231-6_51.
- [6] S. Sandlöbes, M. Friák, S. Zaeferrer, A. Dick, S. Yi, D. Letzig, Z. Pei, L.-F. Zhu, J. Neugebauer, D. Raabe, The relation between ductility and stacking fault energies in Mg and Mg–Y alloys, *Acta Mater.* 60 (2012) 3011–3021.
- [7] Y. Kawamura, M. Yamasaki, Formation and mechanical properties of Mg₉₇Zn₁RE₂ alloys with long-period stacking ordered structure, *Mater. Trans.* 48 (2007) 2986–2992.
- [8] B. Pourbahari, M. Emamy, H. Mirzadeh, Synergistic effect of Al and Gd on enhancement of mechanical properties of magnesium alloys, *Prog. Nat. Sci. Mater. Int.* 27 (2017) 228–235.
- [9] C. Wang, J. Dai, W. Liu, L. Zhang, G. Wu, Effect of Al additions on grain refinement and mechanical properties of Mg–Sm alloys, *J. Alloys Compd.* 620 (2015) 172–179.
- [10] L. Wang, Y. Feng, E. Guo, L. Wang, Y. Fu, S. Zhao, G. Cao, Comparative study on microstructure and mechanical properties of Mg-3Nd-3Al and Mg-3Nd-0.5 Zr alloys under different heat treatment conditions, *JOM.* 71 (2019) 2194–2201.
- [11] A. Bobby, U.T.S. Pillai, B.C. Pai, Investigation on Lead and Yttrium Addition on the Microstructure and Mechanical Properties of AZ91 Magnesium Alloy, *J. Solid Mech. Mater. Eng.* 7 (2013) 273–280.
- [12] S.-R. Wang, P.-Q. Guo, L.-Y. Yang, Y. Wang, Microstructure and mechanical properties of AZ91 alloys by addition of yttrium, *J. Mater. Eng. Perform.* 18 (2009) 137–144.

doi:10.1007/s11665-008-9255-z.

- [13] N. Kashefi, R. Mahmudi, The microstructure and impression creep behavior of cast AZ80 magnesium alloy with yttrium additions, *Mater. Des.* 39 (2012) 200–210.
doi:10.1016/j.matdes.2012.02.036.
- [14] H. Cai, F. Guo, J. Su, L. Liu, B. Chen, Study on microstructure and strengthening mechanism of AZ91-Y magnesium alloy, *Mater. Res. Express.* 5 (2018) 36501.
doi:10.1088/2053-1591/aab0b7.
- [15] K. Korgiopoulos, M. Pekguleryuz, The significant effect of trace yttrium level on the mechanical properties of cast Mg–6Al alloy through a refinement mechanism, *Mater. Sci. Eng. A.* 775 (2020) 138966.
- [16] W.S. Rasband, Imagej, us national institutes of health, bethesda, maryland, usa,
[Http//Imagej. Nih. Gov/Ij/](http://Imagej.Nih.Gov/Ij/). (2011).
- [17] C.W. Bale, P. Chartrand, S.A. Degterov, G. Eriksson, K. Hack, R. Ben Mahfoud, J. Melançon, A.D. Pelton, S. Petersen, FactSage thermochemical software and databases, *Calphad.* 26 (2002) 189–228.
- [18] H.-W. Chang, D. Qiu, J.A. Taylor, M.A. Easton, M.-X. Zhang, The role of Al₂Y in grain refinement in Mg–Al–Y alloy system, *J. Magnes. Alloy.* 1 (2013) 115–121.
- [19] F.-S. Pan, M.-B. Chen, J.-F. Wang, P. Jian, A.-T. Tang, Effects of yttrium addition on microstructure and mechanical properties of as-extruded AZ31 magnesium alloys, *Trans. Nonferrous Met. Soc. China.* 18 (2008) s1–s6.
- [20] H. Zou, X. Zeng, C. Zhai, W. Ding, The effects of yttrium element on microstructure and mechanical properties of Mg–5 wt% Zn–2 wt% Al alloy, *Mater. Sci. Eng. A.* 402 (2005) 142–148.

CHAPTER 5

Mg₁₇Al₁₂ intermetallic modified with Yttrium additions

The previous chapters presented the role of Y on the modification of β -Mg₁₇Al₁₂ intermetallic and the resulting effect on the mechanical properties on Mg-6wt%Al based alloy. The research question here is whether the improvement in mechanical properties with Y additions is due to the morphological refinement of the Mg₁₇Al₁₂ phase in the alloy or to any change in its intrinsic properties. Little is known on the intrinsic properties of Mg₁₇Al₁₂ intermetallic and their possible modification with alloying additions. The current chapter presents a study of the effect of Y on the mechanical properties, microstructure, and crystal structure of Mg₁₇Al₁₂. Experimental techniques including a diffusion couple study of Y/Mg₁₇Al₁₂, characterization methods including XRD and ultrasonic measurements for determining the elastic modulus, and thermodynamic simulations were employed to understand the role of Y in the modification of Mg₁₇Al₁₂.

ABSTRACT

Mg₁₇Al₁₂ is the principal intermetallic second phase in the Mg-Al based alloys (AM series) that significantly affects their mechanical performance. Modification of this intermetallic has been possible with rare earth elements, resulting in mechanical performance improvement of the AM alloys. The modification of the intermetallic has been studied with respect to alteration of the morphology, but little is known about the effect of alloying elements on the intrinsic properties of Mg₁₇Al₁₂ which has a complex crystal structure. In previous studies on first principle simulations of the phase, the effect of alloying additions was not well-investigated. The current experimental study investigates the effect of low and high Yttrium (Y) additions on the mechanical properties, microstructure, and crystal structure of Mg₁₇Al₁₂. Scanning electron microscopy, electron probe microanalysis, X-rays diffraction, ultrasonic and mechanical testing along with thermodynamic calculations are employed to better understand the role of Y in the modification of Mg₁₇Al₁₂. Low Y additions decrease the lattice constant of β phase, but higher amounts present an opposite trend. According to the elastic moduli calculations Mg₁₇Al₁₂ is a ductile phase although Y slightly makes it more brittle. The Young's, shear, and bulk moduli increase with Y additions.

Keywords: Mg₁₇Al₁₂, Intermetallic, magnesium-aluminum alloys, microhardness, elastic modulus

5.1 Introduction

Mg₁₇Al₁₂ (also known as the β phase) is the main second phase in cast Mg-Al based alloys that determines the mechanical properties [1–3]. The β phase is a complex non-stoichiometric compound with cubic crystal structure isomorphous with α -Mn (cI58) that contains 34 Mg and 24 Al atoms [4–7]. According to first-principle calculations and based on the elastic constants,

Mg₁₇Al₁₂ is considered to be a stiff and brittle intermetallic [7–9]. The type of bonding between the different atoms is ionic (Mg-Al), covalent (Al-Al) and metallic (Mg-Mg) [10]. The covalent and ionic bonds are responsible for the brittle nature of β phase [9,10].

The Mg₁₇Al₁₂ intermetallic belongs to a class of intermetallics that are also termed as complex metallic alloys (CMAs); they are characterized by three particularities [11,12]: (1) giant unit cells with up to several thousands of atoms, (2) clustering of atoms in the unit cell, and (3) inherent disorder which may be configurational (different orientation of subclusters) and chemical (substitutional, partial or fractional occupancy). Mg₁₇Al₁₂ as an intermetallic may have a band gap leading to insulating (or only semi-conducting) properties; however, Mg₁₇Al₁₂ is reported to have a 0 eV band gap [13,14] which speaks to its metallic nature. Mg₁₇Al₁₂ is off-stoichiometric at high temperatures and exists in a composition range where chemical disorder (anti-site clusters, unoccupied sites) can exist. At low temperatures it is a line compound (stoichiometric) where it is free from chemical disorder with all sites occupied. Vrtnik et al. [12] have found that the stabilization process (decreasing the kinetic energy of the free electrons) in the β -phase is the Hume-Rothery stabilization mechanism; this is based on the occurrence of a steep pseudogap at the Fermi level at a specific electron-to-atom ratio (e/a) due to Fermi surface-Brillouin zone interactions to assign the electrons to lower levels in the density of states (DOS). It has been also determined via first principles calculations that the pseudo gap in the β -phase is 1-2 eV and occurs at an e/a of 2.38 which is close to the $e/a=2.41$ of the phase calculated at its stoichiometric composition. While the stabilization at absolute zero and low temperatures is due to Hume-Rothery e/a mechanism, at higher temperatures where the β -phase is off-stoichiometric and exists over a wide composition range, it is disordered.

Previous research has also shown that $Mg_{17}Al_{12}$ exhibits plasticity at high temperatures unlike its behavior at room temperature due to dislocations climb as a result of vacancy diffusion [15]; this may be due to the activation of slip modes at high temperatures in ionic bonding. It is also reported that dislocations pile up or form networks inside $Mg_{17}Al_{12}$ [16]. More recently Vaid et al. [17] have made atomistic simulations of basal-dislocation interactions with the β -phase and suggested that the dislocations pass the $Mg_{17}Al_{12}$ phase without shearing the precipitate or presenting any Orowan loop around it.

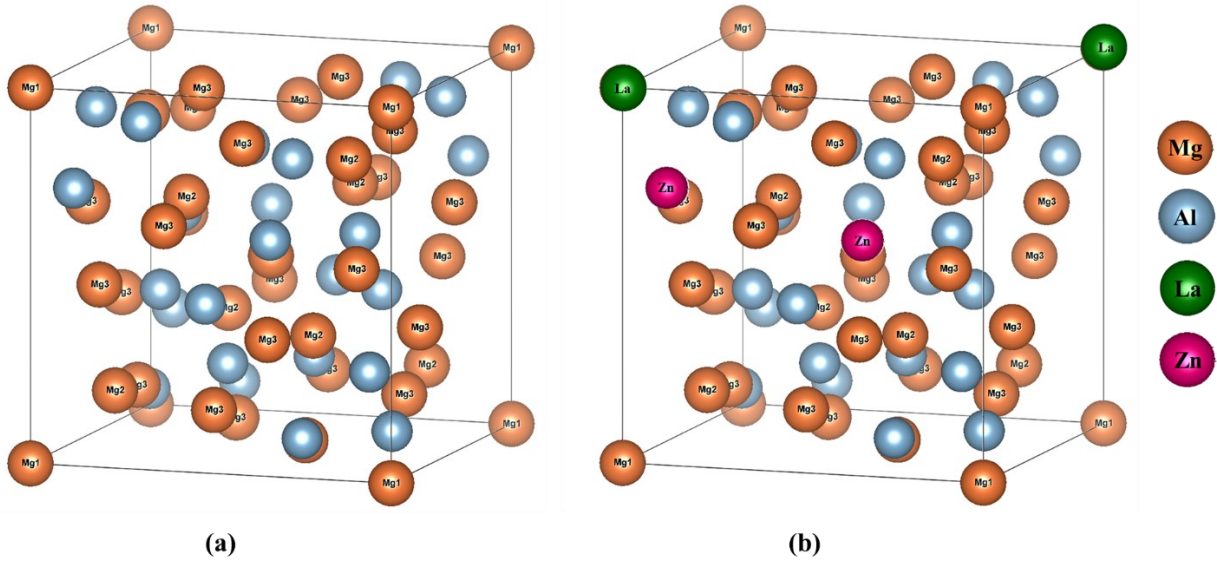


Fig. 5.1 (a) Crystal structure of $Mg_{17}Al_{12}$, (b) Substitution example of Mg(I) atoms with La and Al atoms with Zn according to reference [10].

Alloying can change the characteristics of this intermetallic phase by substituting the Mg and/or Al atoms in the crystal structure of the $Mg_{17}Al_{12}$; substitution can distort the lattice and change the lattice parameter [18,19]. The lattice parameter of the unit cell of the $Mg_{17}Al_{12}$ at its stoichiometric composition is 10.5492 Å [20] but it has been observed that in various Mg alloys lattice parameter ranges from 10.50 Å to 10.69 Å [21]. The substitutional element will occupy positions that will minimize the energy. $Mg_{17}Al_{12}$ has three different positions for Mg atoms

namely Mg(I), Mg(II), Mg(III) and one position for Al [7,22]. Alloying additions Ca, Zr, La substitute the Mg(I) atoms, while the Al atoms are substituted by Zn and Cu (Fig. 5.1) [10].

The site substitution can alter the mechanical properties of the intermetallics [10]. It is shown that the ratio of bulk modulus (B) over shear modulus (G) determines the failure mode of intermetallics; ductile ($B/G > 1.75$) or brittle ($B/G < 1.75$) [7–10,23]. Alloying additions such as Ca, Ni, Cu, Zn, Zr and La make $Mg_{17}Al_{12}$ more brittle due to $B/G < 1.75$. However, Ca and La increase both the bulk and shear modulus [10]. In the case of Y additions, this is not known. Previous research from the authors [18,24] has shown that trace additions of Y and Er in cast Mg-6wt%Al alloy distorted the crystal structure and refined the β - $Mg_{17}Al_{12}$ improving the mechanical properties of the alloy. According to other reports, yttrium (Y) refines the $Mg_{17}Al_{12}$ precipitates in Mg alloys improving their mechanical properties and corrosion resistance [25–28].

In the present study, only the $Mg_{17}Al_{12}$ intermetallic is cast with different Y levels. The intermetallics are investigated via Scanning Electron Microscopy (SEM), Electron probe microanalysis (EPMA), X-rays diffraction (XRD), mechanical testing (microhardness, ultrasonic) and thermodynamic calculations. A diffusion couple between $Mg_{17}Al_{12}$ and pure Y is also studied to understand the effect of Y on the intermetallic.

5.2 Material and Methods

5.2.1 Synthesis

Three $Mg_{17}Al_{12+x}$ ($x=0, 0.03, 0.5$ wt%Y) intermetallics (Table 5.1) were synthesized using commercial purity (99.98%) Mg ingot (Magnesium Electron), 99.9% pure Al granules (Alfa Aesar) and 99.9% pure Y rods (Hefa Rare Earth Canada). These Y levels were considered according to the experimental results of our previous work in [24]. The one Y level is below the solubility limit but close to it and the other level is well above the solubility limit. Pure Mg was

heated to 680 °C inside a graphite crucible in a Norax Canada Induction Furnace under a protective atmosphere of CO₂/SF₆ gas (0.553% SF₆ and balanced CO₂); the alloying elements were added at 680 °C and held for 15 minutes at temperature. The alloy with 0.5wt% Y was held at 700°C for longer time to ensure that yttrium was completely dissolved. The molten alloy was stirred and skimmed before casting in a permanent mold. The alloys were then poured in a preheated (400 °C) steel mold to produce flat plates of 6mm thickness; protective atmosphere of CO₂/SF₆ gas was used during the casting. The actual chemical composition (Table 5.1) was determined by Inductively coupled plasma atomic-emission spectroscopy (ICP-AES).

Table 5.1 Compositions of the Intermetallics (ICP).

Intermetallic*	Sample designation	Mg (wt%)	Al (wt%)	Y (ppm)
Mg ₁₇ Al ₁₂	β	55.07	44.89	-
Mg ₁₇ Al ₁₂ +300 ppm Y	β _{300Y}	54.34	45.59	260
Mg ₁₇ Al ₁₂ +5000 ppm Y	β _{5000Y}	53.07	45.81	5000

*0.043 wt% impurities

5.2.2 Thermodynamic calculations

FactSage thermodynamic calculations software based on the CALPHAD method was used [29] to predict phase formation in the alloys. A three-component system composed of Al-Mg-Y was calculated considering the FTlite data base. Pseudo-binary phase diagrams were plotted considering equilibrium conditions.

5.2.3 Characterization

Specimens for microstructural and microhardness analysis were prepared by manual grinding using a series of SiC papers and then polishing with colloidal silica. The microstructure was investigated using a Hitachi SU3500 scanning electron microscope (SEM) with an energy dispersive X-ray spectroscopy (EDS) detector. Further analysis was conducted by wavelength-dispersive spectroscopy (WDS) using a CAMECA SX 100 FiveFe electron probe micro-analyzer (EPMA) after calibration with standard samples.

A Bruker D8 Discovery X-Ray Diffractometer (Cu source – $\lambda=1.5406 \text{ \AA}$, 300 sec/frame for 4 frames in total) was used to determine the crystallographic information of the intermetallics after Rietveld refinement with the GSAS II software [30]. The bulk samples were filed to create powder which was stressed annealed at 160 °C for 1 hour under Ar protective atmosphere.

5.2.4 Mechanical Properties

A Clark CM-100AT micro hardness tester equipped with CLEMEX CMT software was used to evaluate the hardness of the polished samples after 6 repetitions with 50 gf load. To evaluate the moduli of the synthesized intermetallics, nine position ultrasonic velocity measurements per sample were conducted. The longitudinal (V_L) and shear velocity (V_S) were measured using a longitudinal and shear transducer, respectively. The time of flight was obtained by measuring the time difference between the second and first echo. The density (ρ) was measured with Archimedes method conducting 3 repetitions in each sample. The average Young's modulus, Poissons ratio, bulk modulus and shear modulus were calculated by equations 1 to 4 respectively [31,32].

$$\text{Elastic modulus} \quad E = \rho V_S^2 \frac{(3V_L^2 - 4V_S^2)}{V_L^2 - V_S^2} \quad (\text{eq.1})$$

$$\text{Poissons ratio} \quad \mu = \frac{1-2(V_T/V_L)^2}{2-2(V_T/V_L)^2} \quad (\text{eq.2})$$

$$\text{Bulk modulus} \quad B = \frac{E}{3(1-2\mu)} \quad (\text{eq.3})$$

$$\text{Shear modulus} \quad G = \rho V_S^2 \quad (\text{eq.4})$$

5.2.5 Diffusion Couple

A diffusion couple has been prepared to investigate diffusion of Y in Mg₁₇Al₁₂. Both the intermetallic (with no Y addition) and pure Y were cut to cylinders 1 cm diameter and 50 mm in height. Cylinders were grinded, polished and pressed together by a spring supported mechanism to conserve pressure throughout the experiment. The sample was placed in an electric furnace inside a quartz tube maintaining 10⁻² Pa pressure, held at 450 °C for 2 hrs and then cooled to room temperature inside the quartz tube and under vacuum. The sample and studied by OM and SEM (FEI Quanta450). Local chemical compositions were studied by EDS (Bruker XFlash 610).

5.3 Results

5.3.1 Thermodynamic Calculations

Mg-Al-Y pseudo-binary equilibrium phase diagrams were calculated to investigate crystallization sequence in Mg₁₇Al₁₂ intermetallics containing 300 and 5000 ppm Y (Fig. 5.2a & b). In both Y concentrations Mg₁₇Al₁₂ forms at a range between ~43-46 wt% Al as a non-stoichiometric intermetallic. When Y is present in the system, other than the beta phase, the equilibrium Al₄MgY intermetallic forms at the same Al composition. This precipitate was experimentally observed for the first time by Zarechnyuk et al. [33]; it has the MgZn₂ crystal structure with lattice parameters of a=5.33 Å and c= 8.57 Å. The phase diagrams of Fig. 5.2 indicate that presence of 5000 ppm Y in the system changes the crystallization sequence in the two alloys. The main difference between the low and high Y levels are in the solidification path of the Mg₁₇Al₁₂ intermetallic. This

difference gives more time for coarsening of Al_4MgY . For 300 ppm Y the solidification path (Fig.5.3) is:



However, at 5000ppmY the Al_4MgY phase forms earlier in the liquid state (Fig.5.3):

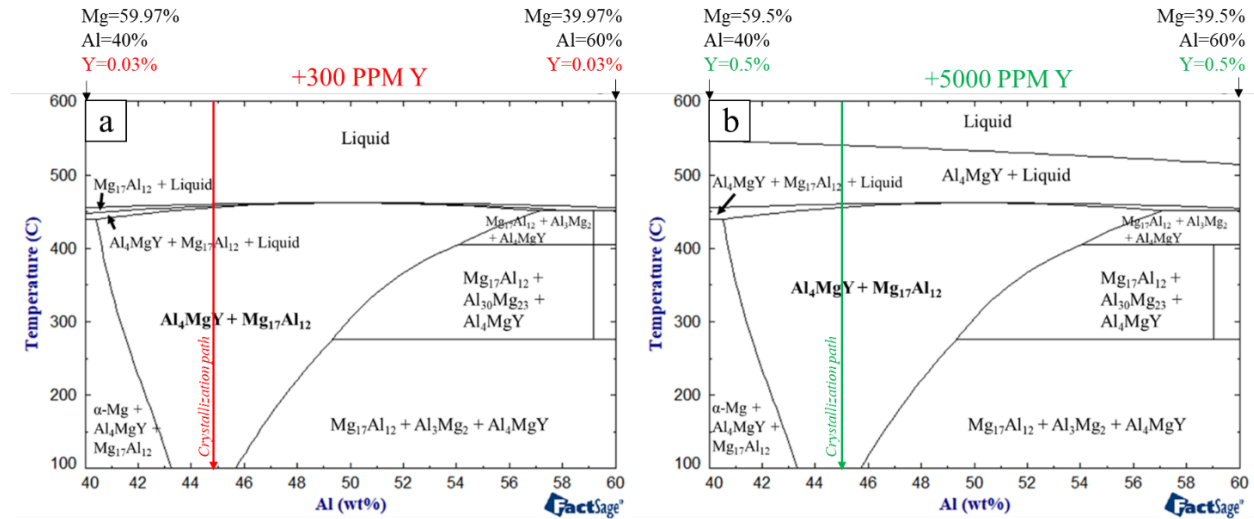


Fig. 5.2 Mg-Al-Y Pseudo Binary Equilibrium phase diagrams, containing (a) 300 ppm and (b) 5000 ppm Y.

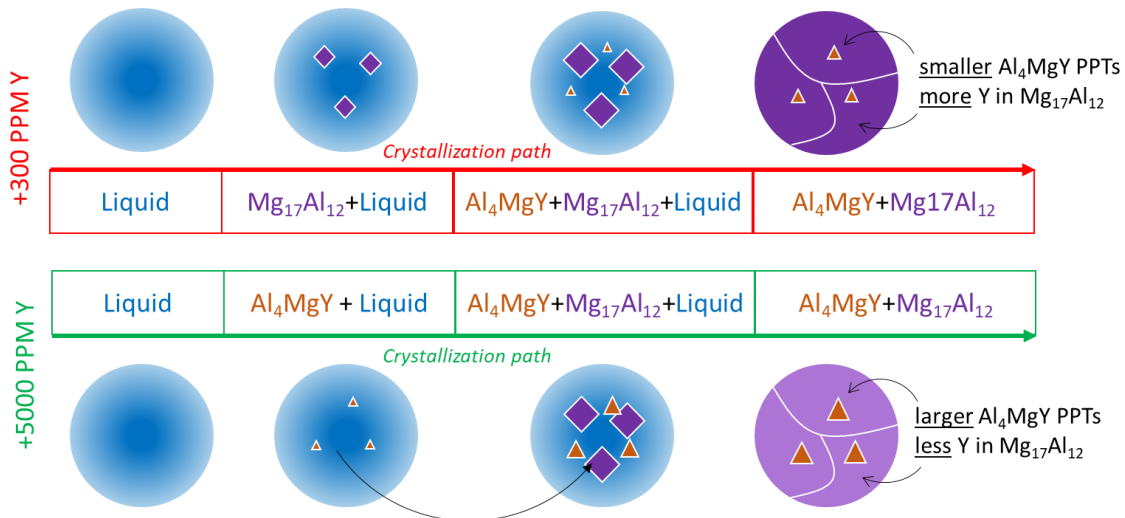


Fig. 5.3 Schematic drawing indicating the crystallization difference of the two intermetallic containing 300 and 5000 ppm Y.

5.3.2 Microstructural Investigation

As-cast Intermetallics

The backscattered electron (BSE/SEM) microstructures of the three intermetallics are shown in Fig. 5.4. Samples β and β_{300Y} (Fig. 5.4 a&b) consist mainly of a Mg-Al phase (dark contrast). Fe enriched rod-like impurities (bright contrast) are also observed due to Fe diffusion from the raw materials. A small amount of Y was observed in some Fe-rich impurities in β_{300Y} as per the EDS analysis. The microstructure of β_{5000Y} (Fig. 5.4c) consists mainly of the Mg-Al phase and cuboidal precipitates that contain Al, Mg and Y (Fig.5.5). The amount of Y in the matrix and in the Y-rich precipitates was determined by WDS (Table 5.2). It is found that Y goes into solid solution in the $Mg_{17}Al_{12}$ phase of the β_{300Y} but the max solubility is at ~ 330 ppm above which it starts to precipitate as Y-rich phase as seen in β_{5000Y} . The WDS of β_{5000Y} (Fig.5.5a) shows that the cuboidal precipitates have a stoichiometry close to Al_4MgY (Table 5.3); this phase is also predicted by the thermodynamic calculations.

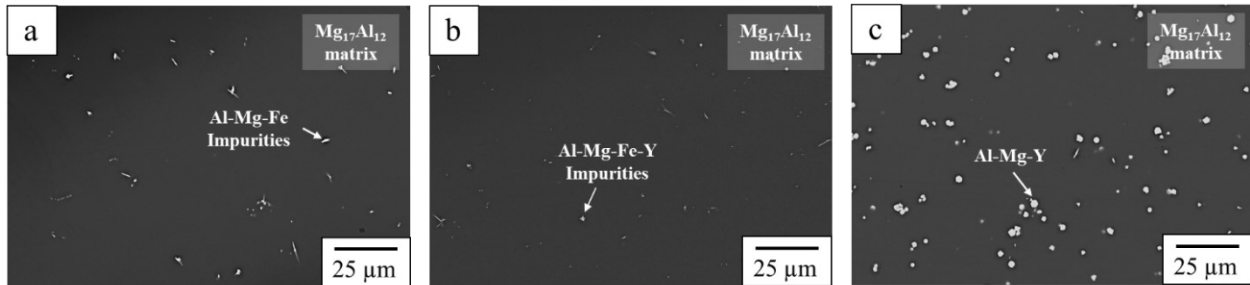


Fig. 5.4 BSE/SEM microstructures of the studied intermetallics (a) β , (b) β_{300Y} and (c) β_{5000Y} .

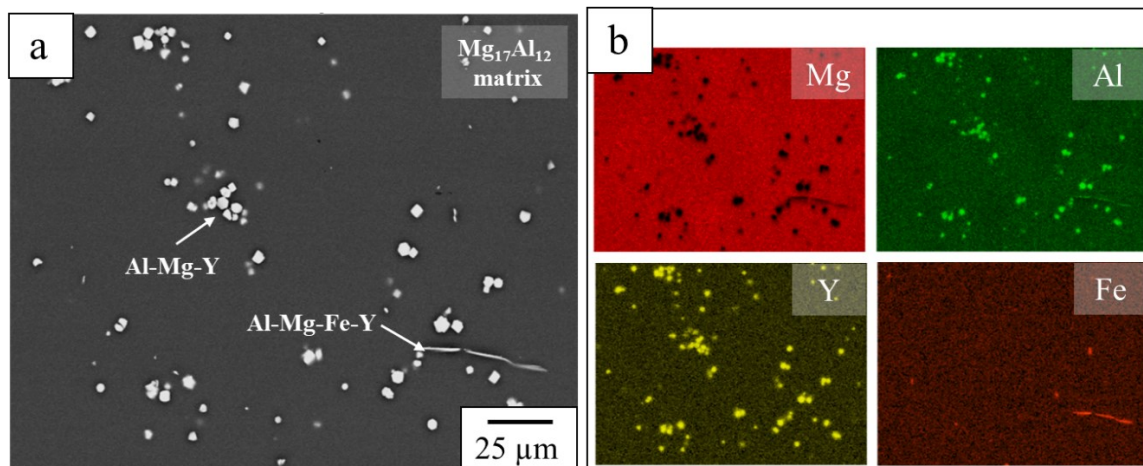


Fig. 5.5 Microstructure of the β_{5000Y} (a) BSE image and (b) EDS mapping of the respective region of a.

Table 5.2 EPMA/WDS chemical analysis of the matrix (solid solution).

Sample	Mg (wt%)	Al (wt%)	Y (ppm)	Mg (at%)	Al (at%)	Y (at%)
β	54.44±0.53	44.75±0.5 8	-	57.45±0.53	42.55±0.53	-
β_{300Y}	51.12±0.43	44.42±0.6 9	259±73	56.09±0.58	43.90±0.58	0.008±0.002
β_{5000Y}	53.68±0.26	45.90±0.1 7	333±81	56.49±0.20	43.50±0.20	0.010±0.002

Detection limits: 80 ppm for β_{5000Y} and 150 ppm for β_{300Y} (Table 2) because EDS cannot detect ppm levels (0.1wt% detection limit).

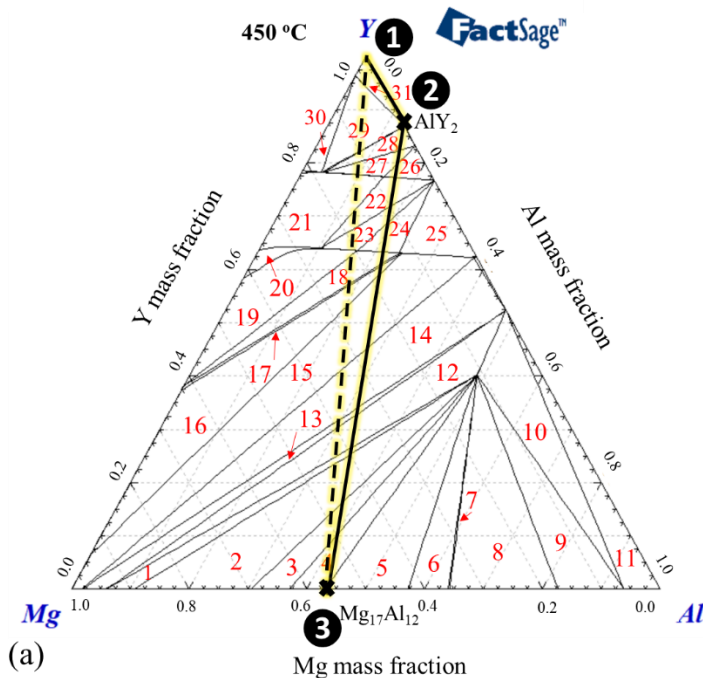
Table 5.3 EPMA/WDS chemical analysis of the Y enriched precipitates in β_{5000Y} .

	Mg	Al	Y	Al/Mg	Al/Y	Mg/Y
Cuboidal precipitate in β_{5000Y}	19.70 ±0.78	65.84 ±0.34	14.46 ±0.71	3.34 ±0.14	4.56 ±0.24	1.36 ±0.12

Diffusion Couple

The diffusion couple was created to investigate Y diffusion into the intermetallic and the phases that form between intermetallic $Mg_{17}Al_{12}$ and Y metal. Fig 5.6. shows the equilibrium isotherms of Mg-Al-Y at 450 °C and 25 °C with the terminal compositions shown in dashed line. The diffusion couple was not quenched from 450 °C, but it was slow cooled to room temperature, so the phases that exist in the diffusion couple sample can be predicted with the isotherm at 25 °C.

SEM/EDS analysis (Fig. 5.7) shows the Y-Al-Mg precipitates that exist at the interface of the diffusion couple. EDS mapping confirms, interestingly, that Y diffuses to the $Mg_{17}Al_{12}$ side and Al diffuses towards Y side (Fig. 5.7d). The phase that is seen in at the interface is AlY_2 (Fig. 5.8). Based on the analysis and isotherm at 450 °C, it can be suggested the diffusion path is $Y \rightarrow AlY_2 \rightarrow Mg_{17}Al_{12}$ as shown with the solid line (1-2-3) in Fig. 5.6.a.



1. $Al_4MgY + HCP_A3$ [P63/mmc (194)]
2. $Al_4MgY + HCP_A3$ [P63/mmc (194)] + Liquid
3. $Al_4MgY + Liquid$
4. $Al_4MgY + Mg_{17}Al_{12} + Liquid$
5. $Al_4MgY + Mg_{17}Al_{12}$
6. $Al_4MgY + Al_3Mg_2 + Mg_{17}Al_{12}$
7. $Al_4MgY + Al_3Mg_2$
8. $Al_4MgY + Al_3Mg_2 + Al$
9. $Al_4MgY + Al$
10. $Al_3Y + Al_4MgY + Al$
11. $Al_3Y + Al$
12. $Al_3Y + Al_4MgY + HCP_A3$ [P63/mmc (194)]
13. $Al_3Y + HCP_A3$ [P63/mmc (194)]
14. $Al_3Y + C15 + HCP_A3$ [P63/mmc (194)]
15. $C15 + HCP_A3$ [P63/mmc (194)]
16. $C15 + Mg_{17}Al_{12} + HCP_A3$ [P63/mmc (194)]
17. $C15 + Mg_{17}Al_{12}$
18. $C14 + C15 + Mg_{17}Al_{12}$
19. $C14 + Mg_{17}Al_{12}$
20. $C14$
21. $BCC-B2$ [Pm-3m (221)] + $C14$
22. $YAl + BCC-B2$ [Pm-3m (221)] + $C14$
23. $YAl + C14$
24. $YAl + C14 + C15$
25. $YAl + C15$
26. $YAl + BCC-B2$ [Pm-3m (221)] + Al_2Y_3 or Mg_2Y_3
27. $BCC-B2$ [Pm-3m (221)] + Al_2Y_3 or Mg_2Y_3
28. $AlY_2 + BCC-B2$ [Pm-3m (221)] + Al_2Y_3 or Mg_2Y_3
29. $AlY_2 + BCC-B2$ [Pm-3m (221)] + HCP_A3 [P63/mmc (194)]
30. $BCC-B2$ [Pm-3m (221)] + HCP_A3 [P63/mmc (194)]
31. $AlY_2 + HCP_A3$ [P63/mmc (194)]

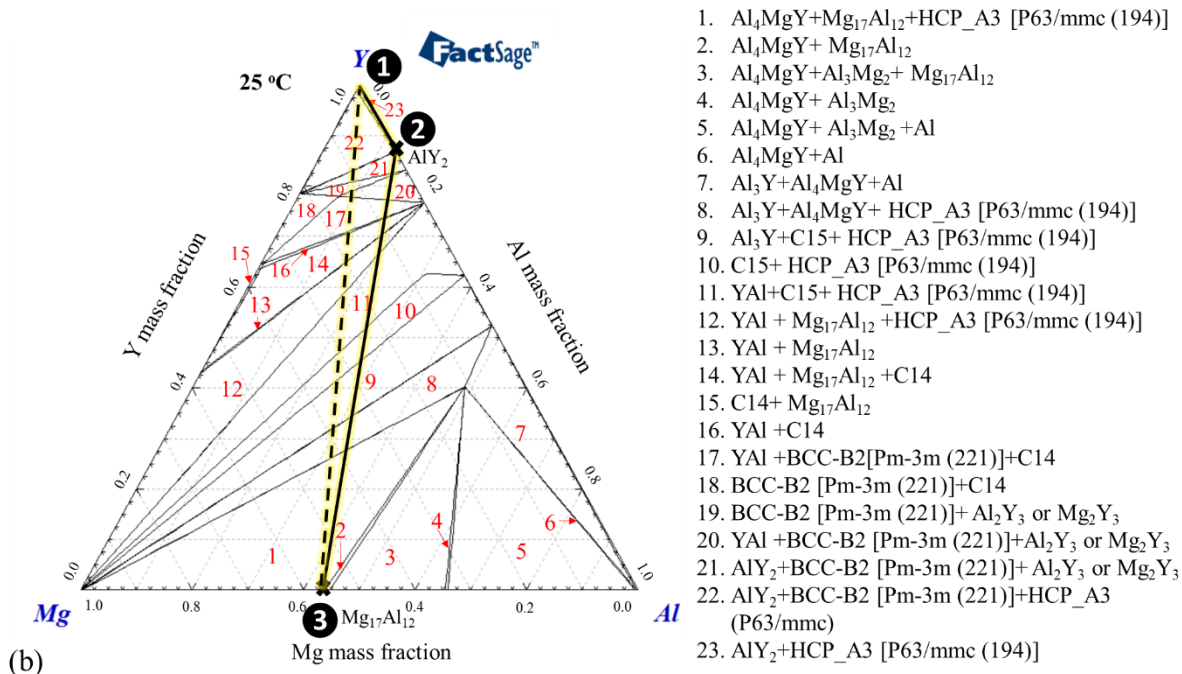


Fig. 5.6 Mg-Al-Y isotherm at (a) 450 °C and (b) at 25 °C with the terminal compositions shown with the dashed line. The diffusion path is shown with the solid line 1-2-3.

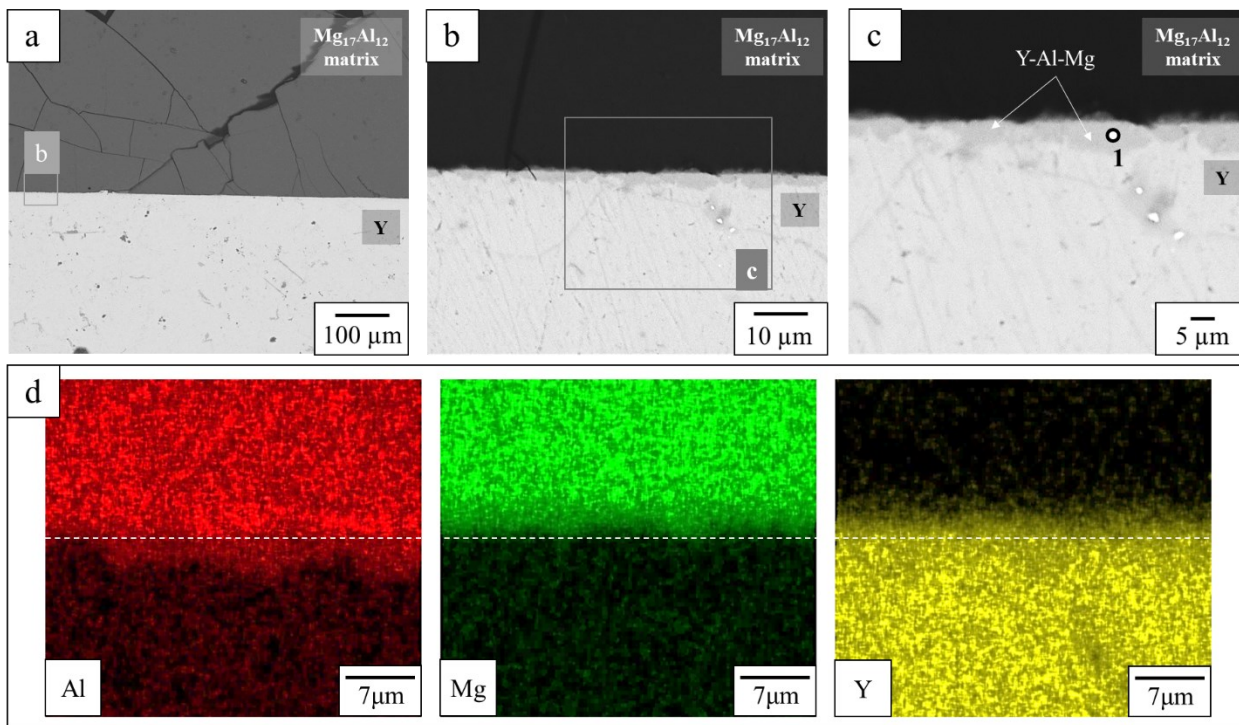


Fig. 5.7 Interface of the $\text{Mg}_{17}\text{Al}_{12}/\text{Y}$ diffusion couple. (a-c) BSE micrographs at consecutive magnifications of squared and labeled regions, (d) EDS elements distribution map of c.

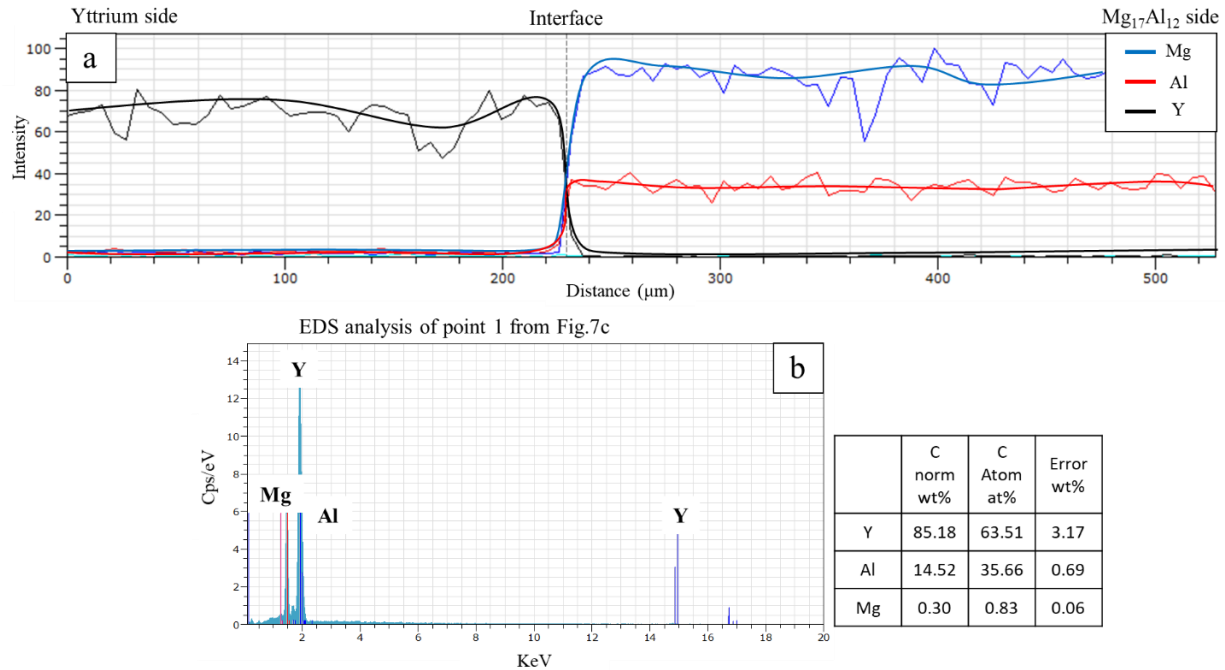


Fig. 5.8 (a) Profile of Mg, Al and Y distribution at the interface of Mg₁₇Al₁₂/Y, (b) EDS of Y rich precipitates on the Mg₁₇Al₁₂/Y interface.

5.3.3 Crystal structure

The XRD (Fig. 5.9) mostly detects the Mg₁₇Al₁₂ phase in all three (β , β_{300Y} and β_{5000Y}) samples due to the low amounts of other possible phases. However, a small peak of Al₄MgY appears in the β_{5000Y} which is not strong due to the low volume fraction of this phase. The lattice parameter of the Mg₁₇Al₁₂ phase was determined using the strongest peak at high angles (2θ between 64-66°) to reduce the error of the calculated lattice parameter. The lattice parameter a (Table 5.4) decreases in β_{300Y} and then it increases in β_{5000Y} ; consequently, the cell volume follows the same trend.

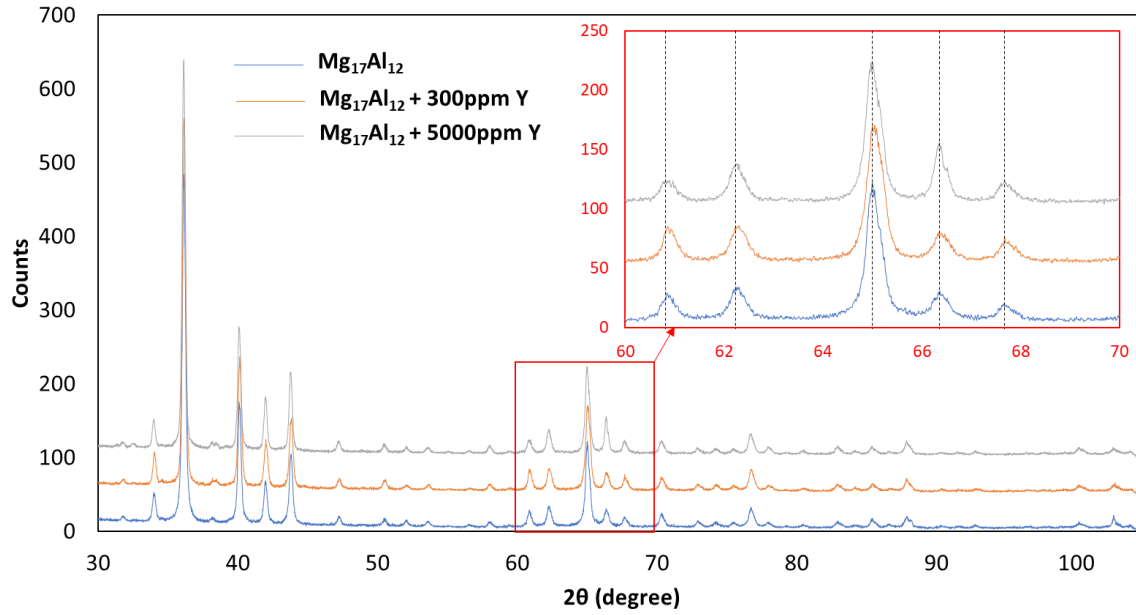


Fig. 5.9 XRD patterns of the three samples.

Table 5.4 Lattice parameter as per XRD results.

Intermetallic	<i>a</i> parameter (Å)	Cell Volume (Å ³)
β	10.5431±0.0011	1171.94
β _{300Y}	10.5426±0.0009	1171.77
β _{5000Y}	10.5437±0.0010	1172.14

5.3.4 Mechanical Properties

Table 5.5 presents the properties experimentally obtained of average elastic moduli, the microhardness and density of the three samples, as well as the theoretical elastic moduli values of Mg₁₇Al₁₂ from first principle simulations. The experimental results indicate the Young’s (E), shear (G) and bulk (B) moduli increase for both β_{300Y} and β_{5000Y}. The microhardness decreases for β_{300Y} but it increases for β_{5000Y}.

Table 5.5 Microhardness and measured moduli values of the three intermetallic samples.

Intermetallic	E (GPa)	G (GPa)	B (GPa)	μ	B/G	Microhardness (HV)	Density (g/cm ³)
β -Mg ₁₇ Al ₁₂	52.16 ±3.06	19.64 ±1.45	43.46 ±2.55	0.3	2.21	249±2	2.11±0.01
<i>Calculated</i> [7–10,34,35]	55.3 -79.62	21.3 -32.49	45.15- 48.30	0.23 -0.3	1.48 -2.20		2.085[20]
β _{300Y}	53.03 ±3.68	20.39 ±1.81	44.19 ±3.06	0.30	2.17	246±3	2.10±0.01
β _{5000Y}	56.32 ±3.54	21.51 ±1.71	46.93 ±2.95	0.30	2.18	253±5	2.13±0.01

5.4 Discussion

The main research question in this study was if Y addition influences the characteristics of the Mg₁₇Al₁₂ (β), the second phase with significant effect on the mechanical properties of Mg-Al based alloys. Various effects of solute Y atoms were seen on the β phase.

Solubility of Y in Mg₁₇Al₁₂ and Phase formation

Thermodynamic simulations show almost zero solubility of Y in Mg₁₇Al₁₂. Microstructural investigation of β _{5000Y} in this study showed that β -phase has solubility for Y and that the maximum level is ~330ppm as per WDS. Above the solubility limit, coarse cuboidal precipitates of Al₄MgY form that coexist with the Mg-Al phase. Thermodynamic calculations show that Mg₁₇Al₁₂ coexists with the Al₄MgY phase in both Mg₁₇Al₁₂ + 300 ppm Y and Mg₁₇Al₁₂ + 5000 ppm Y. The actual Y level in Mg₁₇Al₁₂ in the β _{300Y} sample was 259 ppm which is below the experimental maximum solubility determined in this study.

Lattice Parameters

Size Effect: This study observed that yttrium as solute changed the lattice parameter, a , of the β -

phase (Table 5.4). The change in lattice parameters can be due to size difference that the solute has with respect to the host metal as determined by Vegard's law [36]. Table 5.6 lists the metallic and covalent radii and the valency of Mg, Al and Y. The radius of Y (metallic or covalent) is larger than the radii of Mg and Al. Therefore, the lattice parameter would increase as the larger Y substitutes either Al or Mg sites. Additionally, first principle simulations [10] show that if a trivalent rare earth atom (e.g. La) with larger atomic radius than Mg and Al is added to $Mg_{17}Al_{12}$, an increase in the La-Mg and La-Al bond lengths will occur.

Table 5.6 Radii and Valence of Elements [37]

Element	Metallic radius, pm	Covalent radius (single bond), pm	Valency
Mg	160	136	+2
Al	143	125	+3
Y	181	162	+3

In this study, a different trend is seen, the lattice parameter a first decreases and then increases with increasing Y dissolved in the β -phase (Fig. 5.10, Table 5.7). The effect is not isolated; the increase in Y is accompanied by an increase in the Al content suggesting that the Y possibly substitutes the Mg sites. This is supported by the fact that the e/a calculated using our WDS results increases with Y compared to the β -phase with no Y (Table 5.7).

Table 5.7 Lattice parameter as per XRD results and calculated e/a ratio.

Intermetallic	a parameter (Å)	Cell Volume (Å ³)	Al (at%)	Y (at%)	e/a
β	10.5431±0.0011	1171.94	42.55±0.53	-	2.426±0.037
β_{300Y}	10.5426±0.0009	1171.77	43.90±0.58	0.008±0.002	2.439±0.041
β_{5000Y}	10.5437±0.0010	1172.14	43.50±0.20	0.010±0.002	2.435±0.014

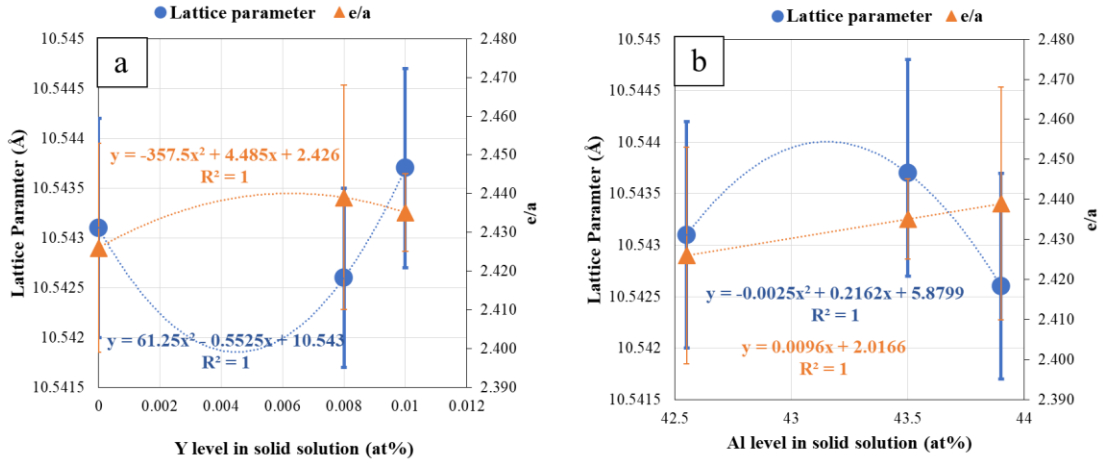


Fig. 5.10 Effect of (a) yttrium and (b) aluminum on the lattice parameter and e/a of the β -phase.

However, there are other underlying trends: sample β_{5000Y} has higher Y but lower Al than sample β_{300Y} which also has higher e/a suggesting that Y here may be substituting Al sites as well. This also agrees with the diffusion couple results where Y diffuses into $Mg_{17}Al_{12}$ and Al diffuse to Y. The reversal in dependence of the lattice parameter on Y and Al occurs at ~ 0.005 at% Y and ~ 43.1 at% Al. The increase in lattice parameter above 0.005 at% Y can be explained by the size effect. However, the initial decrease in lattice parameter with increasing Y and with increasing Al cannot be explained on the basis of the metallic radii. A possible explanation can be sought in the fact that Y at low levels can form covalent bonds, yet the covalent radius of Y is similar to the metallic radius of Mg and larger than the covalent and metallic radii of Al and Mg indicating that the size effect does not offer a plausible explanation for the initial lattice contraction. The effect can be attributed to the inherent chemical disorder of the β -phase that exists at off-stoichiometric compositions and that consists of partial and fractional site occupancy [12]. Shin et al [38] performed first principles calculations and found that the thermodynamic stabilization at off-stoichiometry is complicated in the β -phase; they found that simple native point defects do not account for stabilization which can only be attributed to the formation of complicated defect

mechanisms such as multi-defect clustering. The present study also concurs that the effect of Y on the lattice parameter is not likely due to simple site substitution.

Electron-to-Atom Ratio (e/a): In solid solution metallic alloys, e/a governs the lattice parameters by Brillouin zone overlap. When a sufficient amount of higher valency element is added to a crystal structure, e/a increases and more electrons overlap from the first Brillouin zone [36] to the second zone. The electrons are over a plane of energy discontinuity in the reciprocal space distorting the Brillouin zone [39]. The contraction of the Brillouin zone in the reciprocal space means the expansion of the lattice parameter in the real space. The effect may be masked initially by size effects, however, the usual behavior of increase of lattice parameter with increasing e/a is not seen here, with the addition of +3 valency yttrium to the β -phase (Fig. 5.10.a). There is correlation of the increase in e/a with the increase in Al (Fig. 5.10.b).

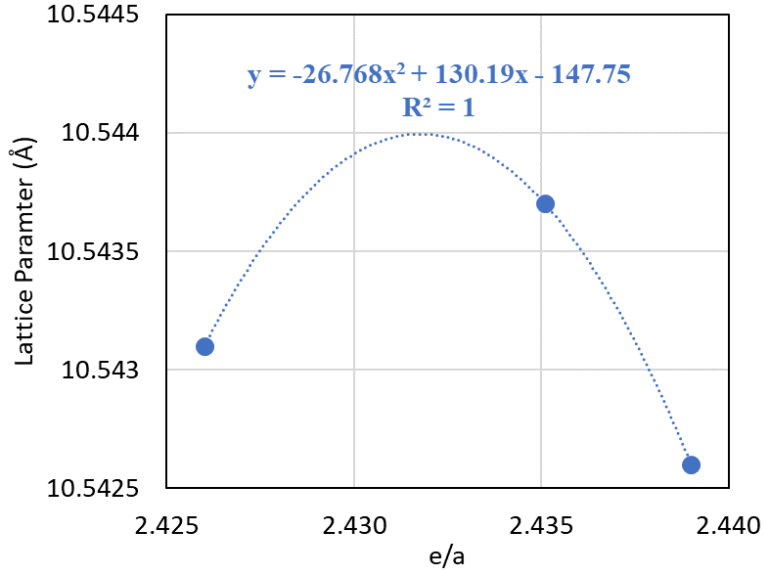


Fig. 5.11 Correlation between the lattice parameter and e/a of the β -phase.

A correlation with e/a and the lattice parameter, a , that shows an initial increase with e/a but then a decrease (Fig. 5.11) is not aligned by the usual effect of e/a on the lattice constant in metallic

solid solution alloys. Vrnk et al.[12] have determined that the Hume-Rothery stabilization with the formation of a pseudo gap occurs in β at the stoichiometric composition with a lattice parameter a of 10.5492 Å and at an e/a of 2.41. The β -phase with and without Y studied in this work is off-stoichiometric and its e/a ratio also implies that its thermodynamic stabilization is not through Hume-Rothery stabilization but through defect structure mechanisms.

Mechanical Properties

Elastic Moduli: It is seen that the elastic moduli of the β -phase increase with Y. This can be attributed partly to the increase in the cohesive energy of the β -phase. Ca addition in $Mg_{17}Al_{12}$ has been reported to increase the cohesive energy of the intermetallic [19]. On the other hand, the steep increase seen in β_{5000Y} has a contribution from the presence of Al_4MgY precipitates in the matrix of $Mg_{17}Al_{12}$ via the inverse rule of mixtures.

Microhardness: Microhardness decreases initially and then increases slightly for the β_{5000Y} . The increase in the latter is likely due to Al_4MgY . Previous research has similarly shown that the addition of Er in $Mg_{17}Al_{12}$ intermetallic has improved its microhardness due to the uniform distribution of Al_3Er precipitates [40]. The initial decrease in hardness in β_{300Y} can be related to the increase in Al; Al increases the e/a ratio and the deviation from stoichiometry at e/a of 2.41 suggesting an increase in disorder.

Ductility: According to the experimental B/G criterion, the $Mg_{17}Al_{12}$ can be characterized as a ductile intermetallic ($B/G > 1.75$) that agrees with previous first principle simulations [34,35]. However, the Y addition seems to slightly weaken its ductility as it reduces the B/G ratio.

5.5 Conclusions

1. Thermodynamic calculations show that the main difference on the solidification path between β_{300} and β_{5000} is that at 5000ppmY the Al_4MgY phase forms earlier in the liquid state. The Al_4MgY phase coexists with the $\text{Mg}_{17}\text{Al}_{12}$ microconstituent after the solidification.
2. The maximum solubility of Y inside the $\text{Mg}_{17}\text{Al}_{12}$ solid solution is at $\sim 330\text{ppm}$ where the $\text{Al}_{4.56}\text{Mg}_{1.36}\text{Y}$ forms with excess amount according to EPMA/WDS.
3. The diffusion couple experiments show that Y diffuses inside the β intermetallic and AlY_2 precipitates form at the $\text{Mg}_{17}\text{Al}_{12}$ /pure Y interface.
4. According to XRD analysis, the lattice parameter and the cell volume decrease for low Y additions (i.e., 300 ppm Y) but increases for higher levels (i.e., 5000 ppm Y).
5. The e/a ratio increases with Y as per the WDS analysis. The intermetallic studied in this work is off-stoichiometric and its e/a ratio implies that its thermodynamic stabilization is not through Hume-Rothery stabilization but through defect structure mechanisms.
6. The microhardness and the elastic moduli increase with Y additions. $\text{Mg}_{17}\text{Al}_{12}$ appears to be a ductile intermetallic according to the criterion B/G. However, Y addition slightly weakens the ductile character.

5.6 Acknowledgements

This project was conducted under the financial support of the Natural Sciences and Engineering Research Council of Canada (NSERC) Discovery Grant (G210358NSERC/RGPIN-2016-05121). The authors would like to thank Christophe Bescond and the National Research Council Canada for the ultrasonic velocity measurements. We would also like to thank Luis A. Villegas-Armenta for his assistance in alloy casting, Ali Jaber for the fruitful discussions and Alireza Zaheri for

conducting diffusion couple tests. Konstantinos Korgiopoulos gratefully acknowledges McGill Engineering Doctoral Award program (MEDA).

5.7 References

- [1] H. Dini, N.-E. Andersson, A.E.W. Jarfors, Effect of Mg₁₇Al₁₂ fraction on mechanical properties of Mg-9% Al-1% Zn cast alloy, *Metals (Basel)*. 6 (2016) 251.
- [2] L. Zhang, Z.Y. Cao, Y.B. Liu, G.H. Su, L.R. Cheng, Effect of Al content on the microstructures and mechanical properties of Mg–Al alloys, *Mater. Sci. Eng. A*. 508 (2009) 129–133.
- [3] H. Lin, M. Yang, H. Tang, F. Pan, Effect of minor Sc on the microstructure and mechanical properties of AZ91 Magnesium Alloy, *Prog. Nat. Sci. Mater. Int.* 28 (2018) 66–73.
- [4] P. Schobinger-Papamantellos, P. Fischer, Neutronenbeugungsuntersuchung der Atomverteilung von Mg 17 Al 12, *NW*. 57 (1970) 128–129.
- [5] A.J. Bradley, J. Thewlis, The crystal structure of α -manganese, *Proc. R. Soc. London. Ser. A, Contain. Pap. a Math. Phys. Character.* 115 (1927) 456–471.
- [6] M. Avedesian, H. Baker, *ASM specialty handbook: magnesium and magnesium alloys.*, ASM International, Ohio, 1998.
- [7] W.-C. Hu, Y. Liu, X.-W. Hu, D.-J. Li, X.-Q. Zeng, X. Yang, Y.-X. Xu, X. Zeng, K.-G. Wang, B. Huang, Predictions of mechanical and thermodynamic properties of Mg₁₇Al₁₂ and Mg₂Sn from first-principles calculations, *Philos. Mag.* 95 (2015) 1626–1645. doi:10.1080/14786435.2015.1040098.
- [8] D. Zhou, J. Liu, S. Xu, P. Peng, First-principles investigation of the binary intermetallics in Mg-Al-Sr alloy: Stability, elastic properties and electronic structure, *Comput. Mater.*

- Sci. (2014) 24-29. doi:10.1016/j.commat.2014.01.007.
- [9] Z.W. Huang, Y.H. Zhao, H. Hou, P.D. Han, Electronic structural, elastic properties and thermodynamics of Mg₁₇Al₁₂, Mg₂Si and Al₂Y phases from first-principles calculations, *Phys. B Condens. Matter.* (2012) 1075–1081. doi:10.1016/j.physb.2011.12.132.
- [10] J. Dai, Y. Song, R. Yang, Influences of alloying elements and oxygen on the stability and elastic properties of Mg₁₇Al₁₂, *J. Alloys Compd.* 595 (2014) 142–147.
- [11] K. Urban, M. Feuerbacher, Structurally complex alloy phases, *J. Non. Cryst. Solids.* 334 (2004) 143–150.
- [12] S. Vrtnik, S. Jazbec, M. Jagodič, A. Korelec, L. Hosnar, Z. Jagličić, P. Jeglič, M. Feuerbacher, U. Mizutani, J. Dolinšek, Stabilization mechanism of γ -Mg₁₇Al₁₂ and β -Mg₂Al₃ complex metallic alloys, *J. Phys. Condens. Matter.* 25 (2013) 425703.
- [13] J.E. Saal, S. Kirklin, M. Aykol, B. Meredig, C. Wolverton, Materials design and discovery with high-throughput density functional theory: the open quantum materials database (OQMD), *Jom.* 65 (2013) 1501–1509.
- [14] A. Jain, S.P. Ong, G. Hautier, W. Chen, W.D. Richards, S. Dacek, S. Cholia, D. Gunter, D. Skinner, G. Ceder, Commentary: The Materials Project: A materials genome approach to accelerating materials innovation, *APL Mater.* 1 (2013) 11002.
- [15] J. Ragani, P. Donnadieu, C. Tassin, J.J. Blandin, High-temperature deformation of the γ -Mg₁₇Al₁₂ complex metallic alloy, *Scr. Mater.* 65 (2011) 253–256.
- [16] R.M. Wang, A. Eliezer, E.M. Gutman, An investigation on the microstructure of an AM50 magnesium alloy, *Mater. Sci. Eng. A.* 355 (2003) 201–207.
- [17] A. Vaid, J. Guérolé, A. Prakash, S. Korte-Kerzel, E. Bitzek, Atomistic simulations of

- basal dislocations in Mg interacting with Mg₁₇Al₁₂ precipitates, *Materialia*. 7 (2019) 100355.
- [18] K. Korgiopoulos, B. Langelier, M. Pekguleryuz, Mg₁₇Al₁₂ Phase Refinement and the Improved Mechanical Performance of Mg-6Al alloy with trace Erbium Addition, *Mater. Sci. Eng. A*. (2021) 141075. doi:<https://doi.org/10.1016/j.msea.2021.141075>.
- [19] D. Zhou, P. Peng, J. Liu, Energetics, electronic structure, and structure stability of the calcium alloying Mg₁₇Al₁₂ phase from first principles calculations, *Mater Sci Pol*. 25 (2007) 145–153.
- [20] J.-C. Crivello, T. Nobuki, T. Kuji, Limits of the Mg–Al γ -phase range by ball-milling, *Intermetallics*. 15 (2007) 1432–1437.
- [21] M.X. Zhang, P.M. Kelly, Crystallography of Mg₁₇Al₁₂ precipitates in AZ91D alloy, *Scr. Mater.* (2003) 647-652. doi:10.1016/S1359-6462(02)00555-9.
- [22] A.A. Kaya, M.O. Pekguleryuz, K.U. Kainer, *Fundamentals of magnesium alloy metallurgy*, Woodhead Publishing, Cambridge, 2013.
- [23] S.F. Pugh, XCII. Relations between the elastic moduli and the plastic properties of polycrystalline pure metals, London, Edinburgh, Dublin *Philos. Mag. J. Sci.* 45 (1954) 823–843.
- [24] K. Korgiopoulos, M. Pekguleryuz, The significant effect of trace yttrium level on the mechanical properties of cast Mg–6Al alloy through a refinement mechanism, *Mater. Sci. Eng. A*. 775 (2020) 138966.
- [25] S.-R. Wang, P.-Q. Guo, L.-Y. Yang, Y. Wang, Microstructure and mechanical properties of AZ91 alloys by addition of yttrium, *J. Mater. Eng. Perform.* 18 (2009) 137–144. doi:10.1007/s11665-008-9255-z.

- [26] J. Zhang, X. Niu, X. Qiu, K. Liu, C. Nan, D. Tang, J. Meng, Effect of yttrium-rich misch metal on the microstructures, mechanical properties and corrosion behavior of die cast AZ91 alloy, *J. Alloys Compd.* 471 (2009) 322–330. doi:10.1016/j.jallcom.2008.03.089.
- [27] N. Kashefi, R. Mahmudi, The microstructure and impression creep behavior of cast AZ80 magnesium alloy with yttrium additions, *Mater. Des.* 39 (2012) 200–210. doi:10.1016/j.matdes.2012.02.036.
- [28] H. Cai, F. Guo, J. Su, L. Liu, B. Chen, Study on microstructure and strengthening mechanism of AZ91-Y magnesium alloy, *Mater. Res. Express.* 5 (2018) 36501. doi:10.1088/2053-1591/aab0b7.
- [29] C.W. Bale, P. Chartrand, S.A. Degterov, G. Eriksson, K. Hack, R. Ben Mahfoud, J. Melançon, A.D. Pelton, S. Petersen, FactSage thermochemical software and databases, *Calphad.* 26 (2002) 189–228.
- [30] B.H. Toby, R.B. Von Dreele, GSAS-II: the genesis of a modern open-source all purpose crystallography software package, *J. Appl. Crystallogr.* 46 (2013) 544–549.
- [31] J. Krautkrämer, H. Krautkrämer, *Ultrasonic testing of materials*, Springer Science & Business Media, 2013.
- [32] P.O. Moore, *Nondestructive testing handbook*, American Society for Nondestructive Testing, 2012.
- [33] O.S. Zarechnyuk, M.E. Drits, R.M. Rykhal, V. V Kinzhibalo, Study of a Magnesium-Aluminum-Yttrium System at 400 in the Phase Containing 0-33.3 at.% Yttrium, *Izv. Akad. Nauk. SSSR Met.* 5 (1980) 242–244.
- [34] Y.-H. Duan, Y. Sun, M.-J. Peng, Z.-Z. Guo, First principles investigation of the binary intermetallics in Pb–Mg–Al alloy: stability, elastic properties and electronic structure,

- Solid State Sci. 13 (2011) 455–459. doi:10.1016/j.solidstatesciences.2010.12.011.
- [35] N. Wang, W.-Y. Yu, B.-Y. Tang, L.-M. Peng, W.-J. Ding, Structural and mechanical properties of Mg₁₇Al₁₂ and Mg₂₄Y₅ from first-principles calculations, *J. Phys. D. Appl. Phys.* 41 (2008) 195408. doi:10.1088/0022-3727/41/19/195408.
- [36] G.V. Raynor, *The physical metallurgy of magnesium and its alloys*, Pergamon, 1959.
- [37] J. Emsley, *The elements*, 3rd ed., Clarendon Press, Oxford, 1998.
- [38] D. Shin, C. Wolverton, The effect of native point defect thermodynamics on off-stoichiometry in β -Mg₁₇Al₁₂, *Acta Mater.* 60 (2012) 5135–5142.
- [39] H. Jones, LIX. The effect of electron concentration on the lattice spacings in magnesium solid solutions, London, Edinburgh, Dublin *Philos. Mag. J. Sci.* 41 (1950) 663–670.
- [40] L.I. Yonggang, W.E.I. Yinghui, H.O.U. Lifeng, G.U.O. Chunli, H.A.N. Pengju, Effect of erbium on microstructures and properties of Mg-Al intermetallic, *J. Rare Earths.* 32 (2014) 1064–1072.

CHAPTER 6

Mg₁₇Al₁₂ Phase Refinement and the Improved Mechanical Performance of Mg-6Al alloy with trace Erbium Addition

Chapters 3-5 discussed the effect of Y additions on the modification of Mg₁₇Al₁₂ and α -Mg phases and the effect on mechanical properties of Mg-6wt%Al based alloys. It was shown that trace Y addition can refine the microstructure more effectively than high additions leading to mechanical properties improvement. The effect of Y was also investigated on the Mg₁₇Al₁₂ intermetallic itself where Y changes its crystal structure and the moduli of elasticity. The current chapter presents the work that extends the knowledge previously acquired on Y-modified Mg-Al alloys to Er additions to Mg-6wt%Al to investigate the possible refinement of the microstructure and the effect on the mechanical properties. Atom probe tomography was used for first time to investigate the possible dissolution of trace Er in Mg₁₇Al₁₂ as well as microstructural investigation and mechanical testing. A comparison between the Y and Er modified alloys is made to rationalize the differences between the two elements on the refinement of Mg-6wt%Al alloy.

ABSTRACT

With an improvement in room temperature ductility, the automotive use of cast Mg-Al alloys can be extended to structural body components. This is challenging since Al readily forms brittle intermetallics with the alloying additions such as rare earths and limits their solid solubility largely, nullifying the potential beneficial effects of rare earth elements on plasticity e.g., on stacking fault energy. In this study, significant improvement of mechanical properties in Mg-6wt% Al (Mg-6Al) casting alloy was seen with low levels of Er additions (60 ppm and 880 ppm) that was related to the modifying effect of Er on the $Mg_{17}Al_{12}$ precipitates and the α -Mg. Thermodynamic simulations, atom probe tomography, scanning electron microscopy, X-rays diffraction and mechanical testing were employed to understand the modification mechanism in Mg-6Al. According to Scheil solidification simulations, Al_2Er Laves co-precipitates at the same temperature as $Mg_{17}Al_{12}$ exerting an inoculating effect when Er is at trace levels in the bulk alloy; however, when Er in the alloy increases, Al_2Er forms at higher temperatures much before $Mg_{17}Al_{12}$ losing its inoculant potential. It was also seen that Er is soluble in $Mg_{17}Al_{12}$ causing changes to its lattice parameter and cell volume. Tensile strength, ductility, compressive strain to fracture and hardness are influenced by microstructural refinement. Yield strength at the higher level of Er (880 ppm) can be explained by the existence of Er-rich intermetallics while the yield strength at low levels of Er (60 ppm) can more likely be explained by the nature of β -phase.

Keywords: Magnesium; $Mg_{17}Al_{12}$ refinement; Mg-Al-Er alloys; Mechanical properties; Atom probe tomography; Thermodynamic simulations

6.1 Introduction

Magnesium (Mg) structural alloys are a viable solution for vehicle weight reduction due to their high strength-to-weight-ratio. While wrought magnesium alloys have enjoyed considerable development effort in recent years, Mg casting alloys have not been subject of concerted alloy optimization or development activities. Mg-6wt%Al based casting alloys with optimum level of strength and ductility are used in automotive interior components [1]. Simultaneous increase in the ductility and strength of these alloys will lead to their extended use also in crashworthy car body components.

Casting alloys which are usually richer in solute levels compared to wrought alloy compositions possess large amounts of intermetallic phases which govern their mechanical properties. In Mg-Al alloys, the β -Mg₁₇Al₁₂ precipitate is the main second phase that significantly affects the mechanical behaviour; it lowers ductility but improves strength. The refinement in the morphology and distribution of this second phase and a change in its crystal structure to improve its strengthening effect have the potential to increase the ductility of the alloy system while maintaining the strength.

Previous work mainly on rare earth (RE) element additions has shown that the refinement of β -Mg₁₇Al₁₂ has exerted an important effect on the ductility of Mg-6Al cast alloy. Minor addition of Gd in AZ91 alloy has simultaneously increased its ductility and strength by forming Al₈Mn₄Gd which act as nucleation sites for Mg₁₇Al₁₂ and α -Mg leading to their refinement [2]. Sankaranarayanan et al. observed that trace erbium (Er) addition in Mg-Al alloy improved the mechanical properties through microstructure refinement which they associated with formation of the Al₃Er intermetallics [3]. Others reported that the addition of Er in cast Mg₁₇Al₁₂ intermetallic improves its microhardness through grain refinement [4]. Studies in Mg-Si alloys have shown that low additions (up to 1wt%) of rare earth elements Nd and Gd can refine the Mg₂Si precipitate

through a poisoning mechanism but the refinement is lost for higher additions [5,6]. In AZ31 [7], trace Er addition (0.03wt%) was seen to refine the grains leading to an increase in UTS and elongation. However, higher Er additions were detrimental for the mechanical properties. Grain coarsening of α -Mg was observed as well as a decrease in the amount and size of $Mg_{17}Al_{12}$ with the formation of Al_2Er phase.

The role of the various RE elements over a wide range of additions is not known. The refinement mechanisms of second phases are known to vary: (i) growth poisoning by segregating to surface or interface, (ii) the alteration of the nature of the phase (crystal structure, bonding), and (iii) inoculation. (i) *Growth poisoning by segregating to surface or interface*: Knowledge on precipitates modification exists from the Al-Si cast alloys where the eutectic Si phase has been refined with low additions elements such as Na[8], Sr[9], Sb[10], Y and Yb[11]. Sr addition in ppm levels can modify the eutectic Si phase due to the co-segregation of Sr with Al and Si within the eutectic precipitate leading to growth poisoning [12]. Overmodification is known to result in a loss of the refinement and in mechanical properties. The previous work of the authors [13] with Y additions to Mg-Al alloy supports that the extensive formation of other intermetallics can be detrimental for the mechanical properties. It is known that RE elements tend to segregate [14,15] to defects (e.g. interfaces, grain boundaries, dislocations) due to their surface active nature in Mg. According to the Yamauchi[16] model, surface segregation occurs when the Wigner-Seitz radius (r) of the solute element is larger than the host. Yamauchi showed that when the ratio of $r_{\text{solute}}/r_{\text{host}}$ is above 1 then surface segregation is likely. Considering this criterion, Er is a promising element (r_{Er} : 0.195nm[17], r_{Mg} :0.141nm[18]) for the modification of $Mg_{17}Al_{12}$. However, in Mg-Al alloys the solubility of Er at room temperature is nil, largely nullifying this effect.

(ii) *The alteration of the nature of the phase (crystal structure, bonding):* Trace additions can change the intermetallic phases altering their bonding, crystal structure and interface properties. First principle calculations [19] have shown that elements such as Ca, Zr, and La substitute the Mg atoms and Zn, Cu, Ni substitute the Al atoms of $Mg_{17}Al_{12}$ phase. This leads to changes in the elastic properties and mechanical stability of $Mg_{17}Al_{12}$. Lattice distortion and change of $Mg_{17}Al_{12}$ lattice parameter has been previously observed due to the existence of a third element in the β phase [13,20,21]. A similar refining effect was found with Y in Mg-6wt%Al alloy[13]. The amount and type of alloying addition determine if the element dissolves in $Mg_{17}Al_{12}$ or creates a new phase.

(iii) *Inoculation:* Theoretically, inclusions and precipitates can have an inoculating role; they can nucleate both the matrix phase and the second phases in the alloy. The previous work of the authors has shown that Y-bearing intermetallic that co-precipitate with the β phase can nucleate and refine this phase [13].

In the present study, the refining effect of ppm levels of Er additions in Mg-6wt%Al (Mg-6Al) alloy was investigated using Scanning Electron Microscopy (SEM), Atom Probe Tomography (APT), X-rays diffraction (XRD), mechanical testing (tensile, compression, hardness) and thermodynamic simulations. The mechanism of refining was related largely to an inoculation effect of Al_2Er on the β - $Mg_{17}Al_{12}$ phase and the additional effect of Er on β -phase and α -Mg was elucidated.

6.2 Experimental Procedures

Three different compositions (Table 6.1) were synthesized using 99.98% pure Mg ingot, 99.9% pure Al granules and 99.9% pure Er pieces. A graphite crucible heated at 700 °C in a Norax Canada Induction Furnace was used to melt the pure Mg. The melt was kept under protective atmosphere all the time with a mix of CO_2/SF_6 gas (0.553% SF_6 and balanced CO_2). The alloying elements

were added at 720 °C and held for 20 minutes at temperature. After skimming and stirring, the alloys were poured under protective gas into a preheated (400 °C) steel mold to produce flat plates (thickness of 6 mm).

Table 6.1 Chemical composition of the alloys using ICP.

Alloy [*]	Al (wt%)	Er (ppm)	Fe (wt%)	Mn (wt%)
Mg-6Al (control) ^{**}	6.23	-	0.027	0.015
Alloy 1	6.28	60	0.018	0.015
Alloy 2	6.07	880	0.020	0.014

^{*} Mg: balance ^{**} Values from author's previous work published in [13] are provided for comparison.

The chemical composition (Table 6.1) was determined by atomic-emission spectroscopy (ICP-AES). Increased levels of inclusions were observed at the Er containing samples, especially at the low ppm level. Three alloy plates were cast in the composition range of 50-90 ppm Er and 5.80-6.28 wt% Al as per ICP. The mechanical properties were evaluated by tensile, compression and hardness tests. The tensile coupons with a gauge length of 25 mm were machined from the as cast plate according to the ASTM E8 standard. The elongation was measured by an extensometer attached on the samples. The compression cylinders were machined from the same plates having 5 mm diameter and 7.5 mm height. Both tests (MTS 810-100kN servo-hydraulic machine) were conducted at room temperature with a strain rate of 0.001 s⁻¹. Lubricated mica sheets with boron nitride were used for the compression samples. A Mitutoyo hardness testing machine (HR-500) was used to evaluate the hardness at room temperature.

Details for the sample preparation can be found elsewhere [13]. A Nikon-Epiphot 200 optical microscope (OM) was used to measure the average grain size by the intercept technique as well as

the secondary dendrites arm spacing (SDAS). The precipitates were characterized with a Hitachi SU3500 scanning electron microscope/Backscattered Electron Detector (SEM/BSE,) with an energy dispersive X-ray spectroscopy (EDS) detector. The OM and SEM micrographs were analyzed with the ImageJ software[22]. A Bruker D8 Discovery X-Ray Diffractometer (Cu source) was used to obtain the crystallographic information of the cast alloys after stress annealing 260 °C for 1 hour as described in [23]. The surface of the samples was flattened after grinding and polishing before the heat treatment. Rietveld refinement using the GSAS II software [24] was used to obtain the crystallographic information. For the atom probe tomography sample preparation, the area of interest was extracted using a standard liftout procedure [25] and sharpened to a needle shape using dual beam focused ion beam FIB-SEM (Zeiss NVision 40), with a 30 kV Ga ion beam. A final sharpening step was performed at 10 kV to reduce ion beam damage to the specimen. The sample was analyzed with a Cameca LEAP 4000X HR atom probe operating in laser-pulse mode (50 pJ/pulse, 200 kHz pulse rate, $\lambda = 355$ nm) at an approximate specimen base temperature of 60 K, with a target detection rate of 0.01 ions/pulse. 462×10^6 total ions were collected during acquisition. Data reconstruction was performed using IVAS 3.8.2 and established algorithms [26].

6.3 Results

6.3.1 Mechanical Properties

Table 6.2 shows the tensile properties; both average and maximum values are reported. Er addition enhances the tensile properties of Mg-6Al binary alloy. Similarly, the hardness shows an increasing trend with Er which agrees with the increasing maximum UTS values. Additionally, the strain to fracture in compression increases with Er addition while the Compression Strength (CS) decreases for Alloy 1 and Alloy 2.

Table 6.2 Mechanical properties of the as cast samples at room temperature.

Tensile Properties	Mg-6Al*	Alloy 1	Alloy 2
UTS (MPa)	206 ± 5 [209]	201± 11 [218]	211±15 [233]
YS (MPa)	74 ± 6 [78]	72± 4 [75]	70±11 [88]
EI (%)	8 ± 2 [9.5]	9± 1 [10]	10±3 [15.8]
Compression Properties			
CS (MPa)	276 ± 8	263 ± 5	264±6
Strain (%)	23 ± 1	28 ± 2	29±1
Hardness			
HRE	47± 2	53 ± 4	54±7

Brackets show max values

*From the authors' previous work [13].

6.3.2 Microstructural Investigation

6.3.2.1 Scanning Electron Microscopy

The SEM/BSE micrographs of the three alloys in the as-cast condition are shown in Fig.6.1. The alloys consist of α -Mg dendrites, partially divorced eutectic $Mg_{17}Al_{12}$ precipitates in the interdendritic regions and Mg-Al-Mn-Fe phases. Table 6.3 shows the results of the image analysis of the OM and SEM micrographs. The average size of $Mg_{17}Al_{12}$ decreases by 56% with trace Er addition (Alloy 1) and then slightly increases in Alloy 2 with higher Er level (~44% decrease from control sample). The area fraction of $Mg_{17}Al_{12}$ increases by ~52% in Alloy 1 and by ~30% in Alloy 2. It has been also observed that Alloy 1 has higher percentage of spherical β phase morphology (i.e., more particles with aspect ratio 0.8-1) comparing to Mg-6Al and Alloy 2 which indicates stronger refinement. The Mg-Al-Mn-Fe-(Er) phase becomes slightly coarser when higher amount of Er is added (Alloy 2). The α -Mg grain size decreases by ~22% in Alloy 1 and by ~18% in Alloy

2 following similar trend with the size of Mg₁₇Al₁₂. The secondary dendrites arm spacing (SDAS) shows a slight refinement in Er containing alloys.

Table 6.3 Effect of Er addition on the size and morphology of second phases.

Alloys	Mg ₁₇ Al ₁₂ Area fraction (%)	Mg ₁₇ Al ₁₂ Size (μm ²)	Irregular Mg ₁₇ Al ₁₂	Spherical Mg ₁₇ Al ₁₂	Mg-Al-Mn-Fe- (Er) Area fraction (%)	Mg-Al-Mn-Fe- (Er) Size (μm ²)	α-Mg Grain Size (μm)	α-Mg SDAS (μm)
Mg-6Al	0.97±0.40*	32 ± 15*	87%	13%	0.09±0.05*	1.56±0.06*	96±13*	23±5
Alloy 1	1.47 ± 0.37	14 ± 3	66%	34%	0.08±0.03	1.47±0.28	75±8	19±2
Alloy 2	1.26 ± 0.46	18 ± 4	82%	18%	0.16±0.06	2.08±0.50	79±10	19±3

*Values from author's previous work published in [13] are provided for comparison.

In Alloy 1 (60 ppm Er), only a small fraction of Mg-Al-Mn-Fe precipitates contains Er compared to Alloy 2 (880 ppm Er) where all the Mg-Al-Mn-Fe precipitates are enriched in Er and depleted in Fe and Mn. A close association of the Mg-Al-Mn-Fe (with or without Er) phase with Mg₁₇Al₁₂ and α-Mg was also seen indicating a co-precipitation/nucleation effect (Fig.6.2).

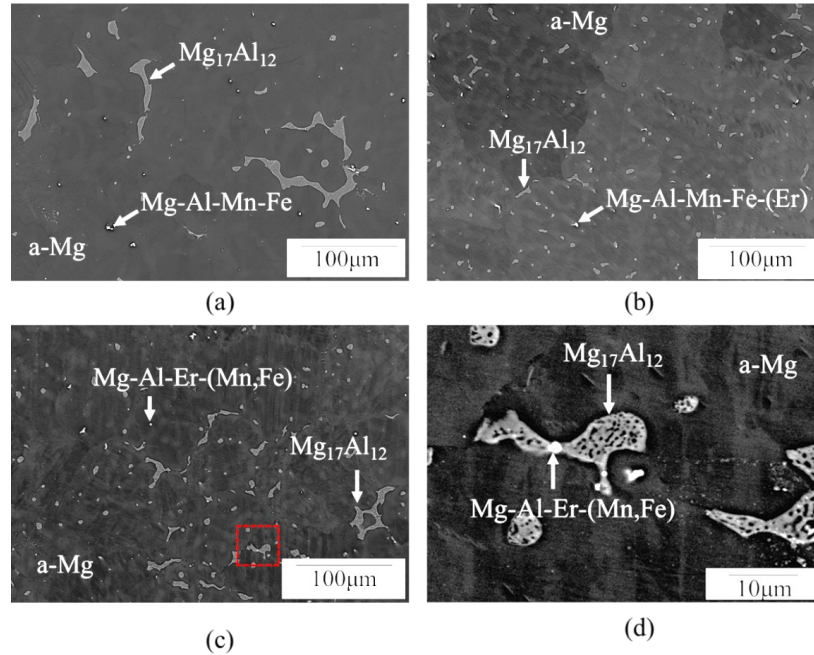


Fig. 6.1 SEM/BSE micrographs of as cast alloys (a) Mg-6Al, (b) Alloy 1 (60ppm Er), (c) Alloy 2 (880ppmEr), (d) Higher magnification of Alloy 2 showing the association between Er enriched phase and $Mg_{17}Al_{12}$.

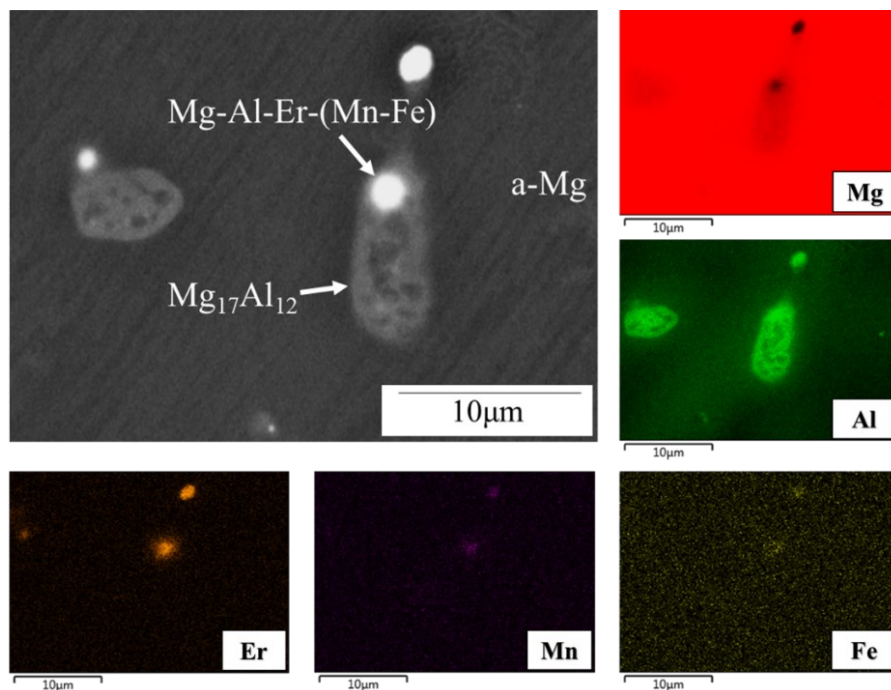


Fig. 6.2 EDS map analysis showing co-precipitated Er-enriched precipitates and $Mg_{17}Al_{12}$ in Alloy 2.

6.3.2.2 Atom Probe Tomography

Atom probe tomography was used to examine the possible segregation of Er inside the $\text{Mg}_{17}\text{Al}_{12}$ phase; The phase was extracted from Alloy 1 (60 ppm Er). A quantitative approach was used to define elemental segregation first by delineating the two phases using an iso-concentration surface (here set at 25 at.% Al) and measuring a 1D concentration profile in the region just adjacent to this surface using a proximity histogram (proxigram). Fig. 6.3 shows the plot of the major elements (i.e., Mg and Al) versus distance. The composition of the secondary phase is close to stoichiometric $\text{Mg}_{17}\text{Al}_{12}$, albeit slightly more Mg-rich. $\text{Mg}_{17}\text{Al}_{12}$ is a metastable non stoichiometric phase and due to the large range of Mg and Al [23] it is often observed to deviate from the stoichiometric composition [27]. Further analysis showed that the $\text{Mg}_{17}\text{Al}_{12}$ is more enriched in Er than the α -Mg matrix (Table 4). The Er peaks are indistinguishable from the background in the Mg matrix (Fig. 6.4). It was also observed that impurities from the raw materials such as Cu and Mn were present in $\text{Mg}_{17}\text{Al}_{12}$. Impurities are common in magnesium alloys and it has been observed that they tend to dissolve in the β - $\text{Mg}_{17}\text{Al}_{12}$ phase [28–30].

Table 6.4 Composition of α -Mg matrix and $\text{Mg}_{17}\text{Al}_{12}$ of Alloy 1 (60 ppm Er).

Element	Mg Matrix (at%)	Mg Matrix (wt%)	$\text{Mg}_{17}\text{Al}_{12}$ (at%)	$\text{Mg}_{17}\text{Al}_{12}$ (wt%)
Mg	94.274 \pm 0.009	93.67	60.701 \pm 0.010	58.15
Al	5.723 \pm 0.003	6.31	39.282 \pm 0.008	41.78
Er	0.002 \pm 0.001	0.01	0.007 \pm 0.001	0.05
Cu	< 0.001	-	0.010 \pm <0.001	0.03
Mn	< 0.001	-	< 0.001	-

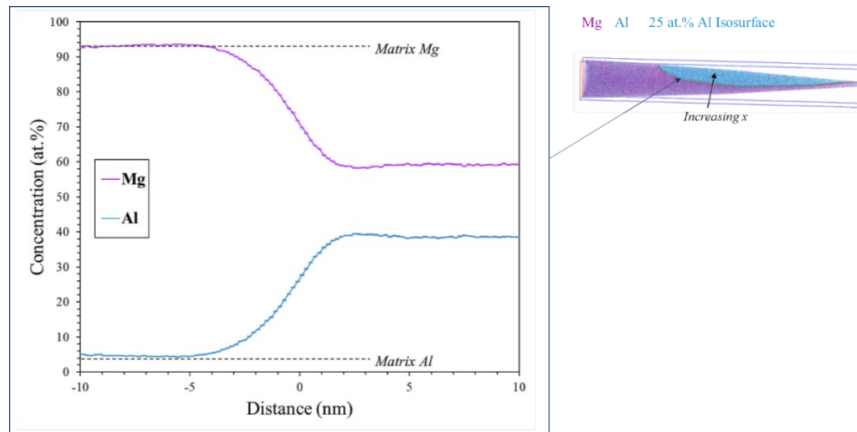


Fig. 6.3 APT plot of Mg and Al inside $Mg_{17}Al_{12}$ of Alloy 1 (60 ppm Er).

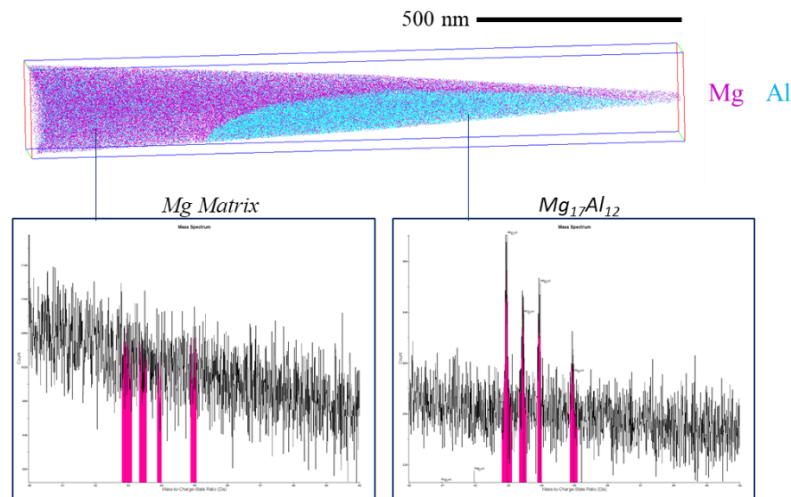


Fig. 6.4 Er peaks (pink) in α -Mg and $Mg_{17}Al_{12}$ of Alloy 1 (60 ppm Er).

6.4 Crystallographic Analysis

The lattice parameter of $Mg_{17}Al_{12}$ for the three alloys was determined via XRD (Fig.6.5) after annealing the samples to relieve the internal stresses. Rietveld refinement at 2θ : 35.6° - 45° was used to calculate the lattice parameter a , the cell volume and weight fraction of $Mg_{17}Al_{12}$ as shown in Table 6.5. The lattice parameter and, by extension, the cell volume of the β phase increase with Er addition. Only the peaks of $Mg_{17}Al_{12}$ and α -Mg matrix appear in the XRD spectra and no Er phase is seen.

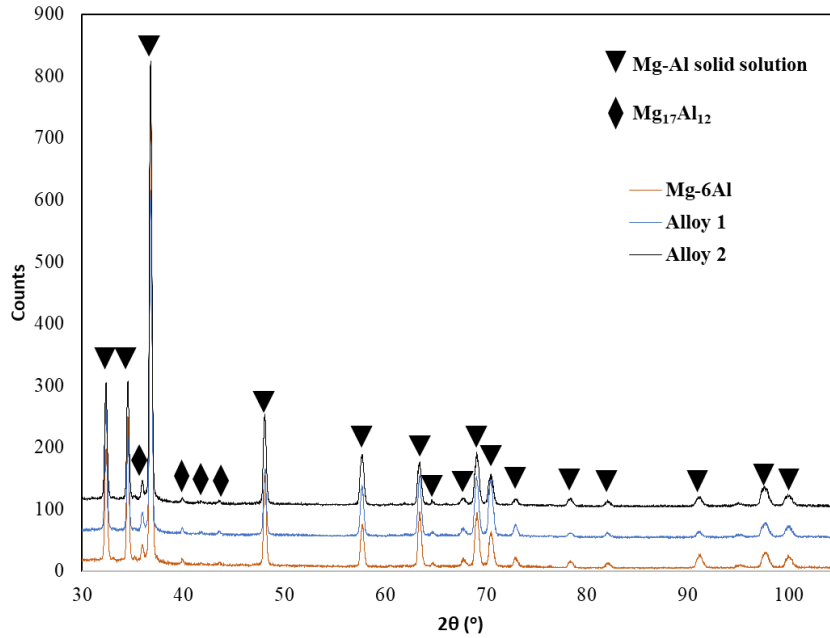


Fig. 6.5 XRD diffraction peaks of the 3 alloys.

Table 6.5 Average lattice parameter of β -Mg₁₇Al₁₂ after Rietveld refinement.

Alloys	a (Å)	Cell Volume (Å ³)	Weight fraction
Mg-6Al ^[13]	10.5841±0.0014	1185.68	0.034±0.003
Alloy 1	10.5846±0.0017	1185.82	0.045±0.003
Alloy 2	10.5861±0.0011	1186.34	0.035±0.001

6.5 Thermodynamic Simulations

Thermodynamic simulations were performed using the FactSage 7.3 Education Package software with the FTlite data base [31]. Equilibrium and non-equilibrium simulations (Scheil cooling) were conducted to predict the formation temperature and type of the phases. Fig. 6.6.a shows the plot of the Mg-(0-60wt%) Al-60ppm Er phase diagram where the β phase co-exists with Er-rich intermetallics. Fig. 6.6.b presents the equilibrium isopleth for the Mg-6wt%Al system with

different levels of Er (0 to 0.1 wt%). Both Alloy 1 and Alloy 2 present the same solidification path leading to the formation of α -Mg+Al₂Er+Mg₁₇Al₁₂ at room temperature. The main differences between alloys 1 and 2 are the following (Fig. 6.6b):

1. Alloy 1 with 60ppm Er experiences a first stage of freezing range (α -Mg+Liq.) of $\sim 70^\circ\text{C}$ before the formation of primary Al₂Er Laves while the corresponding stage in Alloy 2 with 880 ppm Er is only $\sim 20^\circ\text{C}$.
2. In Alloy 1, primary Al₂Er has a short temperature range and less time to coarsen while in Alloy 2, primary Al₂Er has a larger freezing range and more time to coarsen.

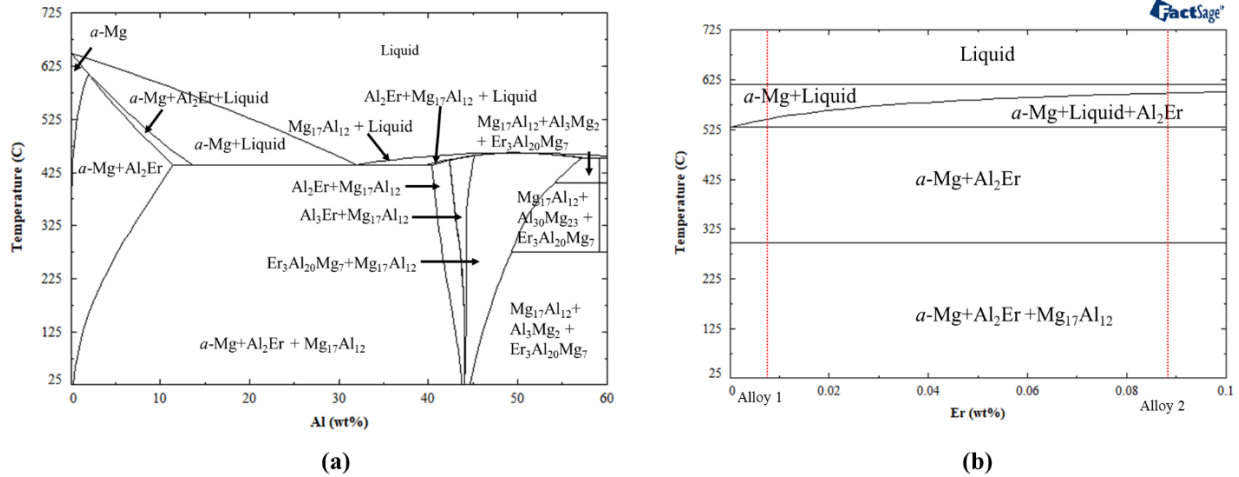


Fig. 6.6 (a) Phase diagram of Mg-(0-60) wt%Al-60 ppm Er. (b) Equilibrium isopleth for Mg-6wt% Al with different Er levels. The red lines show the solidification path for Alloy 1 (60 ppm Er) and Alloy 2 (880 ppm Er).

Scheil cooling simulations were also performed for different levels of Er in the Mg-6 wt% Al alloy (Fig.6.7). It is observed that the Al₂Er precipitate forms at very low Er levels (Fig.6.7a) and its amount increases with increasing Er. The amount of Mg₁₇Al₁₂ shows a decreasing trend with higher Er addition. A notable observation is the formation temperature of Al₂Er and Mg₁₇Al₁₂; the two phases form at a very close temperature in Alloy 1 (60 ppm Er) or even at the same temperature

for lower Er additions. However, the formation of Al_2Er takes place earlier than $\text{Mg}_{17}\text{Al}_{12}$ during the solidification (i.e., at higher temperature) at 880 ppm Er. Another important observation is the segregation of Er inside $\text{Mg}_{17}\text{Al}_{12}$ which confirms the APT results. Table 6.6 summarizes the Scheil cooling results.

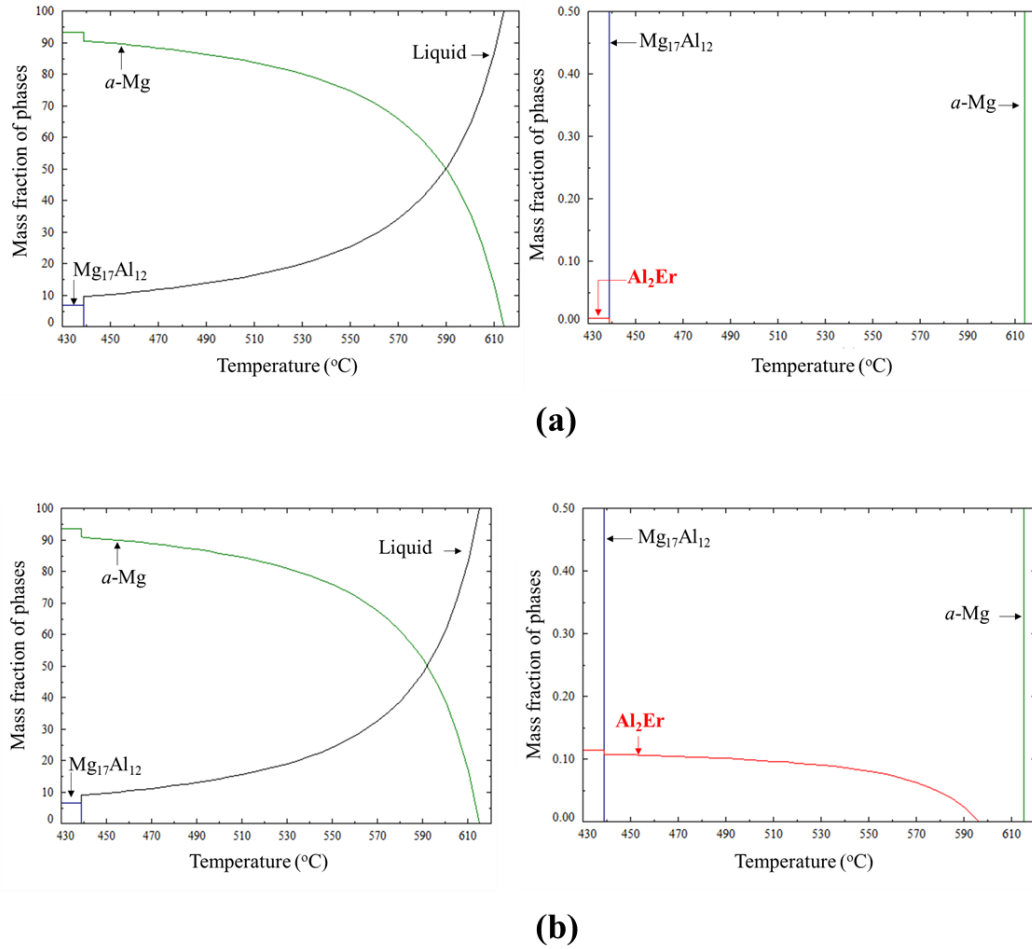


Fig. 6.7 Scheil cooling of Mg-6Al-Er (a)60ppmEr, (b)880ppmEr.

Table 6.6 Formation temperature and amount of each phase predicted by Scheil cooling.

Er level (ppm)	Formation Temperature of Mg₁₇Al₁₂ (°C)	Formation Temperature of Al₂Er (°C)	Amount of Mg₁₇Al₁₂ (%)	Amount of Al₂Er (%)
0	439	-	6.62	-
60	439	440	6.70	0.008
880	439	595	6.35	0.11

6.6 Discussion

This study has shown that low level Er (60 and 880 ppm) additions exert complex effects on the microstructure and the mechanical properties of the Mg-6Al alloy. Microstructural refinement encompassing most microstructural features, the β -Mg₁₇Al₁₂ phase, α -Mg grain size and dendrite arm spacing, as well as Mg-Al-Mn-Fe phases occurs at the lower level of Er. Er also dissolves in both β phase and in Mn bearing phases. In the β -phase, it alters the lattice parameters. Effect of these changes on the mechanical properties is complex. Since the main trust of this study was to understand the effect of low levels of Er on mechanical properties of a Mg-Al alloy, the discussion aims at elucidating the mechanism of the microstructural refinement and interpreting the role of the refinement and of the change in the β -phase on the mechanical properties in Mg-6Al (Er) alloys.

6.6.1 Modification of β -Mg₁₇Al₁₂ crystal structure

Atom Probe Tomography, XRD and thermodynamic simulations indicate that Er is soluble in the β phase. Mg₁₇Al₁₂ is a non-stoichiometric compound which exists over a compositional range for Mg and Al [23,32]. It has a cubic A12 crystal structure isomorphous with α -Mn (cI58). Its unit cell

consists of 34 Mg atoms occupying three different positions Mg(I), Mg(II) and Mg(III) and 24 Al atoms. The bonding of the atoms is homopolar between the Al atoms, heteropolar between Mg and Al and metallic among Mg atoms; $(Al_2)_{12}^{-2} Mg_{24}^{+} Mg_{10}$ [33,34]. Its lattice parameter a ranges from 10.50 Å to 10.69 Å [35]. Elements that dissolve in $Mg_{17}Al_{12}$ (e.g., Ca, Zn, La etc.) substitute Mg or Al atoms. The position of the alloying addition (i.e. Mg(I), Mg(II), Mg(III) or Al) depends on the minimization of the occupational energy. Due to this substitution the elastic constants of $Mg_{17}Al_{12}$ will change [19]. For example, Ca is soluble in $Mg_{17}Al_{12}$ and substitutes the Mg(III) atoms increasing the cohesive energy and its lattice parameter [36]. Similarly, Er is soluble in $Mg_{17}Al_{12}$ substituting Mg or Al leading to lattice distortion and increase of its lattice parameter. This substitution changes its elastic constants affecting its intrinsic characteristics such as its modulus. First principle simulations [19] showed that rare earths such as La increased the bulk, shear, and Young's moduli of $Mg_{17}Al_{12}$ by substituting the Mg atoms. Generally, the modulus increases when the bonded electrons and the coordination number increase while the length of the bond is short [42,43]. XRD investigation shows that Er affects the lattice parameter a of the β -phase which increases with increasing Er in the alloy.

6.6.2 Microstructural Refinement

SEM analysis of this study shows that the addition of low level of Er in Mg-6Al refines the $Mg_{17}Al_{12}$ phase, the α -Mg grain size, and Mg-Al-Fe-Mn phases. The XRD, APT analyses and the thermodynamic simulations indicate that the refinement mechanisms of the $Mg_{17}Al_{12}$ in the Mg-Al-Er based cast alloys can be attributed to an inoculation process. Thermodynamic simulations show that at low levels of Er, the Al_2Er precipitate starts forming at the same or close temperature as $Mg_{17}Al_{12}$ (439 °C). This indicates an effective co-precipitation and inoculation effect. At higher Er levels, the Al_2Er precipitates form earlier at a higher temperature (595 °C) than the $Mg_{17}Al_{12}$

during solidification. This temperature difference allows more time for coarsening of the Al_2Er , resulting to loss of the co-nucleation effect for $\text{Mg}_{17}\text{Al}_{12}$ at the eutectic temperature (439 °C). As a result, the $\text{Mg}_{17}\text{Al}_{12}$ shows an increasing size trend for higher Er additions. The refinement in α -Mg grains can also be attributed to an inoculation effect via the Er modified and refined Mg-Al-Fe-Mn phases that are found in the α -Mg grains (Table 6.3 & Fig. 6.1).

6.6.3 The Effect of Microstructural Refinement and the Modification of β -phase on the Mechanical Properties of Mg-6Al

Effect on Tensile Strength, Ductility and Hardness: The $\text{Mg}_{17}\text{Al}_{12}$ and α -Mg refinement would reflect as an improvement in the mechanical properties of the Er containing alloys. This correlates largely with the trend we see in tensile properties, compression strain to fracture and hardness (Table 6.2). The solubility of REs in α -Mg is very limited when Al is present, resulting in the formation of brittle intermetallics [37–40]. In Mg-Al casting alloys, the embrittlement of the alloy with increasing Al has been related to the increase in the β -phase. It has been reported [41] that dislocations pile up or form networks inside $\text{Mg}_{17}\text{Al}_{12}$ or Al_8Mn_5 . This could possibly lead to the cracking of the precipitates during the deformation of Mg-Al based alloys. Refinement in the β would enhance ductility since cracks that form in the brittle phases would be stopped by the more ductile matrix. Work by Vaid et al [42] sheds more light on the interaction of the β -phase with dislocations where the authors have made atomistic simulations of basal-dislocation interactions with the β -phase. They suggested that the dislocations do not shear the precipitate or Orowan-loop around them but that they pass the β -phase by leaving dislocation segments in the disordered interphase boundary. The β -phase then acts as a sink for dislocations which delays the early onset of dislocation network stage in α -Mg during plastic deformation and improves

ductility. The ductility improvement also explains the increased UTS observed in the Er containing alloys. Hardness defined as resistance to plastic deformation also follows the trend in UTS.

Effect on Compression Strain to Fracture: Compressive fracture in Mg alloys is associated with shear banding that can be twin induced. Al additions to Mg changes the c/a ratio and the twinning mode [43] enhancing tension twins where the twin boundaries accumulate dislocations leading to cracking. The refined grain size can reduce the propensity to twinning and thereby increasing the strain to fracture under compression.

Effect on Yield strength: The yield strength seems to have a complex dependence on β -phase and microstructural refinement. Vaid et al [42] have shown that the critical resolved shear stress τ_c to pass an array of precipitates is proportional to $\ln((1/D + 1/L)^{-1})$ where D is precipitate diameter and L is the interparticle spacing. Er refines the β precipitate diameter and increases its amount in Alloy 1; it also refines the grain size and the SDAS. The consequence of these factors should be an increase in yield strength. However, the yield in Alloy 1 with 60 ppm Er decreases compared to the base alloy but increases in Alloy 2 with 880 ppm Er. To be noted, Alloy 2 has less microstructural refinement and a lower amount of β -phase. Other factors then must be responsible for the trend in yield strength. Vaid et al [42] predicted that a stiffer β -phase would lead to ~15% increase in the critical resolved shear stress. The increased Er dissolved in the β -phase leading to increased modulus would explain partly the increase in yield strength. One other difference between Alloy 1 and Alloy 2 is the appearance of Er-rich intermetallics in Alloy 2 that can provide additional contribution to yield strength. One observation remains elusive and that is the decrease of yield strength in Alloy 1 compared to the base alloy despite the increase in the amount of β -phase, the refinement in grain size and SDAS and the slight change in the lattice parameter indicating dissolved Er in the β -phase (Table 6.5). The increased amount of inclusions that was

observed in this alloy also cannot explain the decrease in the yield strength as the trend is not seen in hardness. A hypothesis that can be put forth can be related to an effect of dissolved Er in the β -phase. If dissolved Er decreases the modulus rather than increase it, then the decrease in yield in Alloy 1 can be accounted for. The increase in the yield strength at the higher Er level (Alloy 2) then can be attributed to the presence of Er intermetallics rather than the stiffening of the β -phase. The authors have previously studied Y additions to Mg-6Al where trace Y additions forms the Al_4MgY at the same temperature as $\text{Mg}_{17}\text{Al}_{12}$ resulting in its refinement. The refinement is lost for higher Y amounts after the formation of coarse Y enriched precipitates [13]. Interestingly substantial differences are also observed between the Y and Er additions in the binary Mg-6wt%Al.

(i) The α -Mg grain size decreases for ppm Y additions but increases for higher levels. In the case of Er, the grain size is smaller than the base alloy for both low and high additions. It is likely that, the Mg-Al-Fe-Mn particles coarsen significantly in the Y containing alloys (from $\sim 2\mu\text{m}$ to $\sim 4\mu\text{m}$) [13] losing their nucleation effectiveness. However, these particles remain $\sim 2\mu\text{m}$ in the Er containing alloys. The Er enriched phases in Alloy 2 with high amount of Er (i.e., 880 ppm) do not coarsen as much as the Y enriched phases in the alloy with high Y (i.e., 300 ppm). It is also noted that the β phase in the Y containing alloys co-exists with the Al_4MgY phase while the β in the Er containing alloys co-exists with Al_2Er , Al_3Er and $\text{Er}_3\text{Al}_{20}\text{Mg}_7$ phases.

6.7 Conclusions

1. Trace Er addition improves the mechanical properties of Mg-6wt%Al alloys. 60 ppm Er (Alloy 1) refine the $\text{Mg}_{17}\text{Al}_{12}$ phase by 56% and 880 ppm Er (Alloy 2) by 44%. Similarly, Er addition leads to refinement of α -Mg grain size and SDAS.

2. An increase on tensile ductility, UTS and hardness was observed in the Er containing alloy with slight changes in YS. Similarly, compression strain to fracture was increased with Er additions; however, the compression strength shows a decreasing trend with Er.
3. Close association of Er enriched precipitates with $Mg_{17}Al_{12}$ was observed proving their nucleation role during the formation of β phase.
4. Atom probe tomography detects Er within the $Mg_{17}Al_{12}$ phase, but not in the α -Mg phase.
5. XRD results show an increase of $Mg_{17}Al_{12}$ lattice parameter and cell volume with Er addition.
6. Non-equilibrium Scheil calculations show that precipitation temperatures of Al_2Er and $Mg_{17}Al_{12}$ coincide at 439 °C for trace Er levels. As Er increases, Al_2Er precipitates at higher temperature before the solid-state formation of the $Mg_{17}Al_{12}$ phase at the end of the solidification.
7. The increase in tensile ductility, compressive strain to fracture and hardness are attributed to microstructural and grain refinement.
8. The increase in yield strength at ~900 ppm Er is attributed to microstructural refinement and the existence of Er-rich intermetallics. Yield strength at 60 ppm Er seems to have complex dependence on microstructural refinement and β -phase modification.

6.8 Acknowledgements

This project was conducted under the financial support of the Natural Sciences and Engineering Research Council of Canada (NSERC) Discovery Grant (G210358NSERC/RGPIN-2016-05121). The authors thank Pierre Vermette, Luis A. Villegas-Armenta and Raul Arriaga Benitez for their assistance in alloy casting and discussions. Konstantinos Korgiopoulos gratefully acknowledges McGill Engineering Doctoral Award program (MEDA).

6.9 References

- [1] H.E. Friedrich, B.L. Mordike, *Magnesium technology*, Springer, 2006.
- [2] J. Wang, X. Li, Simultaneously improving strength and ductility of AZ91-type alloys with minor Gd addition, *J. Alloys Compd.* (2019).
- [3] S. Seetharaman, C. Blawert, B.M. Ng, W.L.E. Wong, C.S. Goh, N. Hort, M. Gupta, Effect of erbium modification on the microstructure, mechanical and corrosion characteristics of binary Mg-Al alloys, *J. Alloys Compd.* (2015) 759–770. doi:10.1016/j.jallcom.2015.05.284.
- [4] L.I. Yonggang, W.E.I. Yinghui, H.O.U. Lifeng, G.U.O. Chunli, H.A.N. Pengju, Effect of erbium on microstructures and properties of Mg-Al intermetallic, *J. Rare Earths.* 32 (2014) 1064–1072.
- [5] J. Hu, C. Tang, X. Zhang, Y. Deng, Modification of Mg₂Si in Mg-Si alloys with neodymium, *Trans. Nonferrous Met. Soc. China.* 23 (2013) 3161–3166.
- [6] L. Ye, J. Hu, C. Tang, X. Zhang, Y. Deng, Z. Liu, Z. Zhou, Modification of Mg₂Si in Mg–Si alloys with gadolinium, *Mater. Charact.* 79 (2013) 1–6.
- [7] Y. Ma, X. Zhang, H. Liu, L. Meng, Effects of Er on the microstructure and properties of AZ31 magnesium alloy prepared via the EMS process, *Rare Met.* 29 (2010) 339–345.
- [8] S.C. Flood, J.D. Hunt, Modification of Al-Si eutectic alloys with Na, *Met. Sci.* 15 (1981) 287–294.
- [9] A.K. Dahle, K. Nogita, S.D. McDonald, C. Dinnis, L. Lu, Eutectic modification and microstructure development in Al–Si Alloys, *Mater. Sci. Eng. A.* 413 (2005) 243–248.

- [10] A.K.P. Rao, K. Das, B.S. Murty, M. Chakraborty, On the modification and segregation behavior of Sb in Al–7Si alloy during solidification, *Mater. Lett.* 62 (2008) 2013–2016.
- [11] A. Knuutinen, K. Nogita, S.D. McDonald, A.K. Dahle, Modification of Al–Si alloys with Ba, Ca, Y and Yb, *J. Light Met.* 1 (2001) 229–240.
- [12] M. Timpel, N. Wanderka, R. Schlesiger, T. Yamamoto, N. Lazarev, D. Isheim, G. Schmitz, S. Matsumura, J. Banhart, The role of strontium in modifying aluminium–silicon alloys, *Acta Mater.* 60 (2012) 3920–3928.
- [13] K. Korgiopoulos, M. Pekguleryuz, The significant effect of trace yttrium level on the mechanical properties of cast Mg–6Al alloy through a refinement mechanism, *Mater. Sci. Eng. A.* 775 (2020) 138966.
- [14] X. Tong, L. Zai, G. You, H. Wu, H. Wen, S. Long, Effects of bonding temperature on microstructure and mechanical properties of diffusion-bonded joints of as-cast Mg–Gd alloy, *Mater. Sci. Eng. A.* 767 (2019) 138408.
- [15] D. Rossouw, B. Langelier, A. Scullion, M. Danaie, G.A. Botton, Multivariate-aided mapping of rare-earth partitioning in a wrought magnesium alloy, *Scr. Mater.* (2016) 174–178. doi:10.1016/j.scriptamat.2016.07.022.
- [16] H. Yamauchi, Surface segregation in jellium binary solid solutions, *Phys. Rev. B.* 31 (1985) 7688. doi:<https://doi.org/10.1103/PhysRevB.31.7688>.
- [17] P. Strange, A. Svane, W.M. Temmerman, Z. Szotek, H. Winter, Understanding the valency of rare earths from first-principles theory, *Nature.* 399 (1999) 756–758.
- [18] P.-G. Reinhard, E. Suraud, *Introduction to cluster dynamics*, John Wiley & Sons,

Weinheim, 2008.

- [19] J. Dai, Y. Song, R. Yang, Influences of alloying elements and oxygen on the stability and elastic properties of Mg₁₇Al₁₂, *J. Alloys Compd.* 595 (2014) 142–147.
- [20] J. Su, F. Guo, H. Cai, L. Liu, Study on alloying element distribution and compound structure of AZ61 magnesium alloy with yttrium, *J. Phys. Chem. Solids.* 131 (2019) 125–130.
- [21] D. Zhou, P. Peng, J. Liu, Energetics, electronic structure, and structure stability of the calcium alloying Mg₁₇Al₁₂ phase from first principles calculations, *Mater Sci Pol.* 25 (2007) 145–153.
- [22] W.S. Rasband, Imagej, us national institutes of health, bethesda, maryland, usa, [Http://Imagej.Nih.Gov/Ij/](http://Imagej.Nih.Gov/Ij/). (2011).
- [23] M. Avedesian, H. Baker, *ASM specialty handbook: magnesium and magnesium alloys.*, ASM International, Ohio, 1998.
- [24] B.H. Toby, R.B. Von Dreele, GSAS-II: the genesis of a modern open-source all purpose crystallography software package, *J. Appl. Crystallogr.* 46 (2013) 544–549.
- [25] K. Thompson, D. Lawrence, D.J. Larson, J.D. Olson, T.F. Kelly, B. Gorman, In situ site-specific specimen preparation for atom probe tomography, *Ultramicroscopy.* 107 (2007) 131–139.
- [26] B. Gault, M.P. Moody, J.M. Cairney, S.P. Ringer, *Atom probe microscopy*, Springer Science & Business Media, 2012.
- [27] S. Barbagallo, H.I. Laukli, O. Lohne, E. Cerri, Divorced eutectic in a HPDC magnesium–aluminum alloy, *J. Alloys Compd.* 378 (2004) 226–232.

- [28] S.T. Auwal, S. Ramesh, Z. Zhang, F. Yusof, J. Liu, C. Tan, S.M. Manladan, F. Tarlochan, Effect of copper-nickel interlayer thickness on laser welding-brazing of Mg/Ti alloy, *Opt. Laser Technol.* 115 (2019) 149–159.
- [29] C. Scharf, A. Ditze, A. Shkurankov, E. Morales, C. Blawert, W. Dietzel, K.-U. Kainer, Corrosion of AZ 91 secondary magnesium alloy, *Adv. Eng. Mater.* 7 (2005) 1134–1142.
- [30] T. Al-Samman, Effect of heavy metal impurities in secondary Mg alloys on the microstructure and mechanical properties during deformation, *Mater. Des.* 65 (2015) 983–988.
- [31] C.W. Bale, P. Chartrand, S.A. Degterov, G. Eriksson, K. Hack, R. Ben Mahfoud, J. Melançon, A.D. Pelton, S. Petersen, FactSage thermochemical software and databases, *Calphad.* 26 (2002) 189–228.
- [32] D. Shin, C. Wolverton, The effect of native point defect thermodynamics on off-stoichiometry in β -Mg₁₇Al₁₂, *Acta Mater.* 60 (2012) 5135–5142.
- [33] A.A. Kaya, M.O. Pekguleryuz, K.U. Kainer, *Fundamentals of magnesium alloy metallurgy*, Woodhead Publishing, Cambridge, 2013.
- [34] W.-C. Hu, Y. Liu, X.-W. Hu, D.-J. Li, X.-Q. Zeng, X. Yang, Y.-X. Xu, X. Zeng, K.-G. Wang, B. Huang, Predictions of mechanical and thermodynamic properties of Mg₁₇Al₁₂ and Mg₂Sn from first-principles calculations, *Philos. Mag.* 95 (2015) 1626–1645. doi:10.1080/14786435.2015.1040098.
- [35] M.X. Zhang, P.M. Kelly, Crystallography of Mg₁₇Al₁₂ precipitates in AZ91D alloy, *Scr. Mater.* (2003) 647-652. doi:10.1016/S1359-6462(02)00555-9.

- [36] D.W. Zhou, P. Peng, H. Zhuang, Y.J. Hu, J.S. Liu, First-principle study on structural stability of Ca alloying Mg₁₇Al₁₂ phase, *Zhongguo Youse Jinshu Xuebao/Chinese J. Nonferrous Met.* 15 (2005) 546–551.
- [37] B. Pourbahari, M. Emamy, H. Mirzadeh, Synergistic effect of Al and Gd on enhancement of mechanical properties of magnesium alloys, *Prog. Nat. Sci. Mater. Int.* 27 (2017) 228–235.
- [38] C. Wang, J. Dai, W. Liu, L. Zhang, G. Wu, Effect of Al additions on grain refinement and mechanical properties of Mg–Sm alloys, *J. Alloys Compd.* 620 (2015) 172–179.
- [39] M. Faruk, A. OezDEMIR, K.U. Kainer, H. Norbert, Influence of Ce addition on microstructure and mechanical properties of high pressure die cast AM50 magnesium alloy, *Trans. Nonferrous Met. Soc. China.* 23 (2013) 66–72.
- [40] L. Wang, Y. Feng, E. Guo, L. Wang, Y. Fu, S. Zhao, G. Cao, Comparative study on microstructure and mechanical properties of Mg-3Nd-3Al and Mg-3Nd-0.5 Zr alloys under different heat treatment conditions, *JOM.* 71 (2019) 2194–2201.
- [41] R.M. Wang, A. Eliezer, E.M. Gutman, An investigation on the microstructure of an AM50 magnesium alloy, *Mater. Sci. Eng. A.* 355 (2003) 201–207.
- [42] A. Vaid, J. Guénolé, A. Prakash, S. Korte-Kerzel, E. Bitzek, Atomistic simulations of basal dislocations in Mg interacting with Mg₁₇Al₁₂ precipitates, *Materialia.* 7 (2019) 100355.
- [43] M. Pekguleryuz, M. Celikin, M. Hoseini, A. Becerra, L. Mackenzie, Study on edge cracking and texture evolution during 150 C rolling of magnesium alloys: the effects of axial ratio and grain size, *J. Alloys Compd.* 510 (2012) 15–25.

CHAPTER 7

Concluding Discussion and Proposed Future Work

7.1 General Discussion

The long-term objective of the current doctoral work was to increase the ductility of Mg-6wt%Al based casting alloys without compromising their strength so that these alloys can be used in structural parts of vehicles. The use of these alloys is important for weight reduction in cars and trucks powered with internal combustion engines for the purpose of emissions reduction. The use of these alloys is also critical in weight reduction in electric vehicles.

The alloy development strategy was focused on the trace additions of rare earths (REs) to modify the β -Mg₁₇Al₁₂ phase which plays an important role in the strength and ductility of Mg-Al casting alloys. REs were selected because of their expected role in improving the mechanical properties of Mg alloys. The usual hesitation in using REs due to their cost and supply concerns was addressed by using trace additions (ppm levels). Trace levels were used to modify the Mg₁₇Al₁₂ phase while minimizing the formation of other phases that could embrittle the alloy. Trace level additions especially as low as ppm levels are not usually used in Mg alloy development with REs. This research choice enhanced both the novelty and the challenges of the alloy development in synthesizing and analyzing the microstructures of the alloys. In the present study Y and Er were studied. The Mg-Al alloy selected was Mg-6Al which is the alloy with an optimum combination of strength and ductility due to the medium amount of Mg₁₇Al₁₂ phase in its structure. The main research questions were:

1. Can trace levels of Y and Er modify either the morphology or the nature of the $Mg_{17}Al_{12}$ intermetallic phase?
2. Can the modification of the $Mg_{17}Al_{12}$ intermetallic enhance the ductility of the Mg-6Al alloy?

This doctoral work was able to show the effects of trace additions of Y and Er on the phase morphology, crystal structure and elastic moduli of $Mg_{17}Al_{12}$. The study also developed Mg-6Al(Y) and Mg-6Al(Er) alloys with enhanced ductility for use in crashworthy structural applications of vehicle-body construction. The forgoing discussion summarizes the key findings of the doctoral work.

7.1.1 The Microstructural Refinement of the Mg-6Al alloy with Y and Er and the Mechanism of such Refinement

Nucleation-Based Morphological Refinement of the $Mg_{17}Al_{12}$ Phase

This doctoral thesis determined that Y or Er additions morphologically refine the $Mg_{17}Al_{12}$ (up to 47% with Y and up to 56% with Er) and that this refinement occurs in a narrow range of trace additions (0.2-1.5 ppm Y and 60 ppm Er). The refinement of $Mg_{17}Al_{12}$ is lost when Y or Er increases to higher levels. At these higher additions, coarse Y or Er phases form.

The mechanisms of morphological refinement in metallic alloys are known to be two-fold: Nucleation based or due growth inhibition. In this study, microstructural characterization, and thermodynamic simulations, both, shed light onto the mechanism of morphological refinement brought about by Y and Er. The close association of Y or Er bearing phases with $Mg_{17}Al_{12}$ in the microstructure indicates a nucleation-based mechanism wherein fine Y-containing or Er-containing intermetallics effectively nucleate and refine the β phase. HRTEM analysis shows that the interface between the $Mg_{17}Al_{12}$ and the Mg-Al-Y precipitate is semi-coherent, with misfit dislocations relaxing the interfacial strain. The near-coherency of the interface strongly suggests

that Y-intermetallic acts as nucleation point of the β -phase. These particles are Al_4MgY in Mg-6Al(Y) alloy and in the Mg-6Al (Er) alloys the nucleant phase was found to be Al_2Er .

The research question on why the nucleant effect occurs with trace levels of Y and Er and the refinement is lost as the amount of these elements increase beyond the optimum range was the principal focus of the project in its early stages. Thermodynamic calculations interestingly pointed out the composition dependence of the nucleation effect. Equilibrium calculations predict that Al_4MgY and Al_2Er , Al_3Er , $\text{Er}_3\text{Al}_{20}\text{Mg}_7$ phases co-exist with $\text{Mg}_{17}\text{Al}_{12}$ phase in Mg-Al-Y and Mg-Al-Er alloys, respectively. Non-equilibrium Scheil calculations show that the precipitation temperatures of Al_4MgY or Al_2Er and $\text{Mg}_{17}\text{Al}_{12}$ coincide at 439 °C when Y or Er are in trace levels. As the alloying addition (i.e., Y or Er) increase, their phases form at earlier stage of solidification (at higher temperature) well before the formation of $\text{Mg}_{17}\text{Al}_{12}$. The phases that form at higher temperatures have time to coarsen and lose their nucleant effectiveness for $\text{Mg}_{17}\text{Al}_{12}$ while at trace additions the phases that co-form with $\text{Mg}_{17}\text{Al}_{12}$ are effective nucleants.

The Refinement of the α -Mg Grain Size

In parallel with the refinement of $\text{Mg}_{17}\text{Al}_{12}$, the α -Mg grain size also decreases for trace Y additions but then it increases for higher amounts of Y. Similar trend is shown with trace Er where the α -Mg grain decreases for trace additions. This can be attributed to the solute content of liquid in the semi solid fields. Since the formation of the Al_4MgY or Al_2Er phases occur at low temperatures at trace additions the liquid phase is enriched in Y or Er yielding a fine grain size. At higher additions where these phases form early, the liquid is dilute leading to coarser grains. However, it is noted that grain coarsening with increasing Er is less significant than that with Y. Here, the effect of another nucleant comes into play: The Mg-Al-Fe-Mn particles are nucleants for α -Mg grains, but they coarsen significantly with high Y additions but not with high Er additions.

7.1.2 Modification of the intrinsic properties of β -Mg₁₇Al₁₂

The Mg₁₇Al₁₂ phase is stoichiometric at absolute zero but exists over a range of compositions at higher temperatures. Stabilization is via-Hume-Rothery rules at stoichiometric composition, but via complex defect structure at off-stoichiometry. This structure is subject to substitution by solutes. Solute substitution while increasing stability can also alter lattice parameters.

Solubility and Lattice Parameter:

The experimental investigation of this study showed that Y and Er dissolves in the Mg₁₇Al₁₂ phase. Y shows a maximum solubility of ~330ppm. Excess Y additions lead to the formation of Al₄MgY phase. Atom probe tomography proved that Er dissolves in the Mg₁₇Al₁₂ phase and no Er was detected in the α -Mg matrix. XRD showed that the lattice constant a and the cell volume increase with Y or Er additions. However, the lattice parameter and cell volume contracts for higher Y additions (i.e.,300 ppm Y).

Once an effect of dissolved Y and Er was seen on the lattice parameter of Mg₁₇Al₁₂, the principal focus, at this stage, was to understand the mechanism of this effect. Lattice constants can change through change in electron-to-atom ratio (e/a) which is Hume-Rothery stabilization effect or through size differences of the solute radii with respect to host radii. Several important observations and findings were obtained in this doctoral study to shed light on the incorporation of Y or Er in the phase.

Y alloys:

- The lattice parameter a first decreases and then increases with increasing Y dissolved in the β -phase; the increase in Y is accompanied by an increase in the Al content suggesting that the Y possibly substitutes the Mg sites, but samples also show that Y may be substituting Al sites.

- There is a complex dependence of lattice parameter with Y and Al with a reversal in dependence at ~ 0.005 at% Y and ~ 43.1 at% Al. The lattice parameter decreases and then increases with Y.
- The increase in lattice parameter a above 0.005 at % Y can be explained with size effect however, the initial decrease in lattice parameter with increasing Y and Al cannot be explained on the basis of the metallic radii. The initial lattice contraction can only be attributed to the inherent chemical disorder of the β -phase that exists at off-stoichiometric compositions and that consists of partial and fractional site occupancy. The present study concurs with previous studies by Shin et al [reference 38 in Chapter 5] that the effect of Y on the lattice parameter is not likely due to simple site substitution but can be explained by the formation of complicated defect mechanisms such as multi-defect clustering.
- A complex correlation exists between c/a and the lattice parameter, a , with an initial increase with c/a (up to 2.439) but then a decrease that is not aligned by the usual effect of c/a on the lattice constant that can also be explained by its complex defect structure.

Er Alloys

- Atom Probe Tomography, XRD and thermodynamic simulations indicate that Er is soluble in the β phase. XRD showed that Er affects the lattice parameter a of the β -phase which increases with increasing Er in the alloy from 10.5841 to 10.5861 angstroms at 880 ppm Er.

Microhardness and Elastic Moduli

The characterization of the $Mg_{17}Al_{12}$ phase as ductile or brittle is complicated. According to first-principle calculations and based on the elastic constants, $Mg_{17}Al_{12}$ is considered to be a stiff and brittle intermetallic [Chapter 5 ref 7–9]. Its presence in Mg-Al alloys is also related to the lowering of the alloy's ductility. However, it was also shown that the ratio of bulk modulus (B) over shear modulus (G) determines the failure mode of intermetallics; ductile ($B/G > 1.75$) or brittle ($B/G < 1.75$) [Chapter 5 ref 7–10,23].

The microhardness and the elastic moduli of $Mg_{17}Al_{12}$ with Y was determined experimentally in this doctoral study and the B/G for β - $Mg_{17}Al_{12}$ is found to be 2.21 indicating that the β -phase can be classified as ductile. The study also determined that the B/G of $Mg_{17}Al_{12}$ decreases to 2.17-2.18 with dissolved Y. It appears that Y weakens very slightly the ductility of $Mg_{17}Al_{12}$ but the intermetallic is still in the ductile category as per B/G.

Atomistic simulations of basal-dislocation interactions with the β -phase suggest that the dislocations pass the $Mg_{17}Al_{12}$ phase without shearing the precipitate or presenting any Orowan loop around it [ref 17 Chapter 5]. This notion leads us to think that the morphological refinement of the $Mg_{17}Al_{12}$ phase would indeed aid the movement of dislocations in cast alloys in interdendritic regions where the $Mg_{17}Al_{12}$ phase concentrate. Hence, the role of Y in ductility improvement seen in this study is attributable to its modifying effect on the $Mg_{17}Al_{12}$ phase rather than in changing its intrinsic ductility.

7.1.3 The Effect of Y and Er on the Tensile Properties of Mg-6Al

The driving force for this study is the need to develop Mg-6wt%Al alloys with enhanced ductility without sacrificing strength for use in structural body components of automotive vehicles. The study shows that Yttrium and Erbium additions at trace levels can meet these objectives.

Yttrium: Trace Y additions significantly increase the tensile ductility and the UTS; hence toughness increases making the alloy crashworthy. The effect is attributed the modifying effect of these additions at these trace levels. The modifying effect and the improvement in mechanical performance is lost as Y or Er is increased above these trace levels. The strong relationship between $Mg_{17}Al_{12}$ and tensile ductility is described as $\%El = 44.38 - 2.648 Mg_{17}Al_{12} \text{ Size} + 0.04724 Mg_{17}Al_{12} \text{ Size}^2$ with $R(\text{adj})^2=99.98\%$. Compressive strain also improves.

Erbium: Er show slightly different effect than Y on the mechanical properties of Mg-6wt%Al. As Er increases, the tensile ductility; UTS and hardness increase too. Similarly, compression strain to fracture was increased with Er; the compression strength shows an opposite trend.

7.2 General conclusions

Y and Er additions can improve the mechanical properties of the binary Mg-6wt%Al alloy by refining the β -Mg₁₇Al₁₂ phase and the α -Mg grain size. Trace additions without the formation of coarse intermetallics, lead to higher refinement and more cost effective alloys than higher alloying additions. The following table provides the highlights of each alloy that was synthesized and tested in the current doctoral thesis.

Table 7.1 Summary of the investigated alloys and their main characteristics.

Mg-6Al

Control sample with coarse Mg₁₇Al₁₂ precipitates.

Mg-6Al-1.5 ppm Y

Refined Mg₁₇Al₁₂ and α -Mg phases with significantly improved tensile and compression properties. Co-precipitation of Al₄MgY with Mg₁₇Al₁₂ at the end of solidification.

Mg-6Al-100, 300 & 3000 ppm Y

Coarser Mg₁₇Al₁₂ and α -Mg phase than trace Y additions. Formation of coarse Y enriched precipitates before the nucleation of Mg₁₇Al₁₂. Deterioration of mechanical properties.

Mg-6Al-60 ppm Er

Refinement of both Mg₁₇Al₁₂ and α -Mg. Slight improvement on tensile properties and hardness but significant improvement on compression strain to fracture. Co-precipitation of Al₂Er with Mg₁₇Al₁₂ at the end of solidification. Er was detected in Mg₁₇Al₁₂.

Mg-6Al-880 ppm Er

Slight coarsening of $\text{Mg}_{17}\text{Al}_{12}$ and α -Mg phases comparing with trace Er containing alloy but still finer than Y containing alloys. Improvement of tensile properties, compression strain to fracture and hardness. Al_2Er forms earlier than $\text{Mg}_{17}\text{Al}_{12}$ but it is not as coarse as Y precipitates.

 $\text{Mg}_{17}\text{Al}_{12}$ with 300 & 5000 ppm Y

Lattice parameter distortion. Formation of coarse Al_4MgY at high (5000 ppm) Y. Improvement of intrinsic mechanical properties.

7.3 Strategies for Future Work

According to the current doctoral thesis, it is possible to design Mg-Al based alloys with high ductility and strength leading to increased toughness through the modification of $\text{Mg}_{17}\text{Al}_{12}$ intermetallics with trace rare earth additions. The following research and commercial objectives are proposed based on the findings of the current thesis:

7.3.1 Scientific research objectives

1. The diffusion of trace rare earths inside $\text{Mg}_{17}\text{Al}_{12}$ as well as in the α -Mg (e.g., grain boundaries, dislocations) should be thoroughly investigated using high resolution techniques such as atom probe tomography and high-resolution transmission electron microscopy with aberration correction. The orientation relationship between nucleant intermetallics and α -Mg and $\text{Mg}_{17}\text{Al}_{12}$ can also be investigated.
2. A study on the phases formation using differential scanning calorimetry (DSC) would be useful to experimentally validate co-nucleation and the solidification path of Mg-Al based alloys with trace Er or Y additions.
3. The mechanism of ductility improvement with morphological refinement should be investigated.

4. Further investigation on the effect of REs on the elastic moduli of $Mg_{17}Al_{12}$ and the Pugh criterion. It would be interesting to study the change of shear modulus and its effect on the dislocation motion through the Peierls-Nabarro equation.
5. An investigation of synergistic effects between Y or Er and Mn on the refinement of $Mg_{17}Al_{12}$ and α -Mg can be conducted.
6. Other RE elements can be investigated for their role in the modification of $Mg_{17}Al_{12}$ phase.

7.3.2 Commercial development objectives

Magnesium casting original equipment manufacturers (OEMs) such as Meridian Lightweight Technologies would be an appropriate industrial partner to evaluate the performance of AM60 alloys with trace Y or Er addition. The focus should be on following aspects:

1. High pressure die cast (HPDC) Mg-Al based components with trace Y or Er should be prepared to evaluate the existence of the refining mechanism at high cooling rates.
2. Mechanical testing of HPDC components to evaluate the effect of trace additions on the crashworthiness of Mg-Al based alloys.
3. Effect of trace Y or Er on the corrosion resistance of Mg-Al alloys. It is expected that the corrosion will be improved as it is observed that both elements dissolve in Mg-Al-Fe-Mn precipitates and modify them.

CHAPTER 8

Contributions to Original Knowledge

The current doctoral research focused on the development of high ductility and strength Mg-6 wt% Al (Mg-6Al) alloy by refining the microstructure using trace and low amounts of Y or Er additions. Mg-6Al is the main magnesium casting alloy considered for car body applications due to its optimum combination of strength and ductility. However, the alloy needs to have improved ductility for wide use in these applications. In this doctoral study new concepts were developed on rare earth additions to Mg-6Al.

8.1 Yttrium (Y) Alloying of Mg-6Al Alloy

1. ***The concept of trace additions:*** Yttrium alloying of Mg-Al alloys to date had focused on levels that can be considered low to moderate. Observations of microstructural modification and improvement on mechanical behavior have been reported but in contradictory versions. The alloys always led to the formation of coarse and brittle Y-bearing intermetallics that overshadowed the microstructural refinement. The alloy design discovery made in this doctoral thesis is on the use of only trace level Y <60 ppm which is a distinct novelty. It was found that this level of addition refines the $Mg_{17}Al_{12}$ phase which is the main strengthening phase in Mg-Al alloys without the formation of coarse brittle Y-intermetallics. The alloy exhibited 63% improvement in ductility over Mg-6Al base alloy. It can have a wide range of applications readily in vehicle body construction.
2. ***The mechanism of the morphological refinement of $Mg_{17}Al_{12}$:*** The refinement mechanism was determined by thermodynamic simulations and HRTEM analysis. It was discovered that in this composition range of the alloy system, an Y-intermetallic does form but it co-precipitates as a fine particle at the same temperature as the $Mg_{17}Al_{12}$ phase thereby nucleating

and refining it. At higher Y additions, the Y-intermetallic forms earlier at higher temperatures in the liquid; it coarsens and loses its nucleating effect. This principle was validated with another rare earth element Erbium and can be effectively used with the aid of thermodynamic simulations to identify other alloying additions that can refine the $Mg_{17}Al_{12}$ phase.

8.2 Erbium addition in Mg-Al Alloy

1. Trace Er additions also proved to be beneficial for the refinement of $Mg_{17}Al_{12}$ phase and improved the tensile properties suggesting a new way for future alloy design where expensive rare earths can be proved beneficial to the mechanical properties of Mg-Al alloys at trace levels.
2. Atom probe tomography was used to identify the Er solubility inside $Mg_{17}Al_{12}$. Erbium amount was higher in the β phase than the α -Mg matrix for trace Er additions.

8.3 Modification of $Mg_{17}Al_{12}$ intrinsic properties

1. The effect of Y and Er additions in the crystal structure of $Mg_{17}Al_{12}$ has been studied and it has been observed that both elements change the lattice constant of the phase.
2. The elastic moduli of $Mg_{17}Al_{12}$ with and without Y were experimentally investigated for the first time. The experimental results are comparable with the first principle calculations and indicate that $Mg_{17}Al_{12}$ presents ductile character and Y additions increase its moduli of elasticity.
3. Based on the Y effect on cast $Mg_{17}Al_{12}$ lattice constant, it is proposed that the intermetallic is off-stoichiometric and its e/a ratio implies that its thermodynamic stabilization is not through Hume-Rothery stabilization but through defect structure mechanisms.
4. Also, notably, it was determined by the elastic moduli that $Mg_{17}Al_{12}$ is a ductile intermetallic and Y slightly decreases its ductility. This led to the important discovery that the main reason

for the decrease of ductility of Mg-Al alloys with an increased amount of $Mg_{17}Al_{12}$ is based mainly on the coarse morphology of this phase and not on its intrinsic properties. It also led to the confirmation that ductility of Mg-Al alloys can be enhanced by the refinement of the $Mg_{17}Al_{12}$ phase morphology.

8.4 Commercial and Environmental Contribution

The discoveries of this doctoral study are positioned to make a significant contribution to the wider use of Mg in lightweight automotive applications for reduced greenhouse gases, and, also, for enabling the construction of electrical vehicles. Mg-6wt% alloy is already commercially used with all its casting processes well established. The use of rare earth additions only at trace levels would require rather minor adjustments in processing, joining and finishing and infrastructure.

Appendix A

Experimental Details and Sources of Error

Castings

Alloy composition

All the alloys were synthesized using raw materials (pure Mg, Al, Y, Er). A recovery factor was used for each element to ensure that the actual composition is close to the target. The recovery factor for Al was 0.95 and for Er was 0.75. Y recovery factor fluctuated from 0.85 to 0.2 as it was challenging to synthesize alloys close to the target. The main assumption of this error is the fast diffusion of Y at the oxide layer of the melt. All the castings compositions in this thesis are the actual after analyzing the samples with inductively coupled plasma mass spectrometry in an external certified lab. There are three main limitations for the chemical analysis; 1) the detection limit for each element, 2) the matrix effect which can affect the measurements and 3) how homogeneous is the matrix. These limitations significantly affect the quantification of trace additions.

Electron microscopy has also its limitations for the detection of trace additions in the alloys. Energy Dispersive Spectroscopy (EDS) has a detection limit of 0.1 wt% for bulk materials making it impossible to detect trace elements. Wavelength-Dispersive Spectroscopy (WDS) has a lower detection limit (~ 0.01 wt%) but still this is not enough to analyze the alloys presented in the current thesis. Atom probe tomography (APT) is a possible technique to detect trace elements, but the biggest challenge is the sample preparation and the low yield of Mg alloys. For example, the alloy with the detected trace Er which was analyzed in the current thesis, is the result of 462×10^6 ion counts from only one tip. Another tip from the same alloy yielded only 34×10^6 ion counts which

was not enough to detect Er. Similarly, APT was conducted on the Y sample but it yielded only 30×10^6 ion counts which was not enough to detect the trace Y.

Casting defects

Magnesium alloys oxidize fast during the synthesis and castings. For this reason, a protective atmosphere of CO_2/SF_6 is necessary to protect the molten alloys all the time. However, oxidation cannot be prevented completely, and inclusions form during the casting in the permanent mold. These inclusions can be large (mm size) and act as stress risers affecting the tensile properties as the alloys present a premature fracture. After each tensile test, the fracture surface was visually evaluated and the samples which had big inclusions, intense oxidation or broke outside the extensometer were rejected. Compression samples were also used to better evaluate the mechanical properties and eliminate the effect of porosity and inclusions.

Tensile and compression samples geometry

The tensile samples were machined from the as-cast plates (6 mm thickness) using the ASTM E8 standard (Fig. I) for flat subsize specimens (1/4-in. wide).

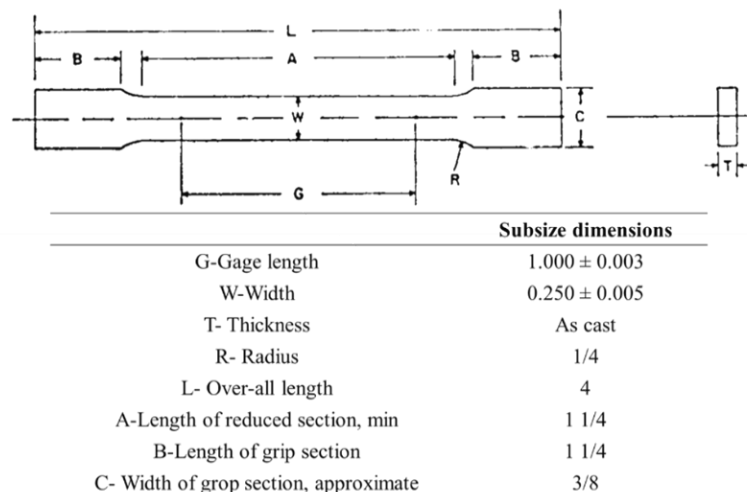


Fig. I Dimensions of tensile samples according to the subsize flat specimen ASTM E8 standard.

The dimensions of the compression samples were machined in that way that the height (7.5 mm) to diameter (5 mm) ratio is always 1.5 to avoid buckling of the samples.

Grain size measurements

To analyze the grain size of α -Mg, the cross section of three samples from different areas of each alloy was observed under the optical microscope (at least seven micrographs per alloy) after grinding, polishing, and etching. Over-etching “burns” the Mg-Al based alloys and makes the grain boundaries (GB) invisible. The etchant composition is given in the previous chapters. The ImageJ software was used to draw lines of known length (at least 7 lines for each micrograph). Then the number of intersections was measured, and the average grain size was calculated by dividing the line length with the number of intersections. Fig. II shows a typical micrograph with the revealed grain boundaries after etching.

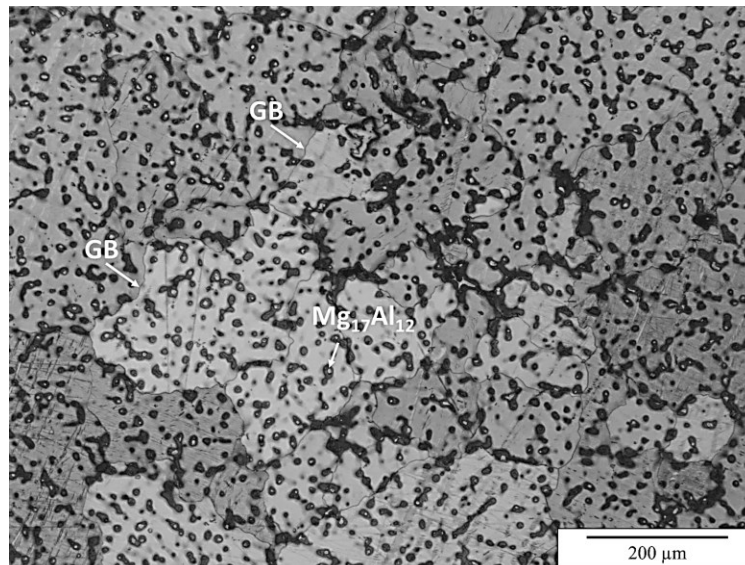


Fig. II Example of Mg-Al-Y micrograph under the optical microscope after etching. The grain boundaries (GB) appear after careful etching. Over-etching makes the GB invisible.

X-rays Diffraction

The calculation of the $\text{Mg}_{17}\text{Al}_{12}$ lattice constant in the Mg-Al alloys can be affected by different types of experimental errors. The lattice constant was measured after doing refinement (Fig. III) using the low angle peaks of $\text{Mg}_{17}\text{Al}_{12}$ because only these peaks were strong enough in the tested alloys. Using low angle peaks can introduce errors in the measurements. Higher angles are more reliable for lattice constant calculations, but this is not always possible due to the low intensity of the peaks. Other possible errors include misalignment of the XRD equipment, temperature fluctuations, sample displacement and texture.

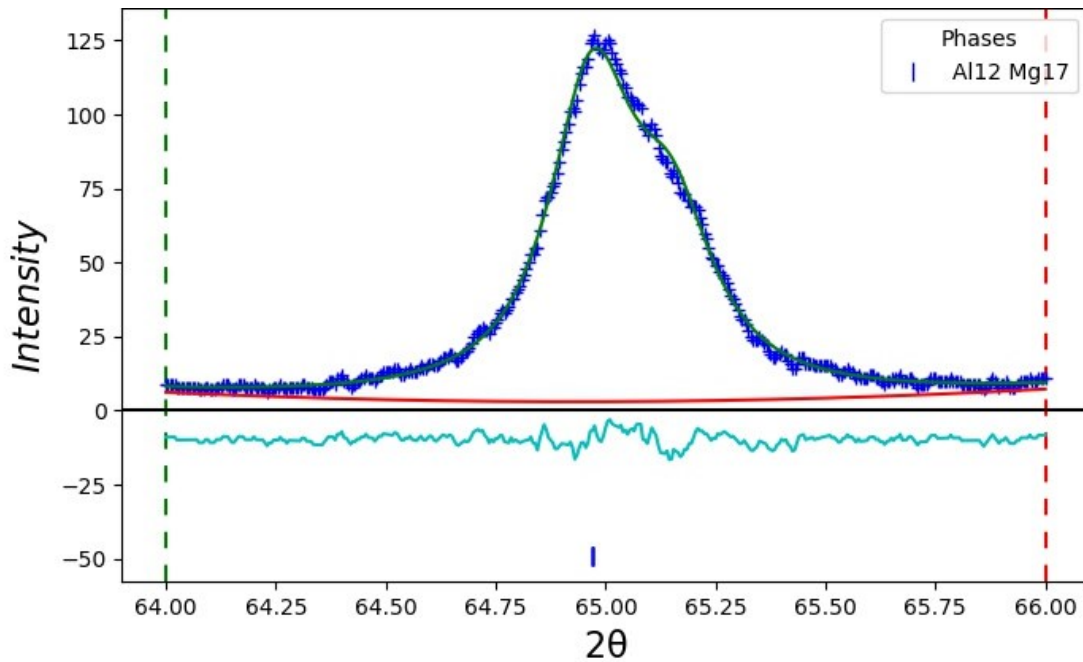


Fig. III Example of Rietveld refinement fitting for the $\text{Mg}_{17}\text{Al}_{12}$ phase.

Thermodynamic Calculations

The thermodynamic calculations are based on databases which were developed over the years. These databases may not contain all the phases that can form during solidification. Updated versions of the software take into consideration new findings which improve the quality of the databases. Scheil cooling which is used to simulate the as-cast microstructures assumes no

diffusion once the solid is formed which may not be real in the actual casting. Kinetics also affect the evolution of the microstructure, but they are not described by the thermodynamic calculations.

Supplemental information

- All the alloys were permanent mold cast and they had a cooling rate of $\sim 10^\circ\text{C}/\text{sec}$ which can be simulated well with no-equilibrium calculations (Scheil cooling).
- $\text{Mg}_{17}\text{Al}_{12}$ has a cubic structure with lattice parameter a (the distance between 110 planes). Changes in lattice parameter with Y (Table 5.4) were explained in the discussion of chapter 5. There is a difference in the effect of Y and Er on the lattice parameter of the β phase (table 3.7 vs table 6.5). When Y is in excess of maximum solubility limit in β phase then Y bearing intermetallics are formed. It is suggested that in β stoichiometry, the defect structure and the lattice parameter change. This behaviour can be different in Er containing alloy. This can be investigated in future work. To remove the internal stresses (i.e., elastic stress), alloys were stressed relieved to remove the effect of strain on the lattice parameter.
- Standard deviations in the β phase size (e.g., table 4.2 and 6.3) overlap but this gives the interesting insight into the refinement and coarsening of β phase. In the refined microstructure the standard deviation is low but in the analysis of the coarse β phase (2D size) the standard deviation increases.
- In chapter 6, it is true that only 3 data points were fitted to give the polynomial relationship but interestingly an extra subsequent experiment drops on this polynomial curve. It has been seen before that lattice parameter can change trend with different levels of alloying additions (Chapter 2).